PROPERTIES OF CEMENT-BASED MATERIALS IN THE PRESENCE OF NANO AND MICROPARTICLE ADDITIVES

A Dissertation
Presented to
The Academic Faculty

by

Amal Raj Puthur Jayapalan

In Partial Fulfillment
of the Requirements for the Degree
Doctor of Philosophy in the
School of Civil & Environmental Engineering

Georgia Institute of Technology
August 2013

PROPERTIES OF CEMENT-BASED MATERIALS IN THE PRESENCE OF NANO AND MICROPARTICLE ADDITIVES

Approved by:

Dr. Kimberly Kurtis, Advisor
School of Civil and Environmental Engineering
Georgia Institute of Technology

Dr. Michael Bergin
School of Civil and Environmental Engineering, School of Earth and Atmospheric Sciences
Georgia Institute of Technology

Dr. Lawrence Kahn
School of Civil and Environmental Engineering
Georgia Institute of Technology

Dr. John Crittenden
School of Civil and Environmental Engineering
Georgia Institute of Technology

Dr. Arun Gokhale
School of Materials Science and Engineering
Georgia Institute of Technology

Date Approved: June 24, 2013

ACKNOWLEDGEMENTS

I would like to express my deepest gratitude to my advisor, Dr. Kimberly Kurtis for her continuous support and guidance throughout my M.S. and Ph.D at Georgia Tech. I truly appreciate her patience and encouragement and am fortunate to have worked with such a great advisor and mentor. I would also like to thank Dr. Lawrence Kahn for his guidance and insightful comments throughout my graduate studies at Georgia Tech. I want to thank Dr. Michael Bergin, Dr. John Crittenden and Dr. Arun Gokhale for being part of my thesis committee and for their time and support for my research.

I would like to thank National Science Foundation for funding my research project under Grant No. CMMI-0825373. I am grateful for the financial support provided by the American Concrete Institute (ACI) Georgia Chapter and Georgia Institute of Technology.

I want to thank Bo Yeon Lee for being an integral part of the research project. I am grateful for the assistance provided by Eva Land, David Tanner and Dr. Greg Huey with the photocatalytic experiments, Arka Pandit and Liz Minne for their help with the life cycle analysis and Nortey Yeboah for assistance with the surface area analysis. I would also like to thank Andy Udell for his help with fabrication of experimental setups. Undergraduate and graduate research assistants Sarah Fredrich, Melinda Jue, Justin Bel, Daniel Glass, Theau Conte, Chen Chris Wenhao, Matthew Treager are thanked for their valuable contributions to this research.

All my current and past research group members have made graduate school life fun and enjoyable at Georgia Tech and I greatly appreciate their friendship and thank

them for all the insightful as well as light-hearted discussions. My sincere thanks goes to Dr. Robert Moser, Dr. Victor Garas, Dr. Jun Chen, Lisa Lindquist Hoeke, Jonah Kurth, Dr. Andrea Mezencevova, Chris Shearer, Dr. Bo Yeon Lee, Sarah Fredrich, Passarin Jongvisuttisun, Nathan Mayercsik, Bradley Dolphyn, Elizabeth Nadelman, Marc Knapp and Alvaro Paul. I also want to thank Dr. Andrew Bechtel, Dr. Benjamin Kosbab, Dr. Jonathan Hurff, Dr. Kennan Crane, Andrea Rose, Falak Shah, Dr. J. Ben Deaton, and countless others for their friendship and for being an invaluable part of my life at Georgia Tech. I would also like to thank my friends Dr. Rakesh Nambiar, Dr. Subodh Jagtap, Rishiraj Bheda, Pawan Moradia, Debesh Bhatta and Sidharth Oommen for their camaraderie and for making life outside graduate school enjoyable.

Most importantly, I would like to express my heartfelt gratitude to my father Jayapalan P.R and mother Lekshmi C.S., as well as my brother Reghuraj Jayapalan and sister-in-law Aathira Prasad for being there for me every step of the way. I will always be indebted to you for your love, encouragement and unconditional support.

TABLE OF CONTENTS

LIST OF TABLES

LIST OF FIGURES

LIST OF SYMBOLS

A	Sample surface area
A_i	area of a triangulated surface
A_{pi}	nominal area of the surface under consideration
CO_{2eq}	Equivalent carbon dioxide emissions
C_2S	Dicalcium silicate (cement chemistry notation)
C_3A	Tricalcium aluminate (cement chemistry notation)
C_3S	Tricalcium silicate (cement chemistry notation)
C_4AF	Tetracalcium alumino ferrite (cement chemistry notation)
E_a	Activation energy
f	air-flow rate
H(t)	Cumulative heat evolved by the cement mixture till time t
H_{cem}	Total heat of hydration of the cement mixture
k	rate of chemical reaction
NO	Nitric oxide (nitrogen monoxide)
NO_2	Nitrogen dioxide
NO_X	sum of nitric oxide and nitrogen dioxide gases
$[NO_X]_{in}$	Supply volume concentration of NO_X
$[NO_X]_{out}$	Output concentration of NO_X
PEF	Photocatalytic Efficiency Factor
r	pore size radius
R	Universal gas constant
RN	Roughness number

SiO_2	Silicon dioxide
T_c	Temperature of concrete
T_{ref}	Temperature of reference sample
TiO_2	Titanium dioxide
V_C	Volume of unhydrated cement
V_{CS}	Volume of chemical shrinkage
V_{CW}	Volume of capillary water
V_F	Volume fraction of filler
V_{gw}	Volume of gel water
V_{gs}	Volume of gel solids
w/c	water-to-cement ratio
w/s	water-to-solids ratio
α	degree of hydration
α_u	ultimate degree of hydration
β	Hydration shape parameter
γ	surface tension
σ_{cap}	capillary stress
τ	Hydration time parameter
τ_c	Hydration time parameter of concrete
τ_{ref}	Hydration time parameter at reference temperature
η_{ads}	Total NO_X adsorbed by test piece (in ISO 22197 test)

LIST OF ABBREVIATIONS

AASHTO	American Association of State Highway and Transportation Officials
ANOVA	Analysis of variance
ASTM	American Society for Testing and Materials
BET	Brunauer-Emmett-Teller
BEES	Building for Environmental and Economic Sustainability
BJH	Barrett, Joyner, Hallenda
CEN	European Committee for Standardization
CSA	Canadian Standards Association
C-S-H	Calcium silicate hydrate (cement chemistry notation)
DALY	Disability-adjusted life year
DE	Diatomaceous earth
EIO	Economic input-output
FE	Field emission
GHG	Greenhouse gas
ISO	International Organization for Standardization
JIS	Japanese Industrial Standards
LCA	Life cycle analysis
LCI	Life cycle inventory
LCIA	Life cycle impact assessment
LEED™	Leadership in Energy and Environmental Design
MIP	Mercury intrusion porosimetry
OPC	Ordinary portland cement

PDF	Potentially Disappeared Fraction
ppb	parts per billion
ppm	parts per million
PLC	Portland limestone cement
PMMA	poly-methyl methacrylate
PTFE	Polytetrafluoroethylene
RCPT	Rapid chloride permeability test
SCM	Supplementary cementitious material
SEM	Scanning Electron Microscopy
UNI	Italian Organization for Standardization
US EPA	United States Environmental Protection Agency
UV	Ultraviolet
VOC	Volatile organic compounds

SUMMARY

Cement clinker production is a highly resource and energy intensive process and contributes substantially to annual global anthropogenic greenhouse gas emissions. One potential pathway to reduce the environmental footprint of cement-based materials is through the reduction of clinker content in concrete by partial replacement of cement with fillers. In this investigation, the partial replacement of cement with chemically inert nano and microsized fillers of titanium dioxide (TiO_2) and limestone was examined. The effects of nano and micro fillers on early-age properties, long-term properties, photocatalytic properties (for TiO_2-cement mixtures) and life cycle costs were measured and compared.

Investigation of early-age properties shows that nanoparticles increase rate and degree of early cement hydration and chemical shrinkage due to heterogeneous nucleation effect. In contrast, coarser microparticles (>3μm in this research) maintain or marginally decrease the rate and degree of early cement hydration and decrease chemical shrinkage due to a dilution effect. In addition, temperature sensitivity of hydration reactions increases in the presence of nanoparticles. Investigation of long-term properties shows that pore size refinement is possible with the partial replacement of cement with nanoparticle fillers. But the long-term tests of filler-cement mixes also demonstrate that, compared to ordinary portland cement mix, the strength decreases and permeability increases.

Analysis of photocatalytic properties of TiO_2-cement mixtures showed a lack of an appropriate testing procedure for nitrogen oxide (NO_X) gas conversion by cement-

based materials. Thus, a new standardized procedure and photocatalytic efficiency factor for characterizing photocatalytic NO_X binding by cementitious materials is proposed. Life cycle analysis demonstrates that although inclusion of TiO_2 increases initial environmental impact of cementitious materials, the innovative photocatalytic properties of TiO_2 could improve sustainability. Life cycle analysis also shows that partial replacement of cement with limestone decreases environmental impact of cementitious mixtures due to lower processing "costs" of limestone compared to cement.

Thus, the results from the current research demonstrate that variation of dosage and particle size of inert fillers can be used to tailor properties and structure of cement-based materials and that environmental sustainability can be improved by partial replacement of cement with inert fillers that introduce additional functionalities or fillers with lower embodied-energy and emissions.

CHAPTER 1

INTRODUCTION

1.1 Background

Cement production is a highly energy intensive process and contributes to the release of pollutants including carbon dioxide, sulfur oxides, particulates and heavy metals [1] into the atmosphere due to both the chemical reactions occurring in the kiln and, in most cases, the burning of fossil fuels for power production. In the United States, the average energy consumption for a cement plants is estimated to be about 5.2 GJ per metric ton of cement. Cement production also releases 0.98 tons of equivalent carbon dioxide per ton of cement clinker produced [2] with the total carbon dioxide (CO_{2eq}) emission by the cement manufacturing industry in 2006 being an estimated 45.8 Tg CO_{2eq} [3]. Thus, along with transportation and energy sectors, the construction industry is identified as one of the major contributors to greenhouse gas (GHG) emissions [4].

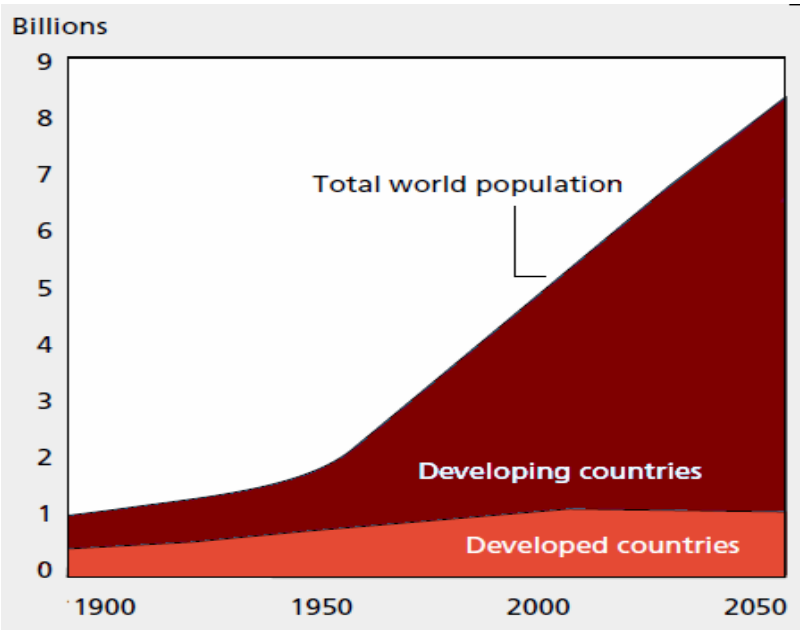

Figure 1.1. Worldwide population history and future trend [5]

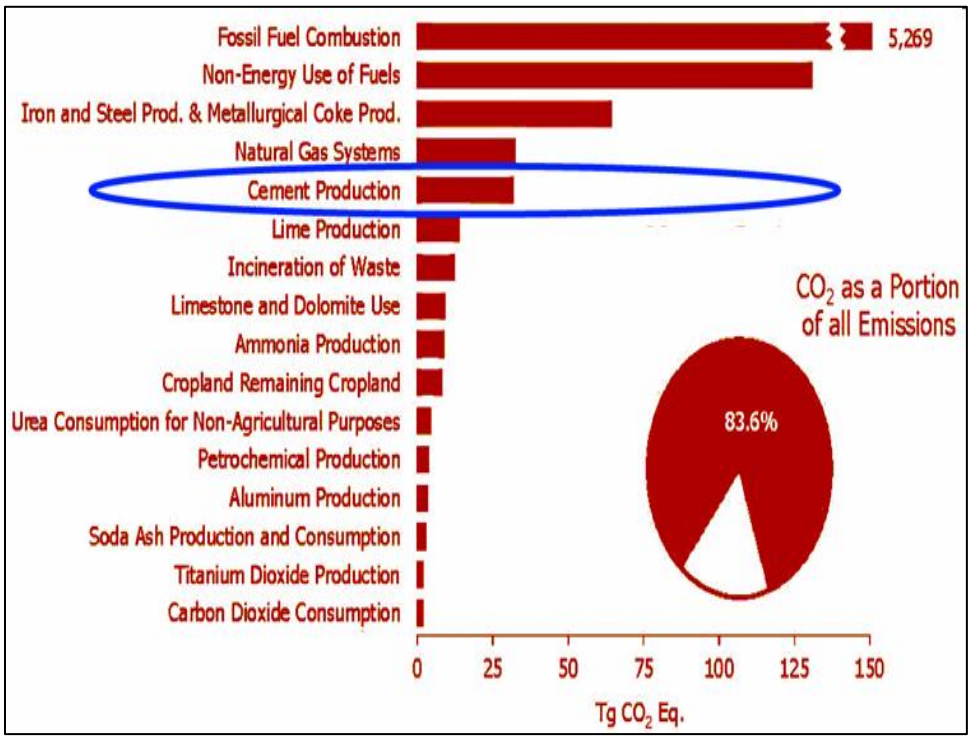

Figure 1.2. US Green House Gas (GHG) emissions inventory [3]

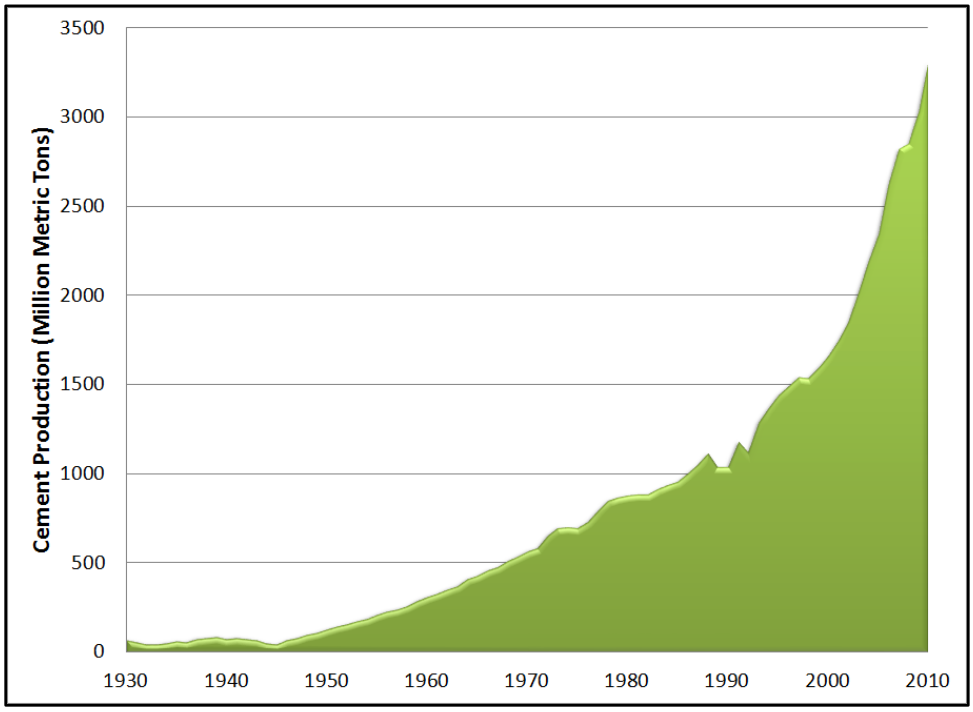

Figure 1.3. Worldwide cement production trend data from USGS [6]

Concrete is the largest volume-manufactured product on earth, other than processed water, with current estimates of global concrete production being approximately around 10 billion m^3 per year or 13.1 billion cubic yards in 2011 [7]. Globally, concrete production is expected to continue to increase due to massive infrastructure developments throughout the world and due to the increasing world population (Figure 1.1). For example 27.9 million m^3 of concrete was utilized for the Three-Gorges Dam project, the largest ever usage of concrete for a single project [8].

Cement is only one of the components used in concrete and the amount of cement in a concrete mixture can vary, typically ranging from 300 to 1000 lb/cu.yd for ordinary to high strength concrete [9]. Thus, high CO_2 emissions from the construction industry are in part due to the large demand for concrete. As shown in Figure 1.2 the cement industry is one of the two largest sources of carbon dioxide emissions among the manufacturing industry in the United States [3]. CO_2 emissions become more significant because of the increasing production of cement in the world, as shown in Figure 1.3, with production in 2012 being estimated at 3.70 gigatons [6]. Life Cycle Analysis (LCA) of cement manufacture, considering processes from transport of supplies (raw materials, fuels and electricity) to cement production, indicates that ~95% of the CO_2 emissions derives from the clinker production phase (burning of fuels in kiln and decarbonation) [10]. Thus, if the cement clinker fraction in concrete mixtures could be reduced, there is a high potential for decreasing CO_2 emissions into the atmosphere from the construction industry and hence achieve sustainability. Developments toward cement reduction, while retaining adequate concrete performance at both early ages and in long-term

performance, can make a tremendous impact, in terms of sustainable development because of the large – and growing – demand for concrete.

Because of this potential to positively affect sustainable development, it is an imperative that the construction industry continues to implement methods and techniques to decrease the total energy use and emissions from concrete construction. In the past, the cement industry has improved cement manufacturing processes to reduce energy use by changing from a wet to a dry kiln, recirculation of heated air for preheating raw materials as well as improved grinding by the use of grinding aids. But further reductions in energy use and emissions are required to achieve sustainability. Suggested pathways for effectively addressing high energy use and CO_2 emissions in cement and concrete production include:

1) reduction of energy use and CO_2 emissions during cement clinker production
2) reduction of cement content used in the concrete industry by the addition of fillers
3) enhancing strength and thus decreasing quantity of concrete used
4) reduction of cement use by increasing the lifespan of existing and new structures [11].

In addition, additional positive contributions to sustainability could be achieved through the introduction of new capabilities or functions to concrete, which positively impact the environment (e.g., photocatalysis).

As a part of this research, the pathway of decreasing the cement content in concrete by the partial substitution of cement using nano and microsized[1] [12] fillers were studied, and the properties of the resulting materials in the presence of these fillers were investigated. In this way, it is ensured that progress toward mitigating the environmental impacts of cement do not compromise performance, including early age properties, mechanical behavior, and durability.

In combination with portland cement in pastes, mortars, or concretes, fillers may modify the early age as well as long-term properties of cementitious materials. Reactive fillers which include all supplementary cementitious materials (SCMs) (e.g., fly ash, silica fume, slag, metakaolin) react with the cement hydration products in the presence of lime and water to form supplementary calcium silicate hydrates (C-S-H), increasing the strength and durability of concrete relative to ordinary concrete [13-15]. The use of SCMs has been generally well-examined. The effects of inert fillers in cementitious materials are, in comparison, not nearly as well-explored or understood. (The term "fillers" will be used to denote finely divided materials which are chemically inert or practically so in combination with portland cement and water.) To gain fundamental understanding on the effect of particle size and dosage of fillers on cement-based materials, in particular, research is needed. Here, the effect of fillers on early and long-term properties of cement-based materials will be assessed with particular emphasis on

[1] In the context of this research nanoparticles are defined as any material that has a size in the order of nanometers (less than 100 nm) and microparticles are defined as any particles with size range larger than a nanoparticle and in the order of micrometers.

the variations in behavior with particle size, from the nano to microscale, and dosage rates.

Prior research has showed that fine fillers affect cement hydration [16], particle packing and permeability of the cementitious systems [17], as further discussed in Chapter 3. The inclusion of fillers to cement could also induce additional benefits to the concrete or mortar mix. For example, the addition of titanium dioxide filler to cement can introduce photocatalytic properties to cementitious materials [18] and addition of limestone can increase the workability of the cementitious mixture [19].

Titanium dioxide and limestone nano and microparticles used as filler in cement and concrete mixes are the focus of this research. Nano and microparticles of these fillers were selected because of the increasing interest in the use of these fillers by the cement and concrete industry, as explained in the following two sections.

1.2 Fillers in Cement

Research on the effect of filler addition to cement has generally focused on fillers with particle sizes comparable to cement grains. For example, when limestone powders (of surface area 0.952 m^2/g) were added to cement up to 15% addition rates, the 7-day strength was 22% and 10% higher than the control mix for 5% and 10% limestone addition and the 28-day strength decreased only marginally [20]. Other researchers have noted that the compressive strength increased as the particle size of the filler decreased. But compared to the reference control mix, the strengths of the cement-filler mix at different ages were found to be higher or lower based on the percentage addition of filler as well as the fineness of filler [21]. When fillers with particle size distribution

comparable to cement were added, researchers have also observed an increase in the degree of hydration [22] as well as chemical shrinkage in the first 24 hours of hydration [23], but the influence of finer inert particles has not been well-examined previously.

For guidance, examination of the use of nano and microscale silica particles in concrete may be helpful. (Although such materials are not inert and are typically pozzolans, lessons learned in this area bear some relevance to inert particles, particularly when considering the relative effects of nano and microparticles.) Use of silica fume in cement-based materials, with sizes in the tens to hundreds of nanometer, affects particle packing and size distribution and with time by its pozzolanic reaction further densifies the microstructure; as a result, the structure and properties of the cement-based material are altered by the introduction of these particles which are much finer than cement [12, 24]. Even smaller nano-SiO_2 particles have been shown to enhance strength and interfacial transition zone properties greater than ordinary silica fume [25], suggesting the potential benefits in decreasing reactive particle sizes below the upper range of nanoscale. However, in part because of this accelerated early hydration and also because of alteration of the pore size distribution in the cementitious system, these reactive particles have also been found to increase shrinkage. For example, researchers have observed that the use of nano-SiO_2 increased 7 day shrinkage by 80% compared to an equivalent mix with micro-silica [26]. Thus, this examination suggests that nano and microparticles of the same composition can have different effects on structure and behavior in cement-based systems because as the particle size decreases from micro to nanoscale the surface area increases considerably.

1.2.1 Nanoparticles and TiO_2 in Cement

While titanium dioxide (TiO_2) is usually present in cement clinker in trace quantities as an impurity from the raw materials used for cement manufacturing, more recently titania is introduced intentionally to ground clinker to impart new functionality through surface-initiated photocatalysis. This results from the discovery of the photocatalytic properties of certain forms of TiO_2 by Fujishima and Honda [27] which has increased the potential application of TiO_2 in cementitious systems [28]. The chain of photochemical surface reactions induced by irradiation of TiO_2 with UV light (hυ), in the presence of water and oxygen is summarized in Equation 1.1 (adapted from Banerjee et al., 2006 [29]). The reactive oxygen species (i.e., $^{\bullet}O_2^-$, H_2O_2) and hydroxyl radicals ($^{\bullet}OH$) are strong oxidizing agents and cause various photocatalytic reactions (Equation 1.1).

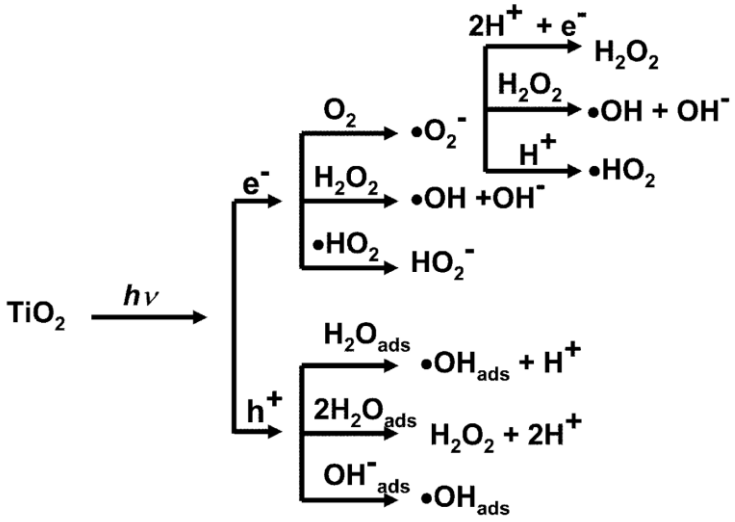

(1.1)

The introduction of nanocrystalline titanium dioxide, particularly in the anatase form, can convert ordinary construction materials, including concrete, to a photochemically active surface. The photocatalytic activity of TiO_2 in construction materials and coatings are being used for smog abatement, biocidal properties super-

hydrophobic/philic and self-cleaning ability [30-34] (Figure 1.4). The initial applications of TiO_2 in civil engineering materials were for self-cleaning ability using which outer walls and facades could be maintained stain free [28]. The application of TiO_2 for decreasing NOx ($NO+NO_2$) [35, 36] and volatile organic compounds (VOC's) has a gained a greater attention of the civil engineering community because of potential benefits with decreasing pollution. Several research projects [31, 37, 38] as well as pilot field application projects [39, 40] were undertaken to further understand the potential applications and effect of various factor on photocatalytic properties.

Research has shown that photocatalytic activity is superior in nanoscale TiO_2 due to the high surface area of the nanosized crystals [18, 41] and thus more nanosized TiO_2 is being used for its photocatalytic properties. This relatively new technology and particle additions are being implemented in various construction materials including ceramic tiles and glass panels (TOTO Hydrotect), aluminum panels (Alcoa's Reynobond® with EcoClean™), stucco tiles (Solar Stucco™, Amcot Stucco™), concrete paving stones [42] and coatings for stone, cement and concrete (StoCoat Lotusan®), and also special cements with TiO_2 additions (TX Active® by Essroc, Italcementi Group). In this research the effects of bulk additions of TiO_2 nanoparticles, at varying dosage rates, to cement paste on the properties of the cement-based material is investigated.

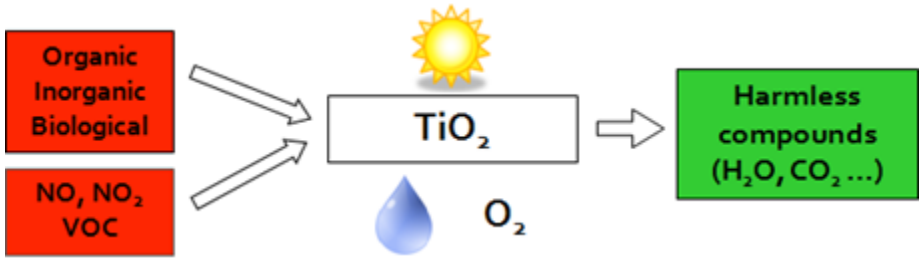

Figure 1.4. Schematic of photocatalytic reaction in the presence of TiO_2

1.2.2 Microparticles and Limestone in Cement

Ground limestone, with typical particle sizes comparable to cement, has long been used in the construction industry to improve the water retention capacity and workability of mortar, where it is a component in masonry cements, and concrete, where it has traditionally been used as a replacement for a portion of the fine aggregate. Researchers have observed that the use of limestone, either as a replacement for cement or sand, increases the flowability and consistency of mortar [43], one of the primary reasons for the use of limestone powder in self-compacting concrete mixes [19]. Limestone additions improves concrete consistency by reducing water demand, and if a low water-to-cement (w/c) concrete mix design is used, high limestone replacement levels can result in almost similar concrete performance as ordinary portland cements mixes [44].

Table 1.1. Maximum prescriptive limits on limestone addition to cement-based materials

Standard	Maximum limestone addition	Comments
ASTM [45]	15%	ASTM has approved 15% limestone in 2013
CSA [46]	15%	CSA has approved 15% in 2009 [47]
CEN [48]	35%	For CEM II/B-L "portland limestone cement"

More recently, the use of ground limestone as a component in portland cement or as blended-hydraulic cement has been permitted by various standards organizations. The prescriptive limits on the maximum percentage addition of limestone to cement vary according to the industry standard and country. As shown in Table 1.1, the maximum prescriptive limits on the addition of limestone vary between 15% to 35% [45, 46, 48, 49]

based on the standard. ASTM C150 *Standard Specification for Portland Cement* [50] specifies only a maximum of 5% limestone in portland cement but ASTM C595 *Standard Specification for Blended Hydraulic Cements* [45] allows up to 15% limestone in blended hydraulic cements.

Limestone could be introduced to cement in two ways: before grinding of clinker or as an additive or replacement to cement, intermixed after cement grinding or during batching of concrete. When limestone microparticles are added to cement clinker before grinding, cement manufacturers also typically grind the limestone blended cement to a finer size to increase the rate of hydration and strength gain [9], especially at early stages of hydration. But the limestone can get crushed to a very fine powder during grinding of clinker, since limestone is soft compared to cement [49]. In this research the effect of addition of limestone microparticles as a bulk additive to cement is investigated to study the effect of limestone particles on the short as well as long-term properties of cementitious systems.

1.3 Research Motivation

The use of inert fillers has been proven to be an effective pathway to reduce the clinker content in cement and concrete and the addition of fine fillers could greatly affect the properties of cement and concrete when compared to coarser filler additives. Hence, comparison of nano and microsized fillers is relevant for understanding the influence of filler particle size on cement hydration, early shrinkage, strength evolution and durability and these properties could be optimized based on the particle size of filler. Thus, as previously stated, one of the main motivations for conducting this research is to improve understanding of the influence of nanoparticles and microparticles on the short-term and long-term properties of portland cement-based materials.

In addition to the short and long-term properties, life cycle costs of these material systems should also be investigated. The total embodied energy and carbon emissions of filler-cement system should be compared to the plain cement system and a life cycle assessment should be conducted to ensure that all critical environmental factors are considered for the selection of a sustainable construction material, particularly because environmental concerns have spurred the use of both TiO_2 and limestone. Since TiO_2 and limestone are relatively new additives to cement, a life cycle assessment of TiO_2-cement and limestone-cement system are conducted as a part of this research and compared to results from plain cement mixes. The results from a life cycle cost analysis in terms of energy and emissions of these various cement-filler systems is critical to understanding the true contribution of these materials to sustainability.

1.4 Purpose and Objective

The main objective of this research is to understand the effect of the replacement of cement with fine fillers - commercially available micro and nanoparticles of TiO_2 and limestone - on the properties of the filler-cement systems. The early age and long-term properties, photocatalytic properties and the life cycle costs of these filler-cement systems are investigated as a part of this research.

The objectives can be classified into the following four main categories.

1. To understand the effect of nano and microparticles of two inert fillers - TiO_2 and limestone - on the early age properties of cementitious materials: Tests including isothermal calorimetry, chemical shrinkage, autogenous shrinkage, flow characteristics, setting time, degree of hydration and activation energy (temperature sensitivity) are conducted. The microstructure of the filler-cement systems is also studied using electron microscopy.
2. To understand the effect on long-term properties of cementitious materials due to the addition of nano and microparticles of TiO_2 and limestone: Strength tests and tests for permeability and pore structure including specific surface area and pore size analysis, chloride permeability and resistivity tests are conducted to characterize the effect of these particles on the structure developed in these binder systems.
3. To evaluate the effects of TiO_2 particles on induced photocatalytic properties of cement-based materials: Applicability of current NO_X tests for testing cement-

based materials are evaluated and NO_X conversion efficiency of cementitious materials with commercially available TiO_2 are characterized and compared.

4. To understand the effect clinker reductions with the use of nano and microsized fillers on sustainability in terms of embodied energy and carbon dioxide emissions: A life cycle analysis (LCA) of the filler-cement systems is conducted to identify the change in sustainability indices due to the fine particle use.

1.5 Organization of Dissertation

The structure of this dissertation is outlined below

- Chapter 2 presents the literature review on the properties of cementitious materials in the presence of nano and micro fillers including early age properties as well as long term properties. The literature review also includes background on activation energy, photocatalytic properties in the presence of TiO_2 and sustainability in the presence of TiO_2 and limestone fillers.
- Chapter 3 presents the effect of fine inert fillers on the early age hydration of cementitious materials. Results from setting time, flow characteristics, isothermal calorimetry, chemical and autogeneous shrinkage, activation energy and microscopy are presented.
- Chapter 4 outlines the long term properties of cementitious materials in the presence of nano and micro fillers. Results from specific surface area and pore size distribution, strength tests, chloride permeability and resistivity tests are presented and discussed.
- Chapter 5 presents the results from photocatalytic properties of TiO_2-cement systems. Testing procedure and results from NO_X tests is discussed and a new efficiency factor for photocatalytic conversion is defined and discussed.
- Chapter 6 presents the results and discussion about the sustainability of cementitious materials in the presence of TiO_2 and limestone. The life cycle analysis and pathways for use of nano and micro fillers is discussed in this chapter.

- Chapter 7 presents a summary of the research performed as a part of this dissertation and the primary conclusions. Further research topics are recommended based on the results from this research.
- Appendices include additional results not provided in the body of the dissertation - the effect of particle dispersion on hydration reaction and life cycle inventory data for plain cement and filler-cement mixtures.

CHAPTER 2

LITERATURE REVIEW

2.1 Properties of Cementitious Materials in Presence of Inert Fillers

The modification of portland cement, especially using fillers, remains of interest to researchers and to industry because of potential opportunities to tailor behavior (e.g. setting time, shrinkage, strength development, durability) and to also contribute to sustainability. As will be explained in this chapter, most of the prior research on the effect of fillers on hydration examined larger micrometer-sized particles [20, 51] and emphasized on strength development characteristics [52]. Therefore, the anticipated contributions of this research include fundamental understanding of the effect of dosage, particle size and type of inert additive on the early and long-term properties and life cycle costs of cement-based materials.

The effect of inert fillers on the properties of cement-based materials depends predominantly on the particle size and distribution of the fillers used. When a filler of a median size smaller than the size of cement is used, the rate of cement hydration could increase due to nucleation effect [22, 53] and the particle size distribution, and thus, the particle packing of the cementitious materials could also be modified. When fillers of size comparable to or larger than size of cement particles are used there could be a decrease in the rate of cement hydration [51]. The addition of fillers could result in a decrease in total hydration product formation and hence an increase in porosity due to this “dilution effect”. Thus, depending on the particle size of the filler used, there is a possibility of an increase or decrease in the rate of reaction and the total hydration product formed or a

modification of the porosity and structure of the hydrated cementitious material. The effect of the particle size of filler on the structure, and hence properties of cement-based materials, is further explored in the following sections.

It should be noted that some researchers have noted marginal reactivity of limestone powder with cementitious minerals [22, 54]. However, in the current research the reactivity of limestone powder is considered negligible as compared to the reactivity of fine pozzolanic fillers such as microsilica and henceforth in this manuscript both limestone particles as well as TiO_2 particles will be categorized as 'inert' or 'fillers'.

2.2 Early Age Properties in Presence of Inert Fillers

The progress of the hydration reaction, shrinkage characteristics as well as the evolution of the microstructure should be researched to fully understand the fundamental effect of micro- or nanoparticles on the formation of hydration product, especially at early age. When fillers with particle size distributions comparable to cement were included in the mix, researchers have observed an increase in the degree of hydration [22] as well as an increase in chemical shrinkage in the first 24 hours of hydration [23]. (The degree of hydration (α) of a cement-based material is the fraction of the cementitious materials that has undergone hydration at any particular time [9].

Chemical shrinkage, also called *Le Chatelier contraction*, is the relative volume reduction between the initial reactants (cement and water) and final hydration products in a closed environment. In a contribution fundamental to the field, Powers suggested using the degree of hydration at any stage of hydration reaction and the water-to-cement or water-to-solid ratio to obtain the chemical shrinkage as well as solids (unhydrated and

hydrated) and water (capillary and gel-water) according to the following equations [47, 55, 56].

$$
\begin{aligned}
&\text{Chemical shrinkage:} && V_{cs} = 0.20(1 - p)\,\alpha\,(1 - V_F) \\
&\text{Capillary water:} && V_{cw} = (p - 1.32(1 - p)\,\alpha)\,(1 - V_F) \\
&\text{Gel water:} && V_{gw} = 0.60(1 - p)\,\alpha\,(1 - V_F) \\
&\text{Gel solids:} && V_{gs} = 1.52(1 - p)\,\alpha\,(1 - V_F) \\
&\text{Unhydrated Cement:} && V_c = (1 - p)(1 - \alpha)\,(1 - V_F) \\
&\text{Volume balance:} && V_c + V_{gs} + V_{gw} + V_{cw} + V_{cs} = 1 - V_F
\end{aligned}
\tag{2.1}
$$

where $p = (w/c)/(w/c + \rho_w/\rho_c)$ is the initial volume fraction of water in the mixture, w/c is the effective water-to-cements ratio, ρ_w and ρ_c refer to the densities of water and cement and V_F is the volume fraction of filler in the blended paste. Gel water is the water held within large surface area of the hydration product (gel solids) and is located between the gel solids in the C-S-H interlayer space (gel pores). Capillary pore is the space not taken up by the cement and hydration product and generally is considered to be pores of size greater than 2.5nm. The water held in the capillary pores is called capillary water. Cement hydration in the presence of fillers could be modeled based on the Powers' equations and compared to experimental results to ascertain the validity of Powers model in the presence of inert fillers.

The presence of fillers can affect other shrinkage characteristics of cementitious mixtures, including autogeneous shrinkage [57] and possibly plastic shrinkage. Autogenous shrinkage is the macroscopic reduction in volume of cementitious mixtures

during hydration. Autogenous shrinkage occurs in cementitious mixtures with low (<0.4) w/c hydrating under sealed conditions [58]. Such low w/c mixtures can self-desiccate due to insufficient water for complete hydration and can create empty pores within the hydrating paste microstructure which can result in cracking [59]. Plastic shrinkage is the volumetric contraction of cement paste due to the loss of water by evaporation or by absorption of water by the substrate or aggregate. Plastic shrinkage is not considered in this research, since plastic shrinkage depends on by rate of water loss to the environment and thus can be controlled externally [9]. Most of the previous research on the effect of fillers on autogenous shrinkage was conducted using reactive fillers, where it was observed that fillers could increase or decrease autogeneous shrinkage based on the type and dosage of filler used [57, 60].

As mentioned earlier, when fillers of various particle size distributions were included in the cementitious mixture, researchers have observed both acceleration and deceleration of cement hydration and a change in shrinkage as well as the porosity and structure of the hydration product. However, little prior effort has examined the influence of a range of sizes of inert particles; variations in cement composition among studies preclude their comparison. Thus the effect of particle size of fillers in the micro and nanoparticle range on hydration rate, chemical shrinkage and microstructure development is likely significant and warrants a comprehensive examination to better understand the role of filler size on early age behavior.

Overall, the partial substitution of cement grains with inert nanoparticles and microparticles may modify the cement hydration kinetics and alter the development of microstructure in comparison to ordinary pates due to three different mechanisms (Figure 2.1) listed below:

- dilution effects,
- heterogeneous nucleation, or
- change in particle size distribution/system porosity [61].

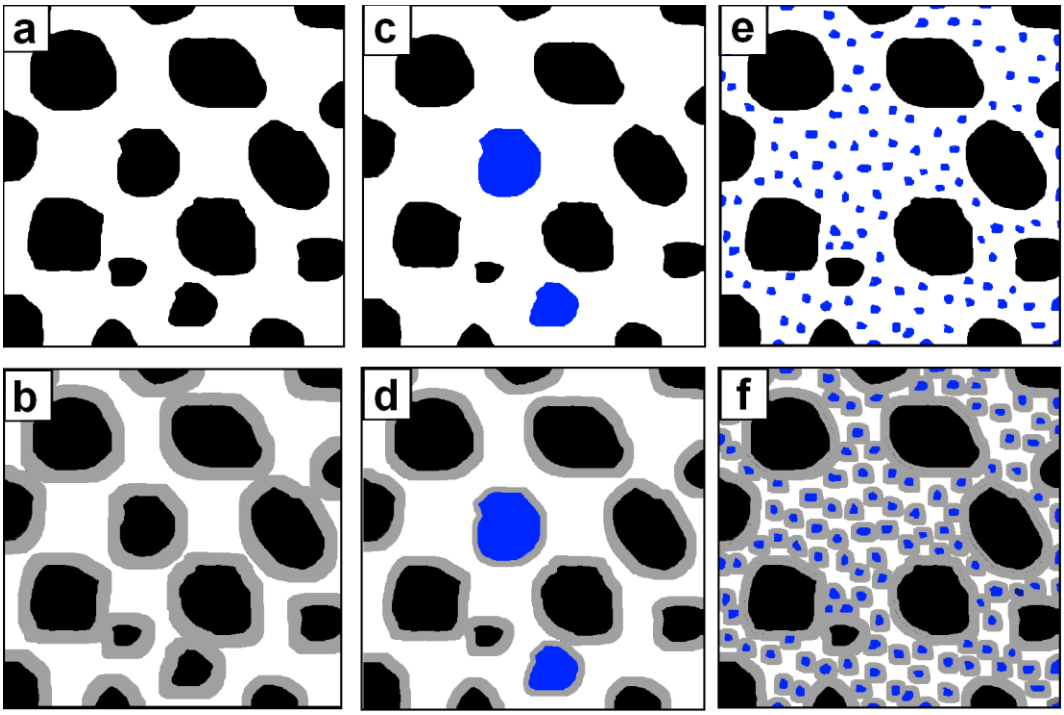

Figure 2.1. Schematic representation of cement hydration: a) Plain cement before hydration, b) Plain cement after hydration, c) Cement with microparticle filler – before hydration, d) Cement with microparticle filler – after hydration (dilution effect), e) Cement with nanoparticle filler – before hydration (change in particle size and porosity), and f) Cement with nanoparticle filler – after hydration (heterogeneous nucleation and changes in particle size and porosity)

When a dilution effect is dominant in the case where inert particles of size similar to or greater than cement grains replaces cement and the particles can be envisioned as

substituting for reactive cement grains, as shown in Figure 2.1c. In this case, the rate of the reaction of the entire mixture will be reduced because of the decrease in the total available cement for hydration reaction, as well as by the resulting increased distance between reacting cement particles. As a result the effective w/c increases and the pore solution become less concentrated and hence results in less hydration product formation for a given age [61] as shown in Figure 2.1d. Chemical and autogeneous shrinkage in cement mixes depend on the degree of hydration. Since the rate of cement hydration decreases when dilution effect is dominant, the chemical and autogeneous shrinkage could also decrease in this scenario.

Heterogeneous nucleation is typically the dominant mechanism when well-dispersed particles of size similar to or less than cement grains are used as a partial substitution for cement (Figure 2.1e) and the hydration reactions are accelerated (Figure 2.1f). Heterogeneous nucleation is a physical process that results in activation of hydration reaction and formation of products on foreign solid surfaces [21]. In the case where fillers are included, the additional surface area provided is believed to increase rate of reaction by decreasing the energy barrier required for the hydration reaction to proceed [62]. The effectiveness of this catalysis depends on the fineness and dosage of the filler [53]; it is understood that finer fillers generally produce greater nucleation effects. Chemical and autogeneous shrinkage could increase when heterogeneous nucleation effect is dominant, since in these cases the rate of cement hydration increases due to surface nucleation of hydration products [23].

Modification of particle size distribution is envisioned to occur with the substitution of chemically inert filler results in a change of the particle size distribution

and hence particle packing in a system. This effect is also dominant when well-dispersed particles of size similar to or less than cement grains replaces cement particles (Figure 2.1e). In addition to altering the initial porosity, the subsequently formed microstructure [17] will vary from an ordinary cement system.

But, while much research has examined the influence of variations in cement particle size and size distribution, this effect of the particle size and size distribution of an inert filler on cement hydration is not well documented in literature. The possible refinement of pore size distribution when nano and microparticles replaces cement grains could increase the capillary tension and therefore the shrinkage could also increase in such scenarios [57]. In addition, other phenomena may occur, including water absorption and/or adsorption by the nanoparticles, interactions with nanoparticle surface treatments, and reaction of materials previously presumed to be inert [63]. Thus, a comprehensive research program is necessary to better understand these complex relationships between particle size of fillers and cement hydration reaction.

2.2.1 Temperature Sensitivity and Activation Energy in Presence of Inert Fillers

The temperature sensitivity of cement hydration reaction is of importance to understand the effect of variation in temperature on the development of properties of cementitious materials [64]. The temperature sensitivity of cementitious mixtures can be evaluated by estimating the apparent activation energy of cement mixtures [65, 66]. The apparent activation energy can also be used in maturity models for estimating the strength development of cementitious mixtures at different ages [67]. The presence of

nanoparticles could affect the temperature sensitivity of cement mixes and this variability can be used to optimize setting and hydration behavior of cement mixes.

The activation energy of cementitious materials can be calculated using various techniques to quantify the effect of additives on cement hydration reaction. Arrhenius equation, defined in Equation 2.2, is used to calculate the activation energy of materials. Arrhenius theory denotes the relationship between the rate of a chemical reaction, activation energy and temperature. According to the classical definition, activation energy for a single reaction system represents the potential energy necessary for the initiation of a chemical reaction. But this definition is not directly applicable to chemical reactions with multiple reactants minerals or where the reaction mechanism and/or products change as the reaction progresses. The activation energy, if calculated for such systems, does not represent the activation energy of separate minerals or their reactions, but rather for a combination of the activation energies of these minerals and reactions [68].

$$k = Ae^{-(E_a/RT)}$$
$$\ln(k) = \ln(A) - E_a / RT \tag{2.2}$$

where k = rate of reaction, A = proportionality constant, Ea = activation energy, R = universal gas constant (8.314 J/mol/K) and T = temperature in Kelvin.

The reaction of cementitious materials with water is an example of a reaction where multiple minerals react simultaneously and the reaction mechanism and products change with time [67]. Thus the activation energy concept is not directly applicable to

cementitious systems. But “apparent” activation energy, an empirically derived value, can be used to represent the combined temperature sensitivity of all the chemical reactions during cement hydration [64]. Henceforth in this research article, the usage of the term activation energy should be considered equivalent to “apparent” activation energy.

Previous researchers have, in fact, applied Arrhenius theory to determine activation energy (and hence temperature sensitivity) of various cement material properties including compressive strength and maturity functions [69], time to end of induction period during hydration [70], time to peak rate of heat evolution during hydration [71], and also to calculate the “apparent” activation energy of the cement hydration reaction for comparison between cementitious mixes [64, 72]. The most common use of the Arrhenius theory on cementitious materials has been to obtain the “apparent” activation energy and for use in maturity functions. The apparent activation energy of cement hydration reaction itself has been calculated using various cement properties including data obtained from isothermal calorimetry [64, 72, 73], free lime measurements [74] and free water index obtained using quasi-elastic neutron scattering [75].

The values of instantaneous activation energies calculated during cement hydration vary as cement hydrates [67]. Cement hydration is initiated as predominantly a surface controlled reaction and slowly changes to a diffusion controlled reaction during later stages of hydration [76]. The transition between surface controlled reaction and diffusion controlled reaction is not clearly discernible and could also vary depending on the temperature and type of cement mix [76]. Researchers have also noted that the

activation energy of surface controlled reactions and diffusion controlled processes are different [68, 72], with diffusion controlled reactions exhibiting lower activation energies. Hence the calculation of activation energy based on the classical Arrhenius equation assuming constant activation energy over the entire hydration curve could be erroneous. The apparent activation energy of cement hydration reaction has been shown to be constant when degree of hydration (α) of cement is less than 0.50 (or 50%), when the reaction is predominantly surface controlled [67]. Thus, in this research it was ensured that the data used for calculating reaction rate and activation energy was limited to a degree of hydration of less than 0.50.

The apparent activation energy calculated for a hydraulic cement or cementitious system (e.g., combinations of cement, supplementary cementitious materials, SCMs, and/or inert fillers) is as a useful tool for understanding the effect of temperature on the hydration of cementitious materials [77]. A higher activation energy for chemical reactions will result in a greater variation of reaction rate with temperature change and hence a "higher sensitivity to temperature". Such understanding is important for appreciating the influence of field temperatures on hydration rates and thus development of microstructure, time to set, and rate of strength development, among other features.

The apparent activation energy of cementitious systems can be affected by various factors related to the chemical and physical properties of the materials used and the mixture proportions. For example, an increase in the water-to-cement ratio has been found to decrease the activation energy [77]. The effect of chemical admixtures on activation energy varied among different researchers. Some researchers found that the inclusion of superplasticizers had minimal impact on the activation energy [78], whereas

others observed that the addition of superplasticizer decreased activation energy [77]. The addition of a water reducing retarder as well as an accelerator was found to decrease the activation energy of cementitious mixtures [77].

With regard to variations in the composition of the cementitious system, previous researchers have noticed that the substitution of cement with ASTM C618 Class F fly ash and silica fume decreases the activation energy [77], while slag increases the activation energy [79]. The higher activation energy in the presence of slag has been attributed to a hydration mechanism that is less dependent on diffusion [79]. Some researchers have noted that the percentage of tricalcium aluminate (C_3A) and alkali content of cement could have an influence on the change of activation energy when ASTM C618 Class C fly ash and slag is added to cement.

Most of the previous research has thus focused on the effect of supplementary cementitious materials and chemical admixtures on the activation energy of cements. But recent interest and research in the use of inert (or largely chemically inert) nano- to micro-sized particles in cementitious has indicated that these particles modify cement hydration kinetics at early ages [12, 80]. Such nanoparticles modify hydration process by increasing the reaction rate due to heterogeneous nucleation on the surface of nanoparticles [53]. Hence the activation energy of cementitious mixtures could also be affected by the presence of nanoparticles. But the effect of nanoparticles on the activation energy of hydration reaction has not been previously quantified. Thus, the current research also examines the effect of nanosized mineral fillers on the activation energy of cementitious systems.

2.2.2 Model for Quantification of Cement Hydration Data and Calculating Activation Energy

Hydration of cementitious materials can be studied by quantifying the cement that has undergone hydration reaction. Degree of hydration of cement, α, is a measure of the proportion of cement that has undergone hydration and is used to track progress of hydration. Degree of hydration is defined as the ratio of the hydrated cement to the original quantity of cementitious material. The degree of hydration varies between 0 and 1, where α=0 denotes no hydration which is the state before water is added to the cement and α=1 denotes a state of complete hydration of the entire quantity of cement. In reality, not all of the cement might hydrate and hence a degree of hydration equal to 1 might never be achieved in typical cements [9]. The degree of hydration could be measured directly by chemically quantifying the amount of reacted and unreacted cement, for example by using thermal analysis [81]. But in this research the degree of hydration was determined indirectly utilizing the heat development data of cement paste mixtures obtained using calorimetry, following the approach in [65]. Previous researchers have shown that the heat released at any time divided by the total heat of hydration provides an appropriate measure of degree of hydration. Thus the equation for degree of hydration (α(t)) at any time t, for mixes without supplementary cementitious, is given in Equation 2.3.

$$\alpha(t) = H(t) \cdot H_{cem} \tag{2.3}$$

where H(t) = cumulative heat evolved by the cement mixture from start of hydration till time t (J/g) and H_{cem} = total heat of hydration of the cement mixture (J/g).

Previous research has shown that the total heat of hydration of cement (at the theoretical 100% hydration) can be calculated from the proportion of the phases present in the cement based on Bogue potential calculations. The equation used to calculate the total heat of hydration of the cement used in this research is: [65].

$$H_{cem} = 500p_{C3S} + 260p_{C2S} + 866p_{C3A} + 420\,p_{C4AF} + 624p_{SO3} + 1186p_{FreeCaO} + 850p_{MgO} \quad (2.4)$$

where H_{cem} = total heat of hydration (J/g) of cement at complete hydration (at $\alpha = 1$) and each p_i term is the mass fraction of that cement mineral phase in the cement. The total nominal heat of hydration of the cement (H_{cem}) used in this research was calculated to be 462.78 J/g, which was constant for all the mixtures, since inert fillers do not contribute to the total heat evolved in cement.

Once the variation (with time) of degree of hydration is calculated using Equation 2.3, the cement hydration data can be mathematically represented using various models. Researchers have suggested a three parameter exponential model to characterize the degree of hydration data [82, 83] and the equation that defines the model is:

$$\alpha(t) = \alpha_u \cdot e^{-(\tau/t)^{\beta}} \quad (2.5)$$

where α_u is the maximum degree of hydration, τ is the hydration time parameter and β is the hydration shape parameter.

The parameters of the model α_u, τ and β can be used as representative parameters for the hydration development of cement mixtures and their values can be used to gain valuable information about cementitious mixes. If two of the three parameters are kept

constant the variation of the third parameter would result in the following trends. An increase (or decrease) in value of α_u indicates a possible greater (or lower) maximum degree of hydration in a cement mix. Although α_u represents the maximum degree of hydration, some researchers have obtained values of α_u greater than 1.0 [73], which is theoretically not possible according to the definition of degree of hydration. Thus α_u should only be considered as a representation of the maximum degree of hydration and as a tool for comparison between different mixes. Relative decrease (or increase) in the hydration time parameter(τ) indicates an acceleration (or deceleration) in the reaction and also lower (or greater) time to reach peak reaction rate and possibly setting time. β represents the slope of the degree of hydration graph, with higher values indicating greater slope. A decrease (or increase) of the hydration shape parameter (β) would indicate a greater (or lower) degree of hydration of the cementitious mix during initial stages of reaction and a lower (or greater) degree of hydration during later stages [82-84]. But when comparing cementitious mixes of different compositions, the values of α_u, τ and β could all be different and thus the combination of the three parameters would result in a more complex representation and trends in the data.

Researchers have demonstrated that, the hydration time parameter (τ) obtained from the three parameter model fit of the hydration data [64] can be used to calculate apparent activation energy of cementitious mixtures. Here, the activation energy (E_a) of cement mixes was determined using the following equation.

$$E_a = \frac{-\ln\left(\frac{\tau_{ref}}{\tau_c}\right)}{\left(\frac{1}{T_{ref}} - \frac{1}{T_c}\right)} \cdot R \tag{2.6}$$

where τ_{ref} and T_{ref} are the hydration time parameter and concrete temperature (in K) at the reference temperature, τ_c and T_c are the hydration time parameter and concrete temperature at different temperatures at which isothermal calorimetry was conducted and R is the universal gas constant (8.314 J/mol/K). For the calculations in this research 25 °C was considered as the reference temperature.

2.3 Long-term Properties in Presence of Inert Fillers

Most of prior research conducted on the effect of fine fillers has focused on the mechanical properties of the cementitious system. When fillers such as limestone were included in cementitious mixture up to 15% replacement rates, the 7-day strength was higher than the control mix and the 28-day strength decreased only marginally [20]. Other researchers have noted that the compressive strength increased as the fineness of the filler increased. Compared to the reference control mix, the strengths of the cement-filler mix at different ages were found to be higher or lower based on the percentage addition of filler as well as the fineness of filler [21, 22].

Because of their potential to modify porosity, pore size distributions and permeability, it can be envisioned that the addition of nano- and micro-sized particles to cement can also affect long-term properties such as durability [9]. The initial pore size distribution and hence permeability of the system depends, at least in part, upon the fineness and amount of filler used in the mixture [61]. The w/c and the particle size distribution of the cement could also affect the properties of the hydration product. But these are beyond the scope of this project and research on the effect of various inert

particles of different particle sizes only would be investigated in this research. The long-term effect on permeability could depend both on the initial pore size distribution as well as the formation of hydration products on the surface of fillers, which could result in a well dispersed hydration product in the microstructure. Thus the relationships between the developed microstructure (e.g., pore size distribution, specific surface area) and parameters which relate to durability (e.g., permeability) warrants further examination.

Ensuring the durability of the material is also critical for the contribution of inert fillers to sustainability [85]. Water penetration, carrying with it aggressive ions, is central to most deterioration mechanisms affecting concrete. Generally in concrete in a hostile environment, low permeability of the concrete reduces the rate of deterioration and results in a longer service life, except for cases such as thaumasite formation which can occur even at low permeability. But thaumasite formation is not considered in this research. A study of chloride solution (3% NaCl by mass) absorption of concrete when replacing cement with limestone indicated that the chloride ion penetration was deeper at 45 days for mixtures with higher limestone contents [86].

Here, the influence between composition, structure and long-term performance, will be assessed through measurements of strength, specific surface area, pore size analysis and rapid chloride permeability test (RCPT according to ASTM C 1202) of pastes prepared with the same cement and varying dosage rates of the inert micro and nanoparticles. Mercury intrusion porosimetry (MIP) was not selected as one of the test methods in this project because of inherent errors in assumptions (e.g., “ink bottle” effect) made when MIP is applied to cement-based materials and other microporous materials and because MIP is not able to measure all pores sizes present in cement paste

[87]. RCPT test was selected such aggressive agents that permeate and diffuse through the concrete microstructure is considered, since the transport of ions depend on the size and chemistry of the molecule, atom or ion moving through the porous media.

Permeability and porosity has a strong inverse correlation with the strength of the cement-based materials, as observed by researchers [88]. Since cement hydration has a strong influence on the change of pore structure, the presence of fine fillers which nucleates the growth of C-S-H could increase degree of hydration and hence could affect the capillary pore volume and structure and have a significant effect on permeability.

Returning to the conceptual model presented in Figure 2.1, the addition of fine particles improves or densifies the pore structure by two main mechanisms [89]. First, the total pore volume is expected to decrease due to heterogeneous nucleation of hydrates on the surface of the fine filler particles and the concomitant acceleratory effect on cement reactions. In addition, the pore structure is refined by the addition of these finer materials, reducing the connectivity of the pores, and thus reduces the permeability and porosity. Based on model-based studies capillary porosity could become disconnected when the value of porosity is below a certain limit. This capillary porosity limit varies based degree of hydration, water-to-cement ratio and there is also significant variation on limit based on the model and ranges from 18% according to [90, 91] or around 30% according to [9]. The effect of size of inert fillers on the permeability and pore size distribution of cementitious materials is also examined as a part of this research.

2.4 Photocatalytic Properties

The photocatalytic activity of titanium dioxide (TiO_2) was discovered accidently when TiO_2 was found to be the cause of degradation on paints containing TiO_2. The interaction of TiO_2 with ultraviolet (UV) light in the presence of water and oxygen was called "Honda-Fujishima effect" and was first described in *Nature* [27]. Photocatalytic titanium dioxide (TiO_2) has been used in various applications predominantly because of the wide range of compounds that can be decomposed at room temperature using only solar energy and moisture [92]. Further research by various research groups has shown that the photocatalytic effect is superior in nanostructured TiO_2 especially in the anatase form compared to the rutile or brookite forms [93]. The major applications of photocatalysis by anatase TiO_2 include removal of organic and inorganic pollutants, photo-degradation of pathogenic organisms [94] and self-cleaning and anti-fogging applications [34]. The photocatalytic effect of TiO_2 has been used in various civil engineering applications including construction materials such as ceramic tiles, asphalt pavements and concrete paving blocks [32, 37]. The TiO_2 in these materials has been shown to oxidize organic and inorganic contaminants on the surface and also as an anti-microbial agent [94, 95].

In the last decade, research and application has increased on the ability of photocatalytic TiO_2 to decrease pollution in the form of NO_X (NO_2 + NO), VOC's and sulfur oxides [18, 35, 96]. The nitrogen oxides are highly reactive and major air pollutants especially in urban areas with high emission of these gases from automobiles. Moreover, NO_X, together with SO_2 and SO_3, produce acid rain, which can be harmful for vegetation (e.g., forests, crops) as well as aquatic life [97] and the built environment [98,

99]. The nitrogen oxides participate in the formation of "photochemical smog" and also in the formation of ozone [97], both of which are detrimental to human health [100]. Thus there has been an increased incorporation of TiO_2 on surfaces exposed to these pollutants in urban areas that include paving blocks and concrete surfaces [32, 40]. Although the complete reaction mechanism remains somewhat uncertain, the photocatalytic oxidation of NO_X broadly follows a set of chemical reactions as given below [101].

$$\begin{aligned} 2NO_2 + H_2O &\xrightarrow{h\nu,\quad TiO_2} HNO_2 + HNO_3 \\ 4NO + 3O_2 + 2H_2O &\xrightarrow{h\nu,\quad TiO_2} 4HNO_3 \end{aligned} \tag{2.7}$$

Most prior research conducted on the utility of TiO_2 for introducing photocatalytic properties to cement [31, 32, 102] for NO_X oxidation have followed the standards ISO 22197-1 2007 [103] or the equivalent JIS R 1701-1 [104] or the UNI 11247 standard [105]. Several researchers have used the JIS R 1701-1 [32, 106, 107] and ISO 22197-1 [31, 42, 102] tests for characterizing the photocatalytic activity of construction materials, whereas the UNI 11247 was introduced recently and thus has not been widely used [108]. Each of these tests were originally developed for studying the NO_X removal properties of relatively impervious "fine ceramic" materials [103-105] and surface coatings (e.g., on ceramics, metals), and, as a result their appropriateness for more porous, heterogeneous, and variable (including time- and environment-dependent variability) cement-based materials should be considered. The applicability of these

existing test methods for measuring the photocatalytic conversion of NO_X on the surface of cementitious materials is reviewed.

2.4.1 Review of Current Test Methods for Photocatalytic NO_X Conversion

Several organizations describe standard test procedures for examination of the air purification capabilities of fine ceramics and other inorganic materials [103-105]. These test methods have begun to be used for the examination of cement-based materials, as well.

Table 2.1. Comparison of testing, sample and analysis parameters of various tests for testing NO_X conversion performance of photocatalytic materials

		ISO 22197-1	**JIS R 1701-1**	**UNI 11247**
Testing parameters	Test gas	NO	NO	NO and NO_2
	Test gas concentration	1000ppb	1000ppb	400ppb NO + 150ppb NO_2
	Gas flow rate (l/min)	3	3	3
	Test duration (h)	5	5	1
	UV light intensity (W/m^2)	10	10	20
Sample parameters	Sample area (cm^2)	49.25	49.25	65
	Sample curing	–	–	–
	Surface preparation	–	–	–
Analysis parameters		η_{ads} (equation 5.3)	Q_{ads} (equation 5.3)	NO_X reduction percentage

The following is a brief review of the existing photocatalytic tests for construction materials, which are based on the flow of reactant gases over photocatalytic samples. Key features of these tests are summarized in Table 2.1. Other tests for photocatalytic activity which were followed by researchers and based on rhodamine [33, 38], atrazine [109], toluene [93] conversion and biological growth [30] on surface of the construction materials are not discussed here.

2.4.1.1 JIS R 1701-1

The standard JIS R 1701-1: "Fine ceramics (advanced ceramics, advanced technical ceramics) - Test method for air purification performance of photocatalytic materials - Part 1: Removal of nitric oxide" [104] was developed by the Japanese Standards Association in 2004. This can be considered as one of the earliest testing method for photocatalytic properties of construction materials, and one which specifically addresses ceramics (i.e. an inorganic non-metallic materials made from heating and subsequent cooling).

In the JIS test, a continuous flow of reactant gases (i.e., this is a "dynamic method") flows over test sample surfaces, and the reactant gas concentration is continuously measured using a chemiluminescent NO_X analyzer. The standard suggests the use of a test piece that measures 49.5mm±0.5mm wide and 99.5mm±0.. The reactant gases are allowed to pass over this flat, plate-like sample in a 5mm thick layer. A light source (300 to 400 nm wavelength) is used to irradiate the surface of the test sample with UV light to produce an irradiance of 10 W/m^2.

The JIS standard specifies using NO gas at 1.0 ppm by volume with 50% relative humidity at 25 °C ± 2.5 °C and at a flow rate of 3.0 L/min. The test samples are stabilized under flowing reactant gases before exposing them to UV light, which is also allowed to warm up before exposure of sample. Once the gases have stabilized at the specified concentration the samples are exposed to UV light and reactant gases for 5 hours. The samples are exposed to the reactant gases and the photocatalytic conversion is measured using an integral of the difference between the input and output concentration of the gas (Equation 5.3). Elution tests are also conducted to confirm the NO_X conversion efficiency of the test sample by measuring the nitrate and nitrite ion produced on the test sample.

2.4.1.2 ISO 22197-1

The standard ISO 22197-1: "Fine ceramics (advanced ceramics, advanced technical ceramics) — Test method for air-purification performance of semiconducting photocatalytic materials — Part 1: Removal of nitric oxide" [103], was developed in 2007 by ISO based on the JIS R 1701-1 standards which was developed earlier. The ISO 22197-1 standard follows the same procedures given in the JIS R 1701-1 standard.

2.4.1.3 UNI 11247

The standard UNI 11247: "Determination of the catalytic degradation of nitrous dioxides by photocatalytic inorganic materials" [105] was developed more recently, in 2008, by the Italian standards organization (UNI). This test is similar to the JIS R 1701-1 and ISO 22197-1 tests and is also a "dynamic" method with a continuous flow of NO_X gases. The concentration of gases is different from the previous tests and uses 0.55 ppm

of total NO_X gas which is a mixture of 0.15 ppm of NO_2 and 0.40 ppm of NO gas. The irradiance in doubled from the ISO and JIS tests to 20 W/m^2 and the samples are tested for 1 hour. The other parameters used are similar the ISO and JIS tests described above.

The use of a combination of NO and NO_2 in the UNI 11247 test could simulate real world conditions, but during photocatalysis there could be a conversion of NO to NO_2 and vice versa. These reactions and conversions cannot be studied accurately using the UNI 11247 test. Moreover, in the current research and in Maggos et. al., [36], it was observed that once cement-based samples are irradiated with UV and exposed to NO_X gases it could take a few hours for gases to stabilize. Thus, the relatively short duration of the UNI 11247 test could be unsuitable for certain construction materials.

2.4.1.4 Other NO_X tests

Among the other tests that have been used by researchers are a "static" tests [36] in which a constant volume of pollutant gas is maintained and recirculated as a closed circuit in the reaction chamber. The pollutant gas concentrations before and after the experiment are measured to calculate the photocatalytic efficiency of TiO_2 surfaces. It should be noted that this test is different from the previous tests which were "dynamic" and used a constant flow of pollutant gases over the photocatalytically active TiO_2 samples. The "static" tests do not represent real world conditions where pollutant gases would move over the TiO_2 surfaces because of air circulation (e.g., air circulation inside buildings or wind). Thus, the dynamic tests are more appropriate to use for measuring the photocatalytic efficiency of cementitious materials with TiO_2 additives.

2.5 Sustainability of TiO_2 and Limestone Cement Mixes

Sustainability has been defined as development that meets the needs of the present generation without compromising the ability of future generations to meet their own needs [110]. Sustainability is often examined in terms of environmental sustainability, societal sustainability and economic sustainability [111, 112]. In the context of this research, the term sustainability refers to the environmental sustainability of the material, product, project or the built system under consideration.

Sustainability of a material or process is assessed by conducting a Life Cycle Assessment (LCA) and calculating the total embodied energy and associated emissions (mainly CO_2) [112-114]. The total primary energy used and emissions generated to abstract, process and manufacture specific goods, services or process and eventual safe disposal of the waste materials to earth have to be considered in the LCA [115]. The embodied carbon dioxide can also be associated with the specific chemical reaction that occurs during the manufacture, which is especially true in the case of cement manufacture [116], where decomposition of limestone releases CO_2 into the atmosphere.

2.5.1 Sustainability Matrices and Life Cycle Analysis

Green building rating systems such as LEED™ (Leadership in Energy and Environmental Design), Green Globes™ or Energy Star certification are simple ways of assessing sustainability. These rating systems are mostly used for assessing the sustainability of an entire building rather than individual components or materials used for construction of the building [117]. Thus for accurate assessment of sustainability,

especially when a new material or composition is considered, it is necessary to conduct a Life Cycle Assessment (LCA) [112, 115].

A life cycle cost analysis is a powerful tool used to make economic and environmental sustainability decisions for selection of any construction material [118]. This analysis accounts for all impacts or "costs" involved over the product's lifecycle [115]. Typically the LCA of a building or material will include the extraction of materials and fuel used as energy for manufacture, transportation of materials, construction, operation including maintenance and repair and demolition, disposal, recycling or reuse of the material at the end of its functional life [4, 117, 119]. Often buildings with a lower first cost for new construction might require higher costs during the entire life cycle [114]. Conversely, durable materials and materials that can offset the "costs" by other means can have a lower life cycle cost [120].

The four major phases of a Life Cycle Analysis are given in Figure 2.2 given below [121].

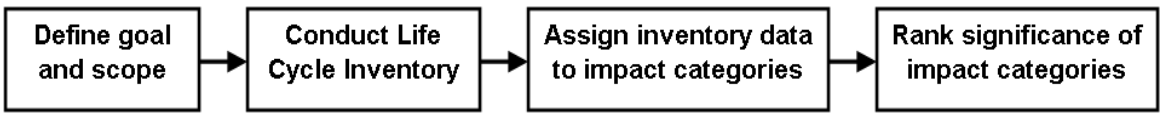

Figure 2.2. The four phases in the process of developing an LCA

One of the first steps of an LCA is to define the scope and boundary of the LCA analysis. A common approach is to consider all the flows related to the system (cradle-to-gate approach). But often in practice, the most significant processes can be analyzed or if

two products are being compared, the processes where the two products differ from each other can also be compared [122]. The latter approach will be followed in this research, where the processes that distinguish the cement systems with and without TiO_2 and limestone additives will be compared.

The second stage of an LCA is the Life Cycle Inventory (LCI) analysis, which accounts for all individual material, energy and emissions inventory and flows to and from the product under consideration. The material, energy and emissions inventory could be conducted for the entire life cycle or only the processes being compared, as defined according to the scope of the LCA analysis. The inventory data could be collected from energy and materials data directly obtained from materials manufacturers (as in [123]) or by utilizing databases embedded in LCA software suites such as Building for Environmental and Economic Sustainability (BEES) or SimaPro.

The third stage called Life Cycle Impact Assessment (LCIA) is to assign and translate the materials and energy use and emissions (the inventory data obtained in the previous step) to various environmental impact categories (based on ISO 14040 standard end points [121]) and some of the impact categories could be land use, resource use, climate change, health effects, acidification and toxicity to the environment [124].

The last stage of an LCA analysis is interpretation of the results including ranking of significance of the impact categories and obtaining a single point score for all effect due to the various inventory items obtained in the LCI. The weightage of the various impact categories from the previous LCA step depends on the assessment method selected (e.g. Eco-Indicator 99E method or BEES). The final single point score or the scores in the impact assessment step obtained for various systems or materials could be

compared to ascertain the sustainability of these systems or as a comparative tool between the various systems under consideration. However, the weights used in the final LCA step are subjective and may affect the conclusions of the LCA. Researchers sometimes use the results obtained from the third LCA stage (LCIA) to compare the different products or processes under consideration [124]. When comparing the results, either from the third or fourth stage of LCA, a lower score indicates a more sustainable and possibly environmentally friendly product or process. If the score for any product or process is negative, the results indicate the products or process has a beneficial impact on the environment, in terms of energy or emissions.

In the context of the current research, the amount of cement in concrete is expected to be reduced with the addition of fillers (TiO_2 and limestone). But production and additional processing of these fine fillers could introduce additional components in the energy and emissions of the composite materials [125]. On the other hand, the use of photocatalytic materials can also decrease pollution in the form of smog, NO_X (NO_2 + NO) gases and volatile organic compounds (VOC's) [32, 35, 36]. All these additions and reductions "costs", energy and pollutants will be included in the analysis. Researchers have examined the effect of fillers on durability of cementitious materials, but most studies were conducted using reactive fillers [106, 126, 127]. The effect of inert fillers on the life-cycle cost due to the effect on durability has not been examined or quantified. Thus the effect of addition of fillers on life cycle analysis due to the effect on durability will not be examined in this research.

It should also be noted that energy is required and carbon dioxide is released during the operation and maintenance of a building [4]. But researchers have found that

the operational energy saving achieved using materials with better insulation could be lower than the premium energy spent on the material manufacturing [128]. In this research the operational and maintenance embodied energy for a building will not be considered as a part of the life cycle or embodied energy cost analysis.

The limitations of LCA are well-documented and include reliance on data (often industry-reported) which may be inaccurate, highly variable, or limited [4, 115, 119]. The goal with the preliminary LCA performed here is not to provide absolute quantitative assessments of environmental impacts, but rather to form a basis for a generalized comparison of nano and microparticle additions to concrete as well as to examine the potential effects of further research.

CHAPTER 3

EARLY AGE HYDRATION STUDIES

3.1 Introduction

In this chapter the effect of nano and micro fillers on the early age properties of cementitious materials is examined. Previous researchers have predominantly examined the effect of inert filler particles with sizes comparable to cement grains. When fillers with particle size distribution comparable to cement were added, researchers observed an increase in the degree of hydration [22] as well as chemical shrinkage in the first 24 hours of hydration [23], but the influence of finer inert particles has not been well-examined previously.

Thus the effect of particle size of much *finer* fillers (in the micro and nano range) on early age cement properties such as hydration rate, setting time, flow, chemical and autogenous shrinkage, microstructure and temperature sensitivity should be evaluated. The particle size of the filler could thus be tailored, to produce desired effects on rate of hydration, workability, time to set, dimensional stability and temperature sensitivity.

Thus, the overall objective of this part of the research is to improve understanding of the influence of two increasingly common portland cement mineral fillers (or additives) - TiO_2 nanoparticles and limestone microparticles - on early age hydration of portland cement when used as partial replacements for cement. The effect of particle size and percentage of fillers on the hydration reaction was investigated. Moreover the effect of dispersion technique/mixing procedure on the hydration in cement paste mixes with nanoparticle fillers was also studied.

3.2 Experimental Procedure

3.2.1 Materials

Commercially available TiO_2 and limestone powders, of different particle sizes and surface areas, were utilized for this research. Ordinary ASTM C 150 Type I portland cement (Lafarge) with median particle size of 10.08 μm used had a potential Bogue composition of 51.30% C_3S, 19.73% C_2S, 8.01% C_3A and 9.41% C_4AF and 0.40% Na_2O_{eq}. Table 3.1 summarizes the properties of the different fillers that were added to the cement and shows that the titania powders' surface areas are greater and the particle size smaller than the limestone powders.

Table 3.1. Properties of TiO_2 (T) and limestone (L) powders added to cement

	Crystal Size (nm)	Agglomerate Size (μm)	Surface Area (m^2/g)	Purity (%)
L1	-	20	0.24	95
L2	-	3	0.5	95
L3	-	0.7	12	98
T1	20-30	1.5	45-55	>97
T2	15-25	1.2	75-95	>95
T3	21	0.58	50±15	99.5

Effect of inclusion of various percentages of TiO_2 and limestone on the hydration of ordinary portland cement at a constant water-to-solids (solids = cement + filler) ratio of 0.50 by mass was examined. The different TiO_2 and limestone powders were added to cement at 5, 10 and 15% percentage replacement rates by mass. In some of the high dosage TiO_2 mixes the workability of the cement-filler paste was reduced, but not to the

extent that chemical admixtures were required. Superplasticizers or other chemical admixtures were not added in any of the mixes because researchers have noticed that the hydration reaction is affected by the presence of these additives [9].

The mixing procedure according to ASTM C 305 [129] was followed, with the following modification to mixing for the cement-filler mixes. In the cement mixes with fillers, the filler was initially added to the entire quantity of the water and mixed for 60 seconds. This was followed by addition of cement and mixing according to the ASTM standard.

3.2.2 Test Methodology

3.2.2.1 Setting Time

Vicat needle tests were used to measure setting time according to ASTM C 191 Method A [130]. Based on consistency test for plain cement paste sample, the w/s was maintained constant at 0.35 in all the samples. Since a constant w/s was used a direct comparison is possible between samples with different fillers and replacement rates with TiO_2. The penetration depth was measured every 15 minutes to measure initial and final set until time of final set.

3.2.2.2 Flow Characteristics

The flow characteristics of cement with TiO_2 and limestone fillers could have implications for the workability of construction materials made with these fillers. The flow of cement paste sample with these fillers was studied using a modified version of the ASTM C 1437 mortar flow test [131]. Test samples were prepared without the filler

as well as with 5% of TiO_2 and limestone filler. A constant w/s of 0.35 was maintained for all the samples to understand on the effect of these fillers on the change in flow characteristics.

3.2.2.3 Isothermal Calorimetry

Isothermal calorimetry was conducted, according to ASTM C 1679 [132], to study the early hydration behavior in terms of the rate of heat release as well as the total heat released. The rate of heat release and total heat released were measured using an isothermal calorimeter (TAM AIR, TA instruments) according to ASTM C 1702 [133], at 25 °C, with a precision of ±20μW and accuracy greater than 95%. To prepare the samples, all materials and mixing equipment were equilibrated at 23±2 °C for 24h before the testing. The w/s (w/cm) was maintained constant at 0.50 in all the samples. Less than 10g of samples were put in plastic ampoules and placed into the calorimeter within 5 minutes after mixing with cement. The calorimetry data from the initial 15 minutes after mixing were excluded to allow the sample to equilibrate within the instrument. Measurements were made at least up to 80 hours from the start of mixing.

3.2.2.4 Chemical Shrinkage

Chemical shrinkage is the total change in volume of the reactants, typically a decrease in volume that occurs during cement hydration. Research has shown that the chemical shrinkage is proportional to the degree of hydration. Chemical shrinkage tests were conducted according to ASTM C 1608-07 Procedure A [134]. For all the mixes, the w/s was maintained constant at 0.50. Around 10g of the cement paste samples were put in

glass vials and the rest of the vial was filled with pure distilled water. The vials were then closed and mounted with a graduated capillary tube. The experimental setup was then placed in an environmental chamber where the temperature was maintained at 23 °C. Measurement of the volume change was conducted every 30 minutes in the first 24 hours, and then every 2 hours up to at least 50 hours after mixing of cement with water. The volume change measurements were obtained using a digital camera set on a time lapse photography mode and the images were analyzed at the end of the test. The use of an environmental chamber as well as time lapse photography allowed maintaining a constant temperature environment in the chamber. At least triplicate samples were used for every mix and the results were averaged for the samples.

3.2.2.5 Autogenous Shrinkage

Autogenous shrinkage is the self-created bulk strain during hydration of a sealed cement paste or mortar sample starting from the time of final set (measured earlier in a previous section). Autogenous shrinkage tests were conducted at w/s = 0.35 according to ASTM C 1698-09 [135], where the cement paste was sealed inside a corrugated plastic mold that offers low resistance to length change and thus allows measurement of length during hydration reaction. The sealed molds are stored in a constant temperature environment of 23 °C and length measurements are taken using a dilatometer after final set of the mix. Measurement of the length change was conducted every 30 minutes in the first 6 hours after mixing of cement with water, and then every 2 hours up to at least 12 hours and subsequently every day. At least triplicate samples were used for every mix and the results were averaged for the samples.

3.2.2.6 Microscopy

A LEO 1530 FE SEM was used for microscopic analysis of the hydrated cement paste samples. The samples used for microscopy were chipped off and were imaged after drying in an oven at 35°C for 3 days. Samples were sputter coated with gold if necessary.

3.2.2.7 Activation Energy of Cement-Nanoparticle Mixes

The procedure used for isothermal calorimetry was followed for the obtaining the data for calculating the activation energy of cementitious mixtures with nanoparticle additives. But in addition to isothermal calorimetry tests at 25°C, the tests were repeated for each of the mixes, at five different temperatures (15, 25, 35, 45 and 55°C) and the collected data used to calculate the activation energy using the two methods described below. Two different techniques were used to calculate the apparent activation energy: 1) a linear method which calculates the rate of reaction based on the linear slope of the heat evolution data and 2) a modified ASTM C1074 procedure that uses calorimetry data.

Linear Method for Calculating Activation Energy

The linear method of calculating the reaction rate and the activation energy of cementitious mixtures is a simple technique based on the calculation of activation energy from the slope of the heat release curve of cement. This method approximates the reaction rate to be the linear slope of the acceleratory region of the cumulative heat release curve of cement mixtures. The procedure for calculating the rate of reaction has

been previously described by other researchers [66, 79], but the main steps are listed below.

1. Obtain the rate of heat release data for each cement mixture from the isothermal calorimeter and calculate the cumulative heat release per gram of cement of these mixtures (Figure 3.12).
2. Calculate the reaction rate (k) as the linear slope of the cumulative heat release curve in the region of maximum slope. The region used to calculate the linear slope would typically include the peak of the hydration curve (which is clearly visible in the rate of heat release curve). Note that the rate of reaction is obtained from the cumulative heat release data and not from the rate of heat release data. Repeat process to obtain the reaction rate (k) at different temperatures for each mix (Figure 3.12).
3. Plot natural logarithm of reaction rate (k) for each mix versus inverse of temperature (in Kelvin) and obtain the slope of the graph (Figure 3.13).
4. According to Equation 2.2, multiply the negative of the slope of the graph of ln(k) vs. 1/T with universal gas constant R (8.314 J/mol/K) to obtain the activation energy for each mix.

The linear method is the simplest technique for calculation of activation energy but has some drawbacks. Activation energy is highly dependent on the degree of hydration and researchers have suggested using data up to a degree of hydration of 0.5 for E_a calculations. In the linear method only the data in a narrow time region is utilized, which typically includes the acceleratory region as well as the peak hydration rate region. The

start of the acceleratory region can also not be easily discernible, especially for the lower temperature calorimetry experiments. Moreover, the determination of linear section of the heat evolution curve can be subjective due to possible multiple peaks due to C_3S and C_3A hydration. Even though these are some drawbacks of the linear technique, the first order differential calculation of reaction rate and hence activation energy obtained using this methods can be used as a simplified initial approximation of activation energy and a comparison for other techniques [66].

Modified ASTM C1074 Method for Calculating Activation Energy

The ASTM C1074 uses a strength data and equivalent time concept to calculate the activation energy of cement mixes. Researchers have demonstrated that instead of using equivalent time in the Arrhenius equation (Equation 2.2), the hydration time parameter (τ) obtained from the three parameter model fit of the hydration data [64] can be used. Here, the activation energy (E_a) of cement mixes using τ was determined using the following equation.

$$E_a = \frac{-\ln\left(\frac{\tau_{ref}}{\tau_c}\right)}{\left(\frac{1}{T_{ref}} - \frac{1}{T_c}\right)} \cdot R \tag{3.1}$$

where τ_{ref} and T_{ref} are the hydration time parameter and concrete temperature (in K) at the reference temperature, τ_c and T_c are the hydration time parameter and concrete temperature at different temperatures at which isothermal calorimetry was conducted and

R is the universal gas constant (8.314 J/mol/K). For the calculations in this research 25 °C was considered as the reference temperature.

The modified ASTM C1074 method calculates the activation energy of cement mixtures using the model fit parameters from the three parameter model of the degree of hydration data (Equation 2.5). The procedure for calculating the activation energy of a cement mix using the modified ASTM C1074 and the three parameter model is listed below and the models and equations used were discussed in a previous section.

1. Obtain the rate of heat release data for each cement mixture from the isothermal calorimeter and calculate the cumulative heat release per gram of cement for these mixtures.
2. Calculate using Equation 2.3 and 2.4, the variation (with time) of degree of hydration by dividing the cumulative heat released with the total heat of hydration of the cement mix (Figure 3.14).
3. Model the degree of hydration using the three parameter model given in Equation 2.5. Use a least square fit of the exponential function to solve for values of α_u, τ and β. Obtain α_u, τ and β values for the cement mix at each temperature tested. Calculate average value of α_u and β for the mix using the values at different temperatures. Using these average values of α_u and β, recalculate the values of τ at each temperature.
4. Using Equation 3.1, plot natural logarithm of hydration time parameter (τ) versus inverse of temperature (in Kelvin) and obtain the slope of the graph (Figure 3.15).

5. According to Equation 3.1, multiply the negative of the slope of the graph of ln(τ) vs. 1/T with universal gas constant R (8.314 J/mol/K) to obtain the activation energy for each mix.

3.2.2.8 Powers' Model for Cement Hydration

The modified Powers' equation [47, 136] was used to model variation of chemical shrinkage with respect to degree of hydration (α) during cement hydration according to equations:

$$\text{Chemical shrinkage:} \qquad V_{cs} = 0.20(1 - p)\,\alpha\,(1 - V_F) \tag{3.2}$$

where $p = (w/c)/(w/c + \rho_w/\rho_c)$ is the initial volume fraction of water in the mixture, w/c is the effective water-to-cements ratio, ρ_w and ρ_c refer to the densities of water and cement and V_F is the volume fraction of filler in the blended paste before hydration (α=0). The variation of chemical shrinkage with respect to degree of hydration was modeled and compared with experimental chemical shrinkage to ascertain the validity of the Power's model for cement hydration in the presence of nano and microsized inert fillers.

3.3 Results and Discussion

3.3.1 Setting Time

The setting time results for portland cement and mixes with cement replaced with 5% TiO_2 and limestone powder are given in Figure 3.1. These results can be used for a comparative analysis between the ordinary portland cement mix and the mixes with fillers. The initial setting time for the portland cement mix was 165 minutes whereas the final setting time was 305 minutes.

The initial and final setting time of the coarsest limestone used in the research (L1) exhibited a similar initial and final setting time compared to the portland cement mix. Other finer limestone powders tested resulted in a decrease in the setting time of the cementitious mix. As the particle size of the inert filler decreased (surface area increased) it was observed that the initial and final setting time decreased, with the finest particle reducing the setting time to the lowest measured value. The greatest decrease in initial and final setting time was observed for the T3-5% mix which had an initial and final setting time of 104 and 164 minutes respectively. Thus, the final setting time for the T3-5% mix was observed to be reduced by 141 minutes, a reduction of 46%, which could have significant implications for construction industry by decreasing the turnover time for concrete elements. These results show that fine inert particles increase the rate of cement hydration, possibly due to heterogeneous nucleation effect.

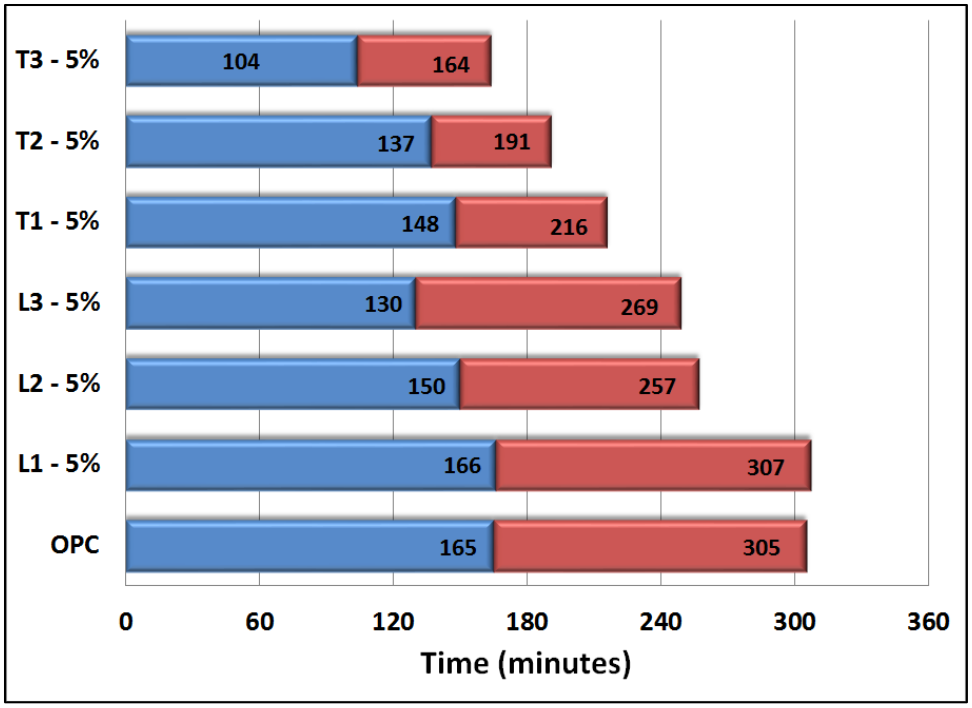

Figure 3.1. Setting time results for cement mixes with 5% replacement of TiO_2 and limestone filler

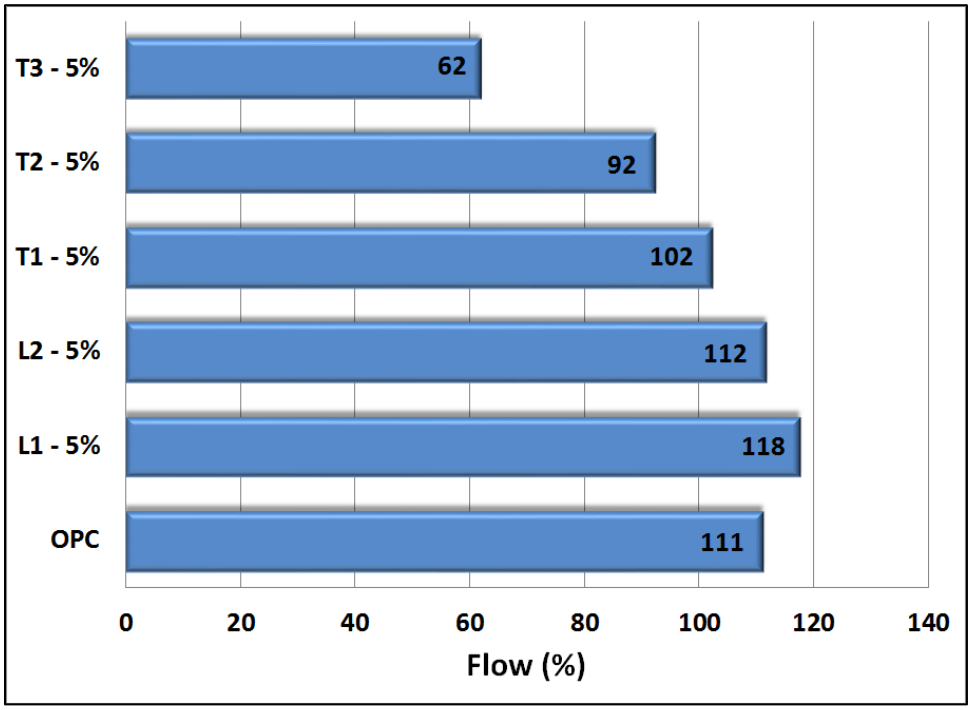

Figure 3.2. Flow characteristics results for cement mixes with 5% replacement of TiO_2 and limestone filler

3.3.2 Flow Characteristics

The flow characteristics results for portland cement and mixes with cement replaced with 5% TiO_2 and limestone powder are given in Figure 3.2. Mixes with L1 and L2 (coarser fillers in this research) had flow values similar to the control mix. But other finer particles (L3, T1, T2 and T3) decreased the flow values compared to the portland cement mix, with finer TiO_2 particles decreasing the flow values greatest. T3 at 5% decreased the flow values to 62% compared to the value of 111% of the portland cement mix. Thus, the use of nano fillers results in a decrease of the flow of cementitious mixtures which could reduce the workability.

3.3.3 Isothermal Calorimetry

3.3.3.1 Calorimetry Studies of TiO_2–Cement Mixes

Figure 3.3 shows the variation of the rate of hydration of ordinary portland cement (OPC) and TiO_2–blended cements at 5and 10% replacement levels. For the control mix, after the initial region of high heat release (heat of dissolution) and dormant stage, the zone of accelerated reaction can be observed from ~1 to ~8 hours of age. The main peak of the hydration reaction corresponding to C_3S hydration was observed at 7.5 hours after mixing and is followed by the secondary peak of the C_3A hydration at 8.5 hours, which in these tests exhibited the highest rate of heat evolution.

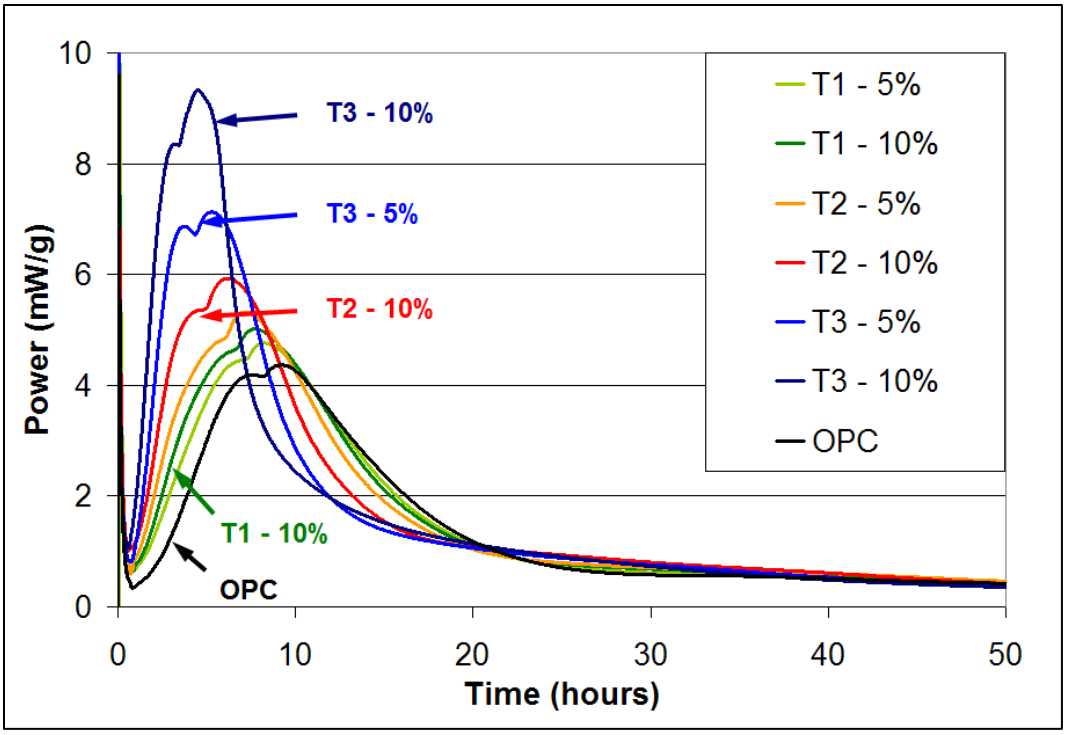

Figure 3.3. Heat of hydration of cement mixes with different types of TiO_2 (T1, T2 and T3) at 5 and 10% replacement rates

When compared to the heat evolution curve for the control mix, it can be observed from Figure 3.3 that as the dosage of TiO_2 is increased, the peak of the hydration curve also increased. This is clearly demonstrated by the increase in peak of C_3S as well as that of C_3A. Since the peak for C_3A is evident for all the mixes, comparison between the various mixes can be conducted using the C_3A peak values. For example, the C_3A hydration peak increased by 21.9% and 35.8% for the T2 mixes with 5% and 10% respectively. A similar trend was observed for the other TiO_2-cement mixes with the maximum increase in the peak hydration rate observed in T3 where 5 and 10% replacement of TiO_2 resulted in an increase of 63.3% and 113.7% of the C_3A peak. Thus the heat evolution by the cement paste mix increases with an increase in the dosage of TiO_2 particles and particularly in the case of T3 at 10% replacement rate, the peak rate of heat evolution was more than double that of the control mix.

Figure 3.3 also shows with TiO_2 fillers resulted in an acceleration of the hydration reaction in all the TiO_2-cement paste mixes. The dormant stage of the reaction was shortened in all the mixes and the slope of the hydration curve was also steeper in the TiO_2-cement mixes compared to the control mix. The time at which the peaks (both C_3S and C_3A peak) of the hydration curve were observed decreased with the replacement with TiO_2. For example it was observed that 10% of T1, T2 and T3 accelerated the hydration reaction by ~80, ~180 and ~280 minutes (by comparing the time at which the C_3A peak was observed). These results suggest that replacement of cement with TiO_2 nanoparticles results in an increased rate of reaction of cement mainly due to heterogeneous nucleation and the effect of dilution was negligible. The results from the current research support the conclusions that were obtained by Lee and Kurtis [63] who also observed that the hydration of C_3S was accelerated by the inclusion of TiO_2 nanoparticles due to heterogeneous nucleation effects. The results from isothermal calorimetry in their research were supported by hydration modeling according to the boundary nucleation and growth model for cement hydration. Thus it can be concluded that the increase in hydration in the presence of fine fillers is due, at least in part, to heterogeneous nucleation which increases the rate cement hydration by boundary nucleation and growth around the fine filler particles.

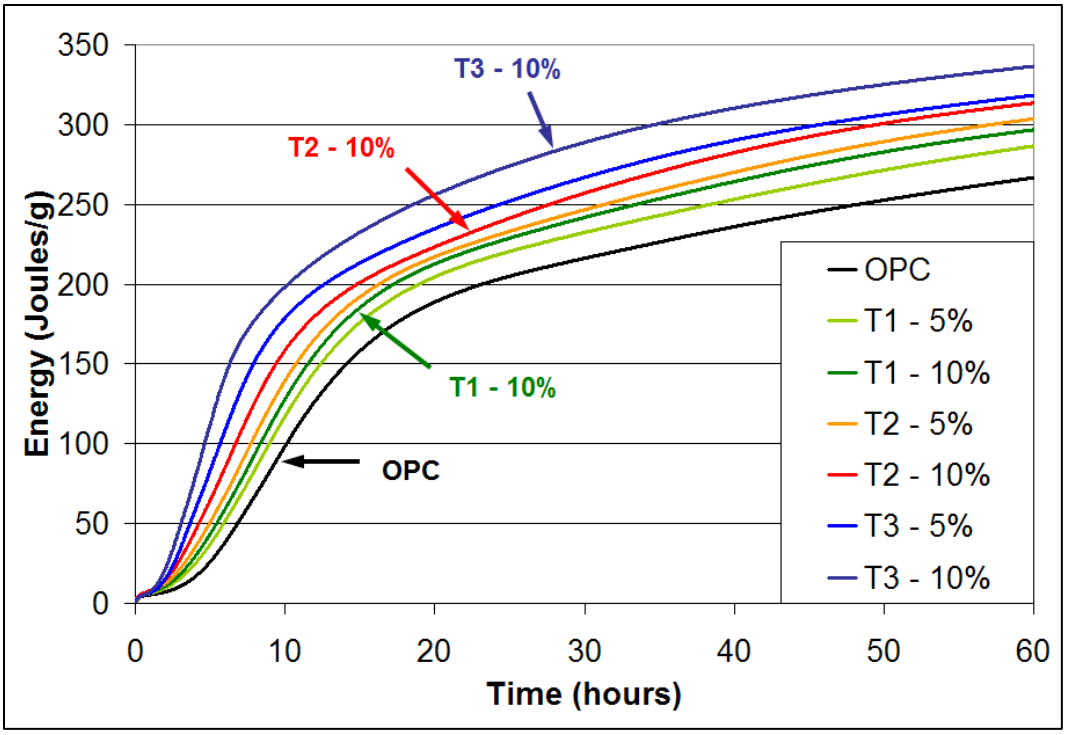

Figure 3.4. Cumulative heat of hydration of cement mixes with different types of TiO_2 (T1, T2 and T3) at 5 and 10% replacement rates

The effect of the fineness of the inert additives on cement hydration is also evident from Figure 3.3. By comparing T1 and T2, which were produced using similar processes by a single manufacturer, it was observed that the TiO_2 with higher surface area (T2) accelerated and increased the rate of hydration more than the TiO_2 with lower surface area (T1). Thus the rate of cement hydration in the presence of TiO_2 depends on the surface area of the particles that are added to the cement, with higher surface area (smaller particle size) particles accelerating the reaction more than particles with lower surface area (larger particle size). This supports the conclusion that heterogeneous nucleation effect, which is dependent on the particle surface area, is the dominant effect compared to dilution, in the case of replacement of cement with TiO_2 nanoparticles to cement.

Figure 3.4 shows the total energy released during the hydration of the control as well as various TiO_2-cement mixes. It can be observed that the total energy evolved was higher for all the TiO_2-cement mixes compared to the control mix. As observed in the heat of hydration curves, higher percentage replacement with TiO_2 resulted in an increased total energy release compared to the control mix. If the total energy released at 48 hours of hydration is compared, 5% and 10% T1 resulted in 7.4% and 12.0% increase in the total energy. The respective increases in energy for T2 was 13.8% and 19.3% whereas the highest increase in the hydration energy were for T3, where a 21.5% and 29.2% increase in the total energy evolved was observed. When comparing the effect of surface area of TiO_2 and comparing TiO_2 that were produced by the same manufacturer, it can be seen that a higher surface area of TiO_2 (T2) resulted in a higher total energy release compared to the lower surface area TiO_2 (T1). Thus the total energy release curve also proves that the higher replacement with TiO_2 and TiO_2 with a higher surface area results in higher energy release by the TiO_2-cement mixes. It should be noted that the total energy released by the mixes eventually will be the same as the cement slowly completes complete hydration. But in the initial stages of the reaction, within the first few days, the inclusion of TiO_2 particles accelerates the energy release and the hydration reaction of cement.

3.3.3.2 Calorimetry Studies of Limestone-Cement Mixes

Figure 3.5 shows the variation of the rate of hydration of ordinary portland cement and limestone–blended cements at 5, 10and 15% replacement levels. Similar to the mixes with TiO_2 filler, it was observed that L2 decreased the duration of the dormant stage of

the reaction, accelerated the rate of hydration and also result in an increased peak release of heat. But when compared to the mixes with TiO_2 filler, the cement paste mixes with limestone L2 filler increased these quantities only marginally. The peak rate of hydration was increased by merely 0.6% and 5.0% for the mixes with 10% and 15% replacement, whereas the mix with 5% replacement showed a 4.1% decrease in peak hydration rate. When the time at which the peaks of the hydration curves are compared, it was observed that hydration was accelerated for all the mixes with L2. Five, 10 and 15% of L2 resulted in an acceleration of the reaction by ~15, ~40 and ~70 minutes when the C_3A peaks are compared with the control mix.

On the other hand all the mixes with L1 (the coarsest of the particles tested) resulted in a decrease in the peak hydration rate as well as a deceleration of the hydration reaction. 5, 10 and 15% replacement by L1 decreased the peak hydration rate by 7.6%, 7.7% and 7.5%. These values suggest that the replacement with L1 resulted in a decrease in the hydration rate due to dilution effect and heterogeneous nucleation was not effective due to the relatively larger particle size of the limestone used. The replacement with L1 also resulted in a marginal deceleration of the reaction by 21, 13 and 8 minutes, when the peaks of C_3A hydration were compared. Thus the results from the two limestone powders that were tested suggest that if the size of the particle additives is larger (or surface area is smaller) than a particular limit, heterogeneous nucleation will occur and the only effect will be a marginal decrease in reaction rate due to dilution effects.

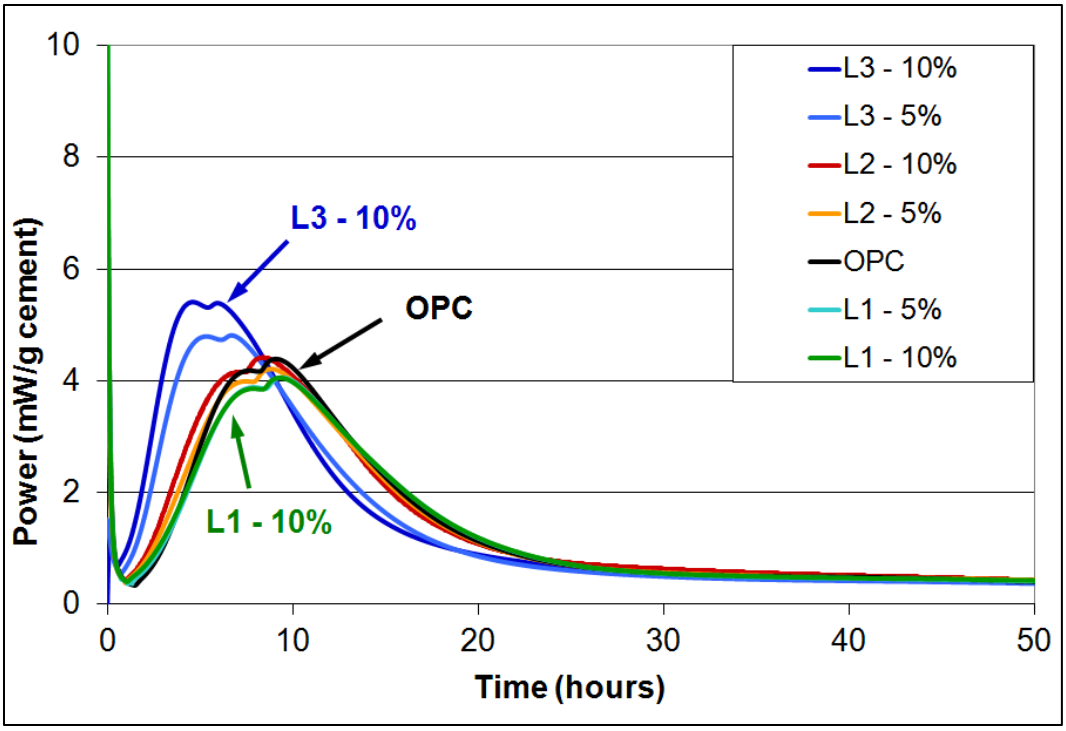

Figure 3.5. Heat of hydration of cement mixes with various percentages of limestone powders (L1, L2 and L3). (Note that the y-axis scale was maintained to be the same as in Figure 3.3)

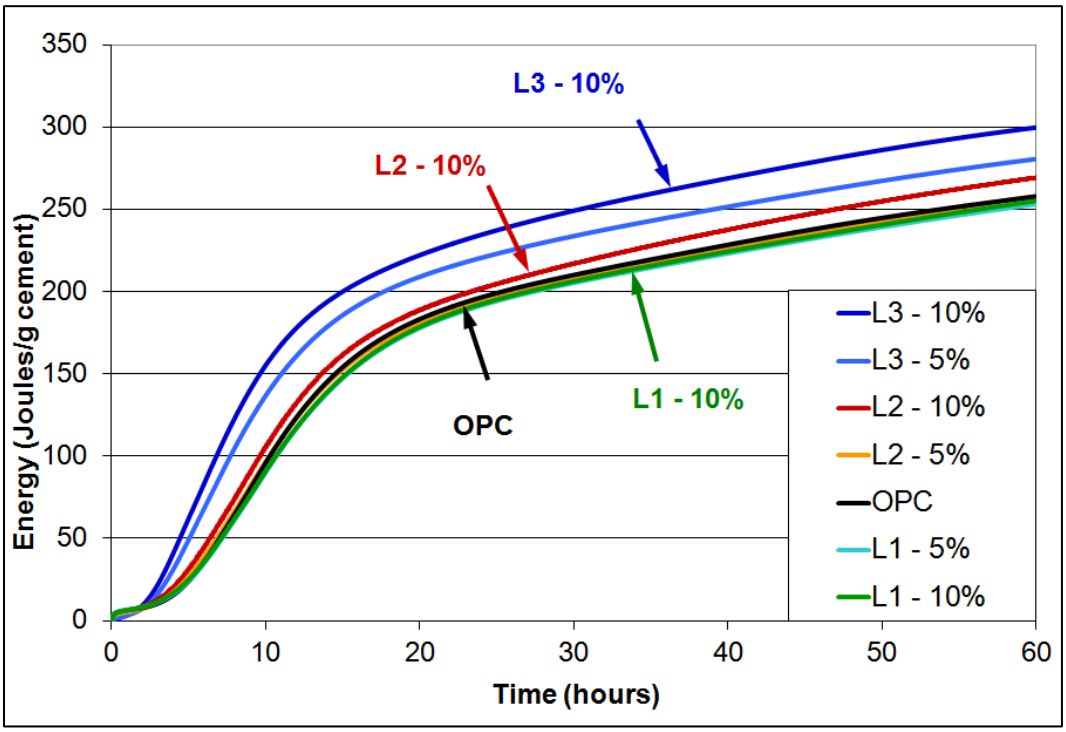

Figure 3.6. Cumulative heat of hydration of cement mixes with various percentages of limestone powders L1, L2 and L3

Figure 3.6 shows the total energy released during the hydration of the control and the limestone-cement mixes. The total energy evolved was higher than or at least equal to the control mix for the mixes made with L2. For example, limestone-cement paste mixes of L2 15% replacement resulted in a 10.6% increase in the total energy released at 48 hours of hydration when compared to the control mix. On the other hand all the mixes with L1 showed a marginally lower total energy released throughout the test duration, as can be observed in Figure 3.6.

3.3.4 Hydration of Cementitious Mixtures at Different Temperatures

Figure 3.7 shows the variation of the rate of hydration and cumulative heat of hydration of ordinary portland cement at different temperatures. It can be observed from Figure 3.7a that as the temperature increases, the peak value of the reaction rate increases. This is expected since a higher temperature increases the rate of cement hydration [137]. The increase in temperature also results in an acceleration of cement hydration, which is evident from the decrease in time required to reach the peak of hydration. For comparison the peaks of the hydration curve at 55°C, 45°C and 35°C were observed approximately at 130, 175 and 265 minutes respectively after mixing. The peaks of hydration are clearly discernable in the higher temperature mixes, whereas in the 25°C and 15°C mixes the peaks are not sharp and it is difficult, for example, to discern between peaks associated with C_3S and C_3A reaction. Some researchers, see for example [71], have used the time to reach peak hydration rate as a measure of the hydration and have applied the Arrhenius equation (Equation 2.2) to calculate activation energy. But as observed in this research, the peaks were not clearly discernable at lower temperatures

and hence calculation of activation energy based on the time to reach the peak temperature release [71] might not be a feasible approach for all cases.

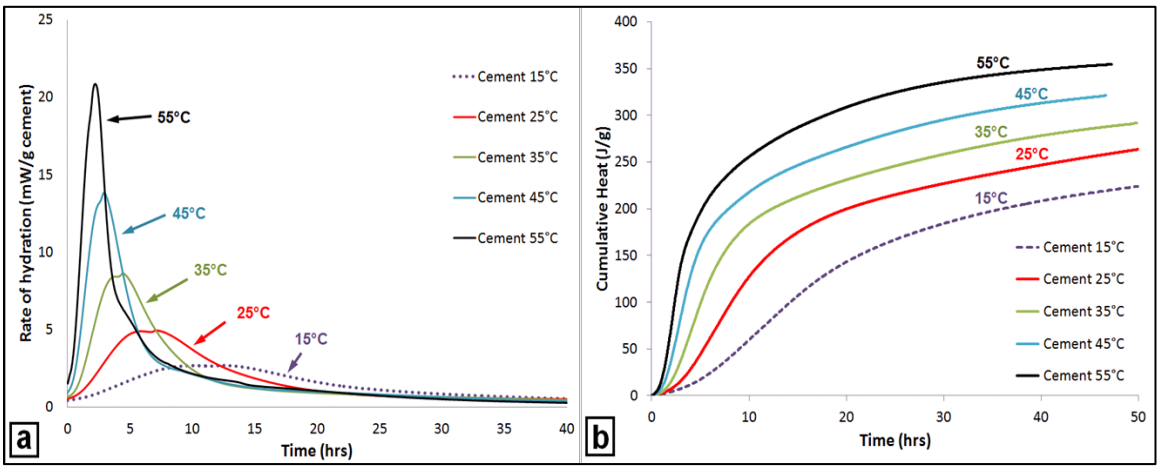

Figure 3.7. (a) Rate of hydration and (b) cumulative heat of hydration of ordinary portland cement at different temperatures (15, 25, 35, 45 and 55°C)

Figure 3.7b shows that the cumulative heat evolved at a particular time by the cement mix increases with an increase in temperature. Based on the increasing slope of the cumulative heat curve in the accelerating region of the hydration curve, it can be concluded that the rate of heat evolution (and hence the rate of cement hydration) increases with increasing temperature.

3.3.5 Chemical Shrinkage

Chemical shrinkage is the reduction in volume of hydrating cement-based materials due to the difference in absolute volume between the reactants and products. Figure 3.8 shows the chemical shrinkage results for the different mixes with TiO_2 and limestone powder fillers. It can also be observed that the chemical shrinkage curves are similar to

the cumulative heat evolution curves that were obtained from the calorimetry tests, as expected. Similar to the cumulative heat curves an initial slow rate of reaction is observed initially, followed by an accelerated reaction up to approximately 24 hours from the time of mixing. The increased duration of shrinkage is followed by a zone of stabilization where the shrinkage rate reduces considerably.

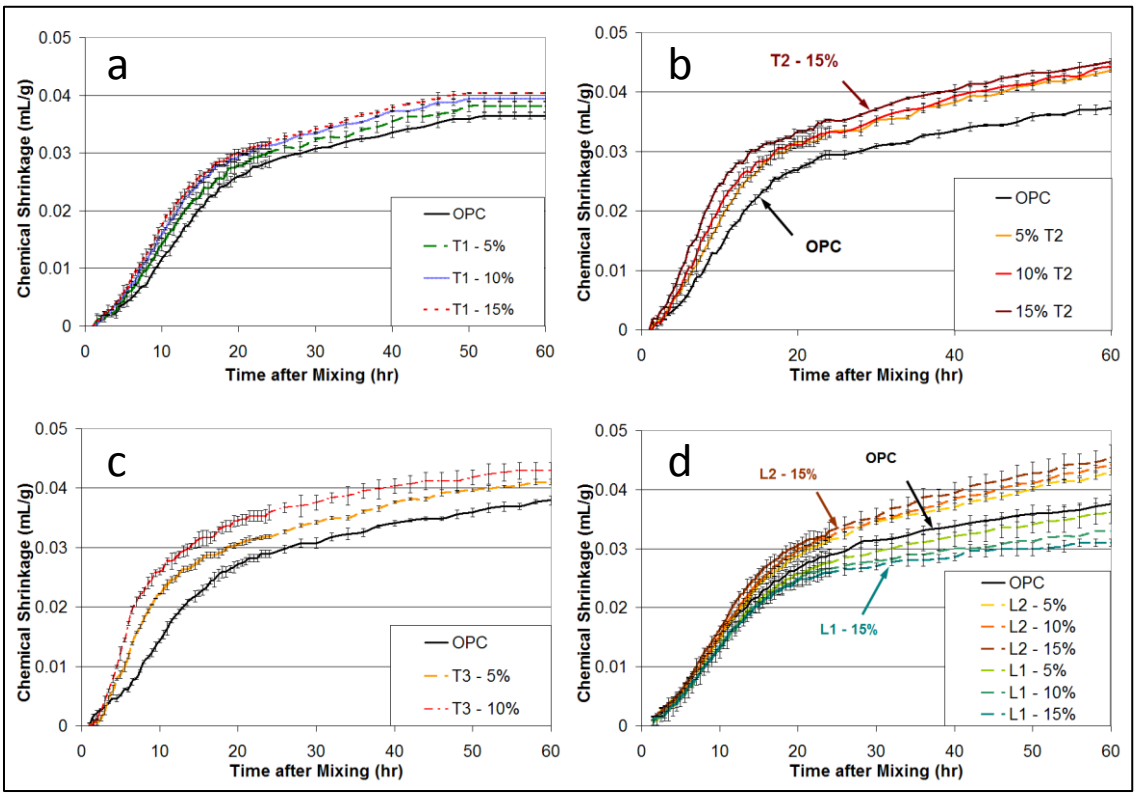

Figure 3.8. Chemical shrinkage observed in samples with different percentages of TiO_2 and limestone powders: a – T1 mixes, b – T2 mixes, c – T3 mixes, d – L1 and L2 mixes

From Figure 3.8 it can clearly be seen that T1, T2, T3 and L2 increased the chemical shrinkage observed in the cement paste compared the control OPC mix. Among the TiO_2 powders tested, the least percentage increase in chemical shrinkage was observed in T1, followed by T2 and T3. For example the increase in chemical shrinkage for the TiO_2-

cement mixes with 10% replacement with TiO_2 of T1, T2 and T3 were 8.13%, 17.58% and 15.69% respectively at 48 hours of hydration.

The limestone-cement mix with limestone L2 also resulted in an increase in the chemical shrinkage as the particle size of the limestone was around 3µm. On the other hand the cement paste mix with replacement of cement with limestone L1 showed a decrease in the chemical shrinkage results, as can be observed in Figure 3.8(d). L1 was the coarsest of the fillers that were used in the current tests and thus it can be concluded that coarser fillers result in a reduced chemical shrinkage of cement paste mixes. As the particle size of the filler increases, as observed from the isothermal calorimetry results the cumulative heat of hydration decreases and hence the total degree of hydration decreases. Thus due to dilution effect the inclusion of coarse inert fillers result in decreased chemical shrinkage in filler-cement mixes.

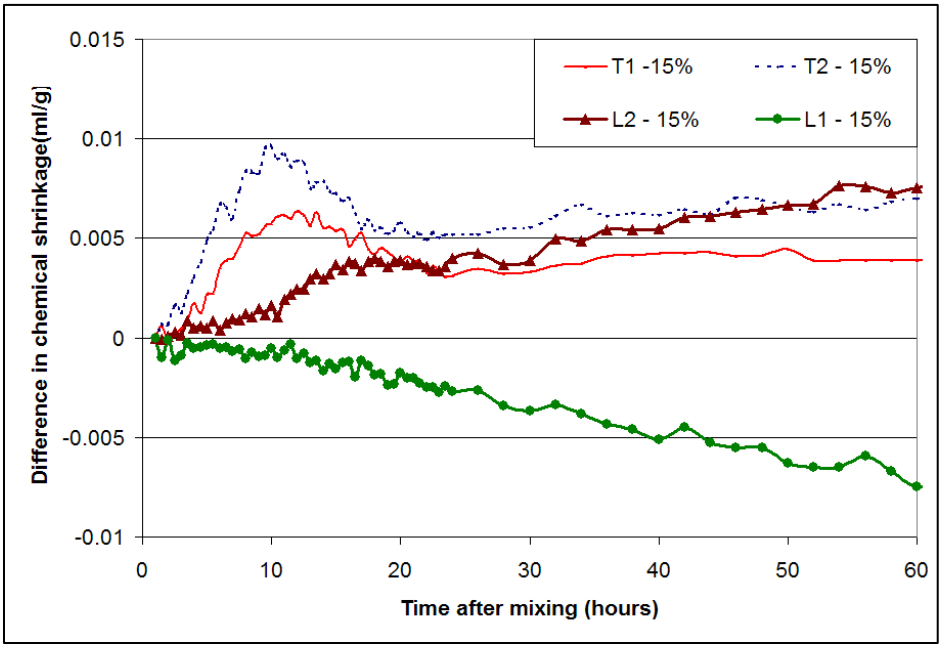

Figure 3.9. Difference in chemical shrinkage observed between samples with different percentages of TiO_2 and limestone powders and the control mix

In all the TiO_2 mixes, the difference between the control mix and the mixes with TiO_2 fillers increased considerably in the first 12 to 24 hours. After the first 24 hours, the curves of the OPC and the TiO_2 mixes were almost parallel to each other with a difference between increase chemical shrinkage being negligible. Figure 3.9 shows the difference of the chemical shrinkage observed between mixes with additives and the control mix. The difference between TiO_2-mixes and control mix increased considerably in the first 12 hours, decreased from this peak until ~24 hours and then remained almost steady after that with only a marginal increase in the chemical shrinkage difference. Thus it can be concluded that the effect of the TiO_2 powders on chemical shrinkage is predominantly during the first 24 hours of the hydration reaction. On the other hand, in the mixes with limestone powder fillers, the difference between the OPC mix and the limestone mixes increased continuously with time and even after 24 hours the difference between the limestone-cement paste mix and the control mix continued to increase, as can be clearly seen in Figure 3.8(d) and Figure 3.9. For mixes with TiO_2 filler, high chemical shrinkage was observed in the initial stages (first 12 hours) of hydration reaction but at this stage the cement paste mix is still plastic and gaining strength.

For the limestone-cement mixes it can be observed that chemical shrinkage when compared to the control mix increases even after 24 hours. This increase in chemical shrinkage should be considered while designing mixes with finer limestone filler to reduce the likelihood of cracking. For example, Bentz et al., [86] showed that the coarsest limestone (with median particle size of 100 μm) used in their research did not result in cracking of the mortar specimens when tested according to the ASTM C 1581 [138] standard test for cracking of mortar specimens but all the other limestone-cement (with

median limestone particle size of 3-17 μm) mixes cracked. Thus higher shrinkage is induced by the use of fine fillers and result in cracking of cementitious materials during the hydration process, but further research has to be conducted on this topic.

3.3.6 Autogenous Shrinkage

Autogenous shrinkage is defined as the volume change in cement-based materials occurring without moisture transfer to the surrounding environment. Figure 3.10 shows the autogenous shrinkage results for the different mixes with TiO_2 and limestone powder fillers. Similar to cumulative heat curves an initial slow rate of reaction is observed initially, followed by an accelerated reaction up to approximately 24 hours from the time of mixing. The increased duration of shrinkage is followed by a zone of stabilization where the shrinkage rate reduces considerably. In the ordinary portland cement mix and L1-cement mix, expansion was observed during initial stages of hydration. This behavior has been observed by other researchers and is due to bleed water reabsorption possible in cementitious mixtures with w/c greater than 0.30 [139]. In the filler-cement mixes with fine fillers (particle size <3μm), the higher filler surface area could have caused adsorption of water on the filler surfaces, and hence reduced free water available for bleeding.

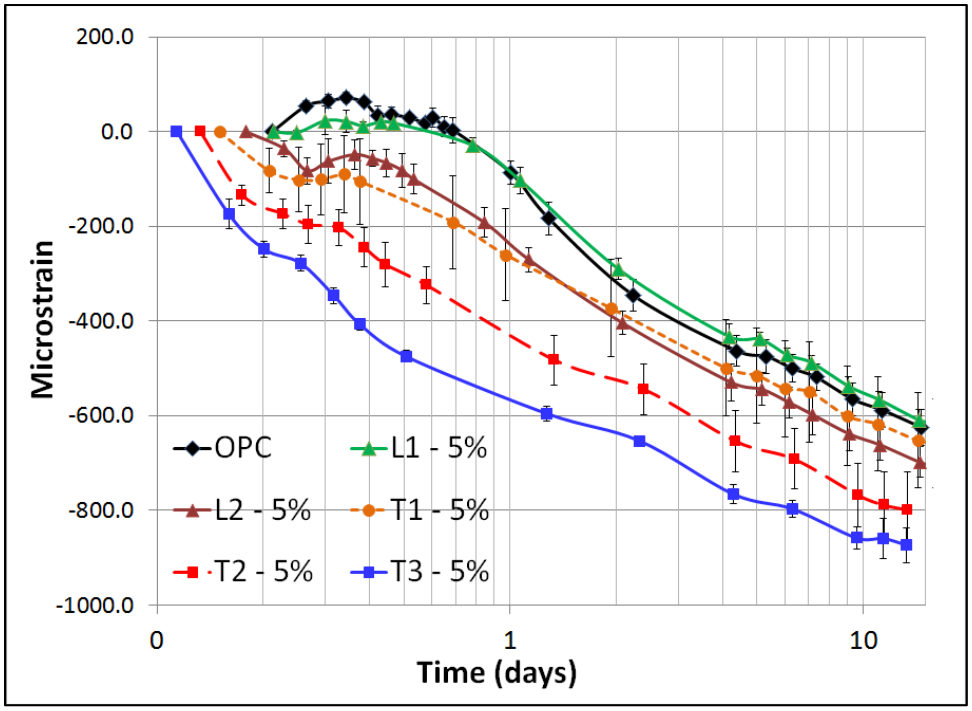

Figure 3.10. Autogenous shrinkage results for cement mixes with 5% replacement of TiO_2 and limestone filler

From Figure 3.10 it can clearly be seen that T1, T2, T3 and L2 increased the autogenous shrinkage compared the control mix. Among the TiO_2 powders tested, the least percentage increase in autogenous shrinkage was observed in T1, followed by T2 and T3 which is the decreasing order of filler particle sizes. For example the increase in autogenous shrinkage for the TiO_2-cement mixes with 5% replacement with TiO_2 of T1, T2 and T3 were 200%, 400% and 550% respectively at 24 hours of hydration. It should be noted that the cement paste mix exhibited a minor expansion during the autogenous shrinkage tests, which could be due to bleeding in the cement paste mix.

The limestone-cement mix with limestone L1 resulted in an autogenous shrinkage behavior similar to the control cement paste mix till 24 hours of hydration. After 24 hours the L1 mix had a marginally lower shrinkage compared to cement paste mix. The

decrease in autogenous shrinkage in the coarsest limestone L1 is similar to the chemical shrinkage results. L2 and L3 limestone filler cement mixes exhibited an increase in the autogenous shrinkage compared to control cement paste mix. But with increasing time, it was observed that the difference between autogenous shrinkage of control mix and these limestone-cement mixes decreased.

The increase in autogenous shrinkage observed in the fine inert filler-mixes, the decrease in shrinkage in L1 mix and the marginal difference between control mix and L2 and L3 mix could be due to variation of interparticle spacing (pore size) which affects capillary stress, according to Kelvin/Laplace-Gibbs equation:

$$\sigma_{cap} = 2\gamma / r \tag{3.3}$$

where σ_{cap} = capillary stress, γ = surface tension of the pore water, and r = pore size radius, where the radius for the smallest water-filled pore is generally used. That is, if interparticle spacing (pore size) increases, the capillary stresses decreases and hence the shrinkage decreases, which is possibly occurring in the case of L1. In the case of fine inert fillers (T1, T2 and T3) the interparticle spacing (pore size) could be decreasing which increases the capillary stresses and hence increase the autogenous shrinkage.

3.3.7 Microscopy

The size of the TiO_2 particles was in the nanometer scale and once mixed, differentiating the TiO_2 particles from the rest of the cement mix was difficult in the backscattered mode since the atomic weight of calcium and titanium are similar (40.078 g/mol and 47.867 g/mol respectively). Hence when imaging samples the TiO_2 filler, the

areas around agglomerates of TiO_2 was imaged for easy characterization of cement paste in different regions. The agglomerates of TiO_2 were easily distinguishable in the TiO_2-cement paste mix due to the differences in the morphology of the paste and TiO_2.

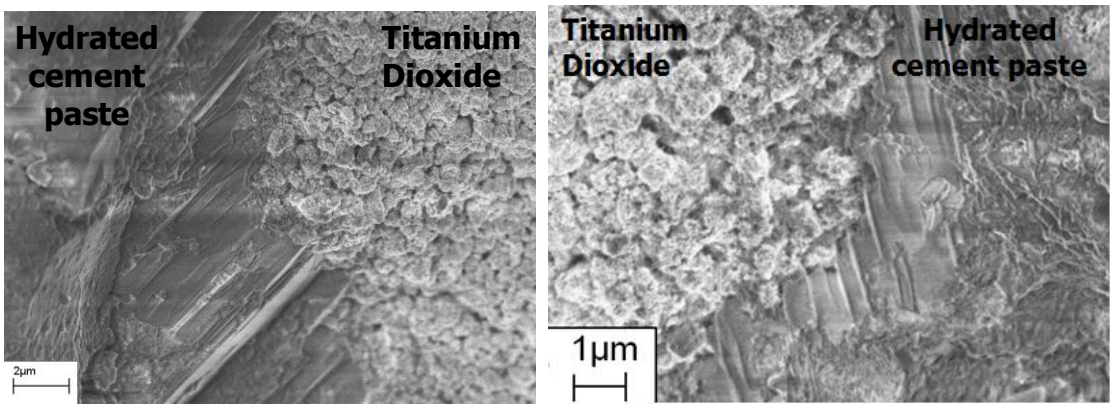

Figure 3.11. Scanning Electron Microscopy image of interface between TiO_2 and cement paste

Figure 3.11 shows that the cement paste in the region immediately adjacent to the TiO_2 particles is dense and the morphology is significantly different from the cement paste away from the TiO_2 agglomerate. The cement paste microstructure away from the TiO_2 particles was found to be less dense and more porous. This suggests that hydrated cement paste immediately adjacent TiO_2 particles could have a higher density and higher strength compared to the rest of the cement paste microstructure. It should also be noted that if the particles of TiO_2 was well dispersed in the cement matrix rather than being agglomerated, the cement paste that formed could have a higher density and strength compared to the cement mix without any such fillers. Further investigation is necessary to understand the effect of TiO_2 on the microstructure of cement paste.

3.3.8 Activation Energy Using Single Linear Approximation Method

The apparent activation energy of cementitious materials represents the temperature sensitivity of the chemical reactions during hydration. A higher activation energy for chemical reactions will result in a greater variation of reaction rate with temperature change and hence a "higher sensitivity to temperature". Such understanding is important for appreciating the influence of field temperatures on hydration rates and thus development of microstructure, time to set, and rate of strength development, among other features.

As described previously, in this approach, the reaction rate (k) for each mix at different tempeartures was calculated using the maximum slope of the cumulative heat of hydration curve obtained at varying temperatures during isothermal calorimetry testing. For comparison of trends between mixes, the data and calculation procedure are explained for two mixes: ordinary portland cement mix and 5% T3 mix. The same procedure was followed for all the mixes, and activation energy for each are listed in Table 3.3.

Figure 3.12a and 3.12b shows the cumulative heat release of ordinary portland cement and 5% T3 mixes at various temperatures (15, 25, 35, 45 and 55 °C). As observed earlier, the slope of the cumulative heat release graph increases with temperature for both the cement paste mixes. If corresponding mixes of ordinary portland cement and 5% T3 mix are compared (for example the data at 15°C), it can be observed that the slope of the 5% T3 mix is greater than the ordinary portland cement paste mix. This clearly shows that the accelerated hydration occurs in the nanoparticle-cement mixes, as was observed earlier in the rate of hydration and cumulative heat of hydration graphs (Figure 3.3 and

3.4). The reaction rates (k) of each mix at different temperatures were calculated as the linear slope of the cumulative heat release curve in the region of maximum slope. The regions used for calculating the linear slope are marked in bold on the cumulative heat of hydration graphs. In general a minimum R^2 value of 0.99 was ensured while calculating the slope in the region of maximum slope in the cumulative heat release graph.

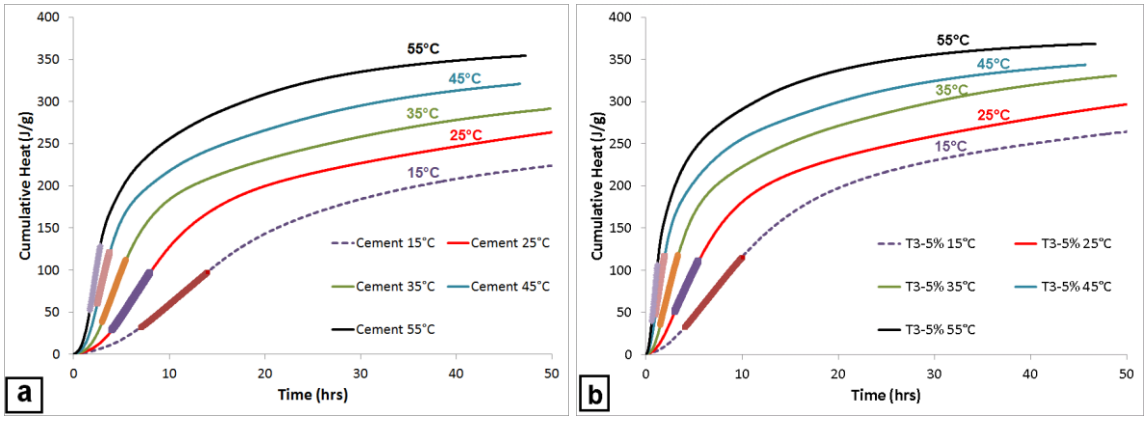

Figure 3.12. Cumulative heat released by (a) ordinary portland cement and (b) 5% T3 cement paste mix at different temperatures showing the linear regions used for calculating reaction rate

Table 3.2 lists the values of the reaction rates (k) of ordinary portland cement and 5% T3 cement mixes. From the data, it is evident that at each temperature the reaction rate of the T3 mix was greater than that of the ordinary portland cement mix. Similarly increased rates of reaction was observed in all the cement-filler mixes in this reseach when compared to the ordinary portland cement mix. The increase in reaction rate is attributed to increased hydration due to heterogeneous nucleation on the surface of fine fillers, which is similar to earlier observations by the current authors [53]. But it should be specifically noted that even though the rate of reaction at each temperature is higher for the 5% T3 mix, the activation energy does not necessarily have to be greater for the

5% T3 mix. The activation energy depends on the rate of change of reaction rate (k) at different temperatures and not the individual reaction rate at each temperture.

Table 3.2. Reaction rate of ordinary portland cement and 5% T3 mix using single linear approximation method

Temperature (°C)		15	25	35	45	55
Reaction rate (J/kg/s)	**OPC**	2.65	4.83	8.36	13.34	20.12
	5% T3	3.91	6.79	12.49	20.57	32.70

The variation of natural logarithm (ln(k)) versus the inverse of absolute temperature (1/T) for the two mixes are given in Figure 3.13a and 3.13b respectively. According to Arrhenius equation (Equation 2.2), the slope of the graphs of ln(k) versus 1/T were multiplied with negative of universal gas constant to obtain the activation energy. The calculation was repeated to obtain the apparent activation energy for each of the mixes for which isothermal calorimetry tests were conducted.

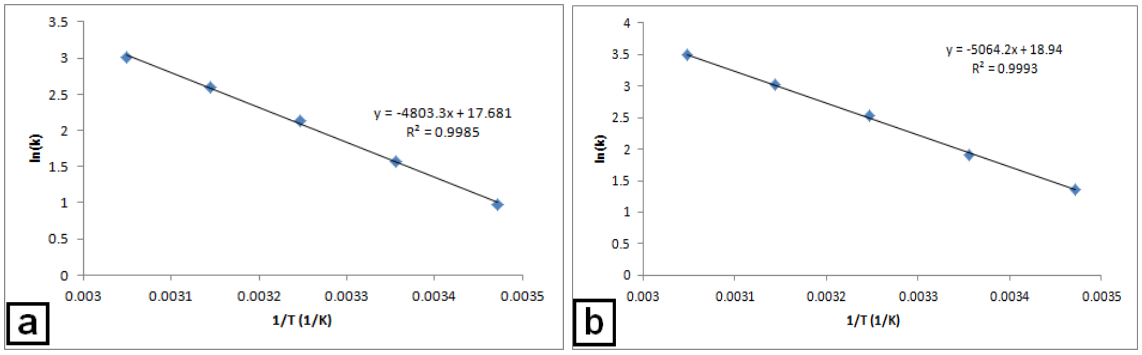

Figure 3.13. Variation of natural logarithm of reaction rate (ln(k)) with inverse of temperature (1/T) for (a) ordinary portland cement and (b) 5% T3 cement paste mix obtained using single linear approximation method

Table 3.3 lists the activation energies calculated using the linear method for all the mixes. Compared to the portland cement, all the cement-filler mixes exhibited a higher activation energy. The activation energy for the 10% mix for each filler was greater than the activation energy for the 5% mixes of the same filler. That is, increasing the dosage of filler resulted in an increase of the activation energy of the cement-filler mixture. Thus, it can be concluded that the inclusion of very fine but inert fillers can increase the activation energy of cementitious mixtures.

Table 3.3. Activation energy calculated according to linear approximation method

OPC	5% L3	10% L3	5% T1	10% T1	5% T2	10% T2	5% T3
39.93	40.23	40.85	39.96	40.45	40.43	41.15	42.10

3.3.9 Activation Energy Using Modified ASTM C1074 Method

The modified ASTM model calculates the activation energy of cement mixes using the parameters obtained from the three parameter model for cement hydration data. The degree of hydration was obtained from the calorimetry data for each mix, using Equation 2.3 and 2.4. The degree of hydration was modeled according to the three parameter model given in Equation 2.5 to obtain the parameters α_u, τ and β. The hydration time parameter (τ) at different temperatures for a mix was used to calculate the activation energy using Equation 3.1. For comparison of trends between different mixes, the data and calculation procedure are explained for two mixes: ordinary portland cement mix and 5% T3 mix. Similar procedure was followed for all the mixes and activation energy for all the mixes tested are listed in Table 3.4.

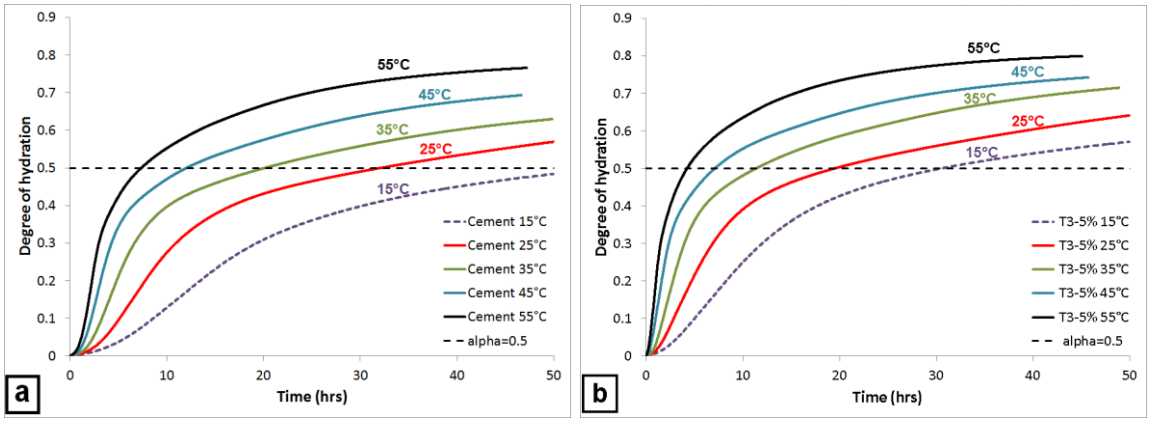

Figure 3.14. Degree of hydration of (a) ordinary portland cement and (b) 5% T3 cement paste mix obtained from isothermal calorimetry data at 15, 25, 35, 45 and 55 °C

Figure 3.14a and 3.14b shows the degree of hydration obtained at various temperatures for ordinary portland cement and 5% T3 mix respectively. The degree of hydration data is similar to the cumulative heat release curve shown in Figure 3.4. In each graph it can be observed that the degree of hydration at any time increases with an increase in temperature. This shows that cementitious mixes hydrate faster with an increase in temperature.

If the data at the same temperature are compared for the two mixes, it can be observed that 5% T3 attains a greater degree of hydration at any time when compared to the ordinary portland cement mix. For example, the degree of hydration at 50 hours for the 15°C experiments were 0.48 and 0.57 for the ordinary portland cement and 5% T3 mixes respectively. Alternatively, the time required to attain a certain degree of hydration is lower for the 5% T3 mix. For example, comparing the 15°C data, 5% T3 attains a degree of hydration of 0.50 at 30.45 hours compared to ordinary portland cement mix, which attains α=0.50 at 56.10 hours. Similar higher degree of hydration was observed for all the nanoparticle-cement mixes when compared to the ordinary portland cement mix.

The degree of hydration data was modeled according to the three parameter model given in Equation 2.5 to obtain the parameters α_u, τ and β using a least square fit of the exponential function. The values of α_u, τ and β obtained for all the mixes are listed in Table 3.4. Comparing the value of α_u, it can be observed that the inclusion of nanoparticles results in an increase in the value of α_u demonstrating that the maximum degree of hydration is higher for the nanoparticle-cement mixes. The increase in α_u and hence the maximum degree of hydration is greatest for the most dispersed nanoparticle (T3) and α_u increases with increasing dosage of the nanoparticle. It was also observed that β decreases due to the inclusion of nanoparticles. Thus nanoparticles result in higher degree of hydration during initial stages of the reaction due to heterogeneous nucleation.

For each of the mixes, it can be observed that an increase in the temperature resulted in a decrease in τ. Thus the increase in temperature accelerated the reaction as well as decreased the time at which the peak rate of hydration occurs. This was earlier observed in the rate of hydration graph, cumulative heat of hydration data as well as the degree of hydration data. When different cementitious mixes at the same temperature are compared it can be observed that the inclusion of nanoparticles resulted in a decrease in τ, reiterating the observation from previous data that nanoparticles accelerated hydration of cement. From Table 3.4 it can also be observed that higher the dosage of nanoparticles the lower is the value of τ, showing a greater acceleration of hydration with higher dosage of nanoparticle. The greatest decrease in value of τ was observed in the 5% T3 mix, which was the smallest nanoparticle tested in this research. Thus by comparing the values of α_u, τ and β it can be concluded that nanoparticles results in acceleration of

hydration, greater initial degree of hydration and possibly greater final degree of hydration due to heterogeneous nucleation.

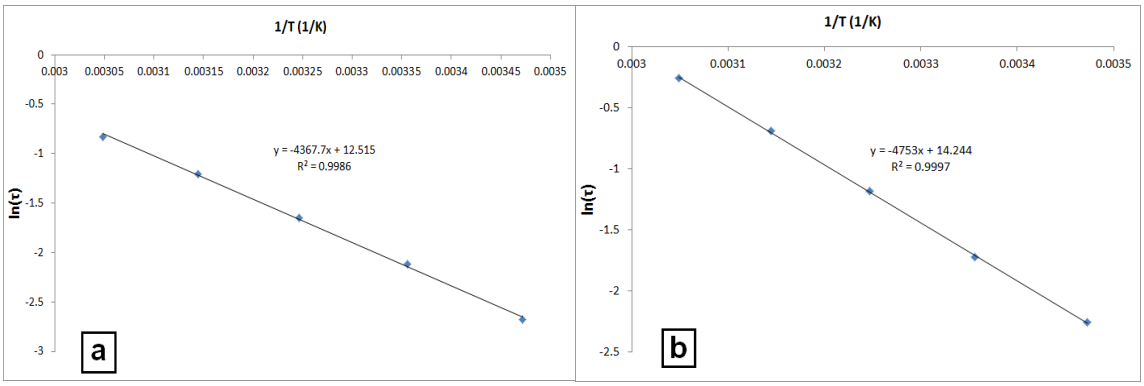

Figure 3.15. Variation of natural logarithm of hydration time parameter (ln(τ)) with inverse of temperature (1/T) for (a) ordinary portland cement and (b) 5% T3 cement paste mix obtained using modified ASTM C1074 method

Figure 3.15 shows the variation of the natural logarithm of the hydration time parameter (ln(τ)) versus inverse of absolute temperature (1/T) for ordinary portland cement and 5% T3 mix, according to Equation 3.1. The apparent activation energy was calculated by multiplying the negative of the slope of plot of ln(τ) versus 1/T with the universal gas constant. The activation energy for ordinary portland cement and 5% T3 mix was calculated to be 36.31 kJ/mol and 39.52 kJ/mol respectively. The activation energy was calculated similarly for all the mixes and is listed in Table 3.4. Thus it was observed that the inclusion of nanoparticles resulted in an increase of the activation energy of the cementitious mix. This was the same trend that was observed when activation energy was calculated according to the linear slope method.

Table 3.4. Activation energy (Ea) and parameters of three parameter model (α_u, τ and β) cement mixes calculated according to modified ASTM C1074 method

Mixture	T (°C)	α_u	β	τ (h)	R^2	E_a (kJ/mol)
Cement	15	0.60	1.30	14.60	0.996	36.31
	25			8.31	0.998	
	35			5.19	0.998	
	45			3.33	0.999	
	55			2.30	0.995	
5% L3	15	0.64	1.19	12.56	0.998	36.82
	25			7.45	0.997	
	35			4.35	0.999	
	45			2.84	0.998	
	55			1.96	0.998	
10% L3	15	0.68	1.10	11.89	0.997	37.97
	25			7.08	0.997	
	35			4.03	0.999	
	45			2.57	0.998	
	55			1.77	0.999	
5% T1	15	0.65	1.16	14.02	0.998	36.82
	25			8.13	0.998	
	35			4.95	0.998	
	45			3.28	0.998	
	55			2.12	0.998	
10% T1	15	0.70	1.05	13.87	0.998	37.65
	25			8.83	0.991	
	35			5.02	0.998	
	45			3.18	0.997	
	55			2.11	0.998	
5% T2	15	0.71	1.02	13.52	0.998	37.58
	25			7.77	0.998	
	35			4.35	0.992	
	45			2.94	0.997	
	55			2.02	0.998	
10% T2	15	0.70	0.97	11.70	0.995	38.79
	25			7.24	0.998	
	35			4.20	0.994	
	45			2.50	0.998	
	55			1.69	0.999	
5% T3	15	0.68	0.97	9.51	0.997	39.52
	25			5.60	0.999	
	35			3.27	0.998	
	45			1.99	0.997	
	55			1.29	0.998	

The classical definition of activation energy could result in a notion that since reaction rate at all temperatures are lowered the activation energy of hydration should also be lower when nanoparticles are added to cement. But activation energy is calculated based on the relative change of the reaction rate at different temperatures and not on the absolute reaction rate at any temperature. Thus, the authors would like to reiterate that the acceleration (or deceleration) of cement hydration reaction at a temperature does not

imply that the activation energy would be lowered (or increased). For example, researchers have earlier observed a decrease in the apparent activation energy of cement hydration when retarding admixtures were used in cement [77]. In the current research it was observed that the inclusion of nanoparticles increased the cement hydration rate as well as increased the apparent activation energy of cement mixes.

The activation energy calculated for cementitious materials is a representation of "apparent" activation energy of the combined hydration reaction that includes reaction of several minerals, producing several products based on a reaction mechanism that changes with time. Thus, apparent activation energy for cement should not be treated as potential energy to be overcome for a reaction to proceed as defined in the classsical definition of the Arrhenius theory. Apparent activation energy should instead be considered as a measure of the temperature sensitivity of the hydration reaction and as a tool to understand and compare the temperature sensitivity of different cementitious mixtures. In the current research it was observed that the inclusion of nanoparticles of various sizes resulted in an increase in the activation energy of the cement mixes. The increase in activation energy with nanoparticle additives thus demonstrates an increased sensitivity to tempearture.

Portland cement reacts with water as a combination of surface controlled (homogeneous nucleation) reaction and diffusion controlled reaction. The presence of nanoparticles in cement results in increased cement hydration due to heterogeneous nucleation, an additonal reaction mechanism [53, 140]. The hydration reactions is less dependant on diffusion controlled process in the presence of nanoparticles. Aqueous diffusional-controlled processes have activation energies less than 20 kJ/mol, while

processes controlled by rates of chemical reaction tend to have significantly higher activation energies [71]. Previous research has shown that higher apparent activation energies are observed during hydration that is less dependent on diffusion (in the presence of slag) [79]. Thus the combination of reactions due of heterogenous nucleation, homogeneous nucleation and diffusion controlled reaction could result in an apparent activation energy which is greater than ordinary portland cement mix.

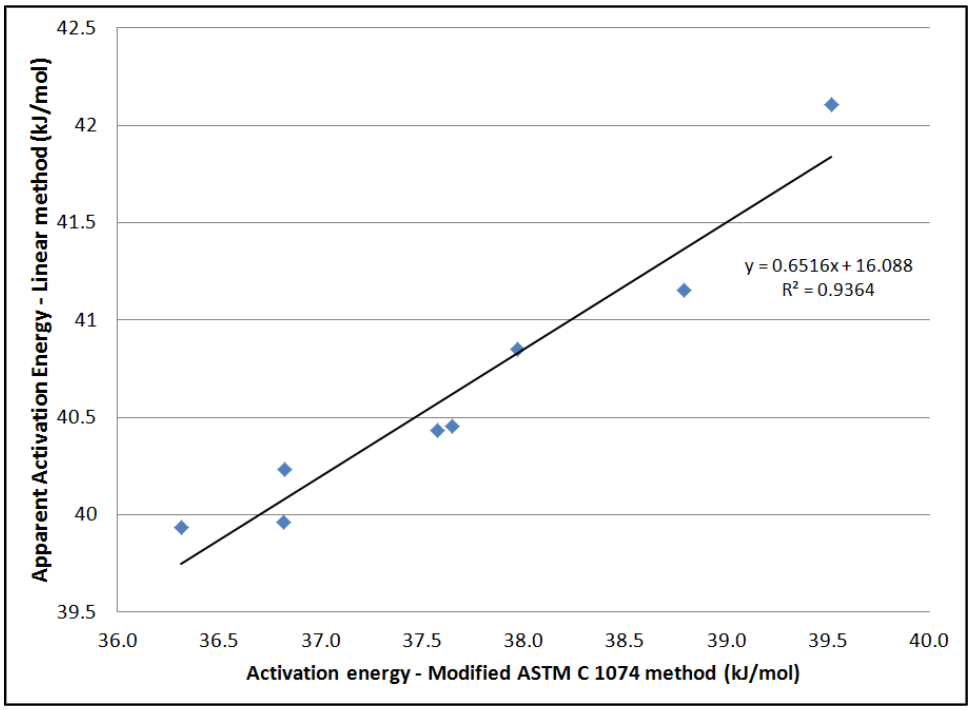

Figure 3.16. Comparison of activation energy of nanoparticle-cement mixtures calculated using linear method and modified ASTM C1074 method

The values of apparent activation energy calculated using the linear slope method was greater than the values calculated using modified ASTM C1074 method. But of greater significance is the for comparison of the relative trends between the different mixes when compared to ordinary portland cement. Figure 3.16 shows the comparison of the activation energy obtained using linear method and modified ASTM C1074 method.

It can be observed in Figure 3.16 that the trend followed by activation energy calculated using both the methods is similar with good correlation between the R^2 values (0.936). Thus for cementitious mixtures containing nano and other fine fillers, both linear as well as modified ASTM C1074 method can be used to calculate the apparent activation energy values, especially when used as a tool to compare between different combination of materials.

These results show that the temperature sensitivity of cement hydration reactions increase due to the inclusion of these nanoparticles. Hence reaction of cement with water is accelerated much greater in nanoparticle-cement mixes compared to ordinary portland cement mixes, when exposed to similar changes in temperature. A higher ambient temperature could result in much faster setting and strength gain in nanoparticle-concrete mixes and hence a faster turnover time. But, the negative impacts of increased thermal stresses should also be considered due to increased temperature sensitivity and higher temperatures.

3.3.10 Powers' Model for Cement Hydration

The Powers' model was utilized to model variation of chemical shrinkage with respect to degree of hydration according to Equation 3.1. Filler-cement mixes at 0%, 5%, 10% and 15% of cement replacement with filler was modeled and compared with experimentally chemical shrinkage results.

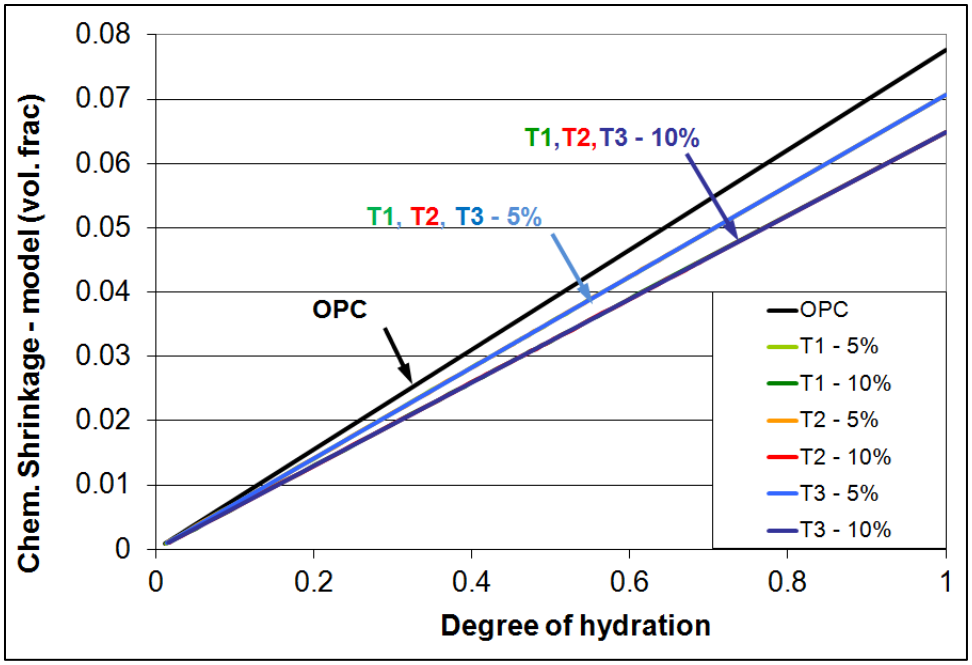

Figure 3.17. Variation of chemical shrinkage of TiO_2-cement mixes with degree of hydration according to Powers' model

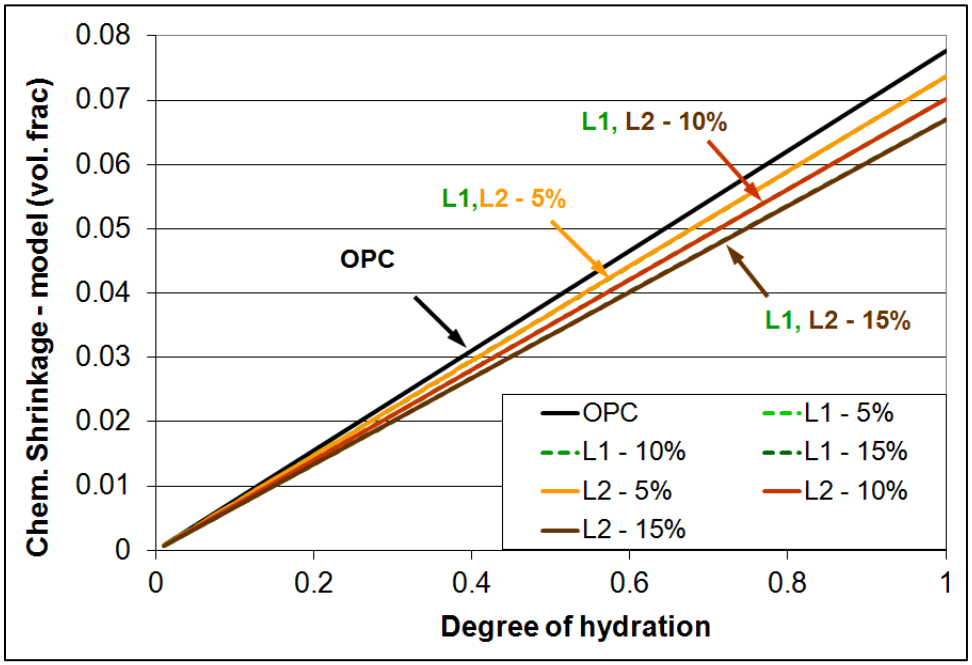

Figure 3.18. Variation of chemical shrinkage of limestone-cement mixes with degree of hydration according to Powers' model

Figure 3.17 and Figure 3.18 shows the variation of chemical shrinkage of filler-cement mixtures with TiO_2 and limestone respectively, according to the Powers' model.

Table 3.5 lists the modeled chemical shrinkage values of the TiO_2 and limestone filler cement mixes at complete hydration (α=1). It can be observed from Figures 3.17 and 3.18 and Table 3.5 that the replacement of cement with filler decreased the chemical shrinkage of the filler-cement mixture. The decrease in chemical shrinkage is proportional to the degree of hydration as well as the dosage of filler, as would be expected.

Table 3.5. Chemical shrinkage of cement mixes at 100% hydration obtained using Powers' model and experimental data (extrapolated)

		Powers' model	Experimental data (extrapolated)
OPC		0.078	0.066
L1	5%	0.074	0.067
	10%	0.070	0.063
	15%	0.067	0.060
L2	5%	0.074	0.076
	10%	0.070	0.074
	15%	0.067	0.073
T1	5%	0.071	0.063
	10%	0.065	0.064
T2	5%	0.071	0.066
	10%	0.065	0.064
T3	5%	0.071	0.597
	10%	0.065	0.602

Figure 3.17 and the data in Table 3.5 (Powers' model) for the TiO_2–cement mixtures demonstrate that the chemical shrinkage of filler-cement mixtures depends only on the dosage of the filler and not on the type (i.e., size) of TiO_2 used. Similar behavior

was observed in the limestone-cement mixes. It is clear, based upon the model parameters, that Powers' equation only considers the dosage and the density of the filler and does not consider effect of particle size of filler on hydration reaction.

To examine the goodness of fit as hydration proceeds, Figure 3.19 shows the variation of the experimental chemical shrinkage with degree of hydration for the TiO_2-cement mixes. During initial stages of hydration ($\alpha<0.3$) there is a greater difference between the experimental chemical shrinkage of the TiO_2-cement mix, and with increasing degree of hydration the difference between chemical shrinkage decreases. Thus, at initial stages of hydration ($\alpha<0.3$), a higher chemical shrinkage is observed in the ordinary portland cement mix compared to the TiO_2-cement mixtures, an opposite trend as observed in the Powers' model calculations.

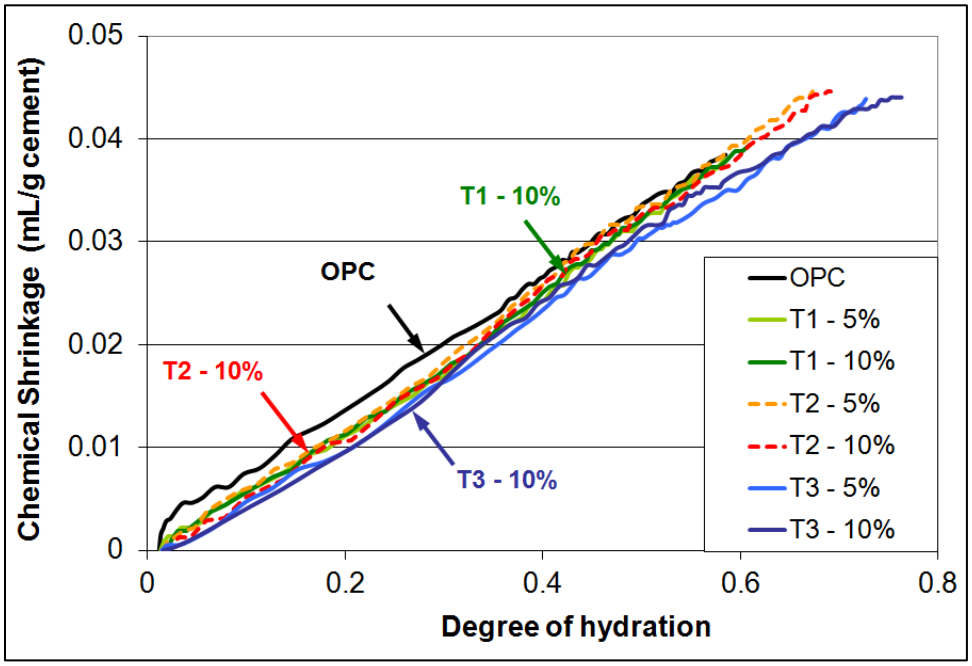

Figure 3.19. Variation of chemical shrinkage of TiO_2-cement mixes with degree of hydration using experimental data

Figure 3.19 also shows that the type of TiO_2 affects the chemical shrinkage; T3 resulted in greatest difference compared to the plain cement mix. The difference of experimental chemical shrinkage from the modeled chemical shrinkage (Figure 3.17) could be due to heterogeneous nucleation effect in the presence of fine inert fillers. The Powers' model [47] considers only dilution effect of fillers and does not consider heterogeneous nucleation effect. Thus the increased rate of hydration in the presence of fine inert fillers and hence the variation in chemical shrinkage could not be modeled according to the Powers' model.

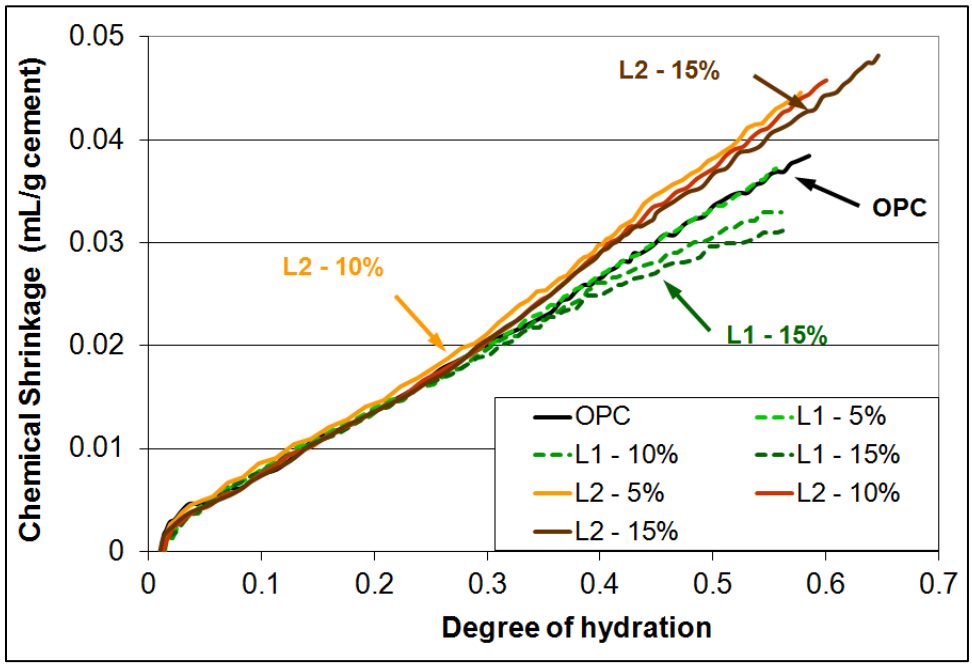

Figure 3.20. Variation of chemical shrinkage of limestone-cement mixes with degree of hydration using experimental data

Figure 3.20 shows the variation of experimental chemical shrinkage for the limestone-cement mixes. The chemical shrinkage values of L1-cement mix during initial stages of hydration were similar to plain cement. With increasing degree of hydration the L1-cement mixes exhibited a decreasing chemical shrinkage compared to plain cement

mix. Thus, the trend of experimental chemical shrinkage of limestone L1 compared to plain cement paste is similar to that observed in the Powers' model chemical shrinkage (Figure 3.18). These results show that Powers' model can be used to predict the trend of chemical shrinkage of filler-cement mixtures when coarse fillers (>3μm particle size) are used, or, that is, when dilution effect is dominant.

Figure 3.20 also shows that the experimental chemical shrinkage of L2-cement mix was greater than the plain cement mix, at later stages of hydration. Although this graph is similar to the variation of chemical shrinkage with time (Figure 3.8d), the trend is not similar to the Powers' model chemical shrinkage since the Powers' model predicted a lower chemical shrinkage in filler-cement mixes when compared to plain cement mix. The effect of finer limestone fillers and model parameters thus needs further research, since the possible formation of hemi- or mono-carboaluminate phases in the presence of limestone could be resulting in additional reaction products not considered in the model and affecting chemicals shrinkage results [54].

The comparison of Powers' model with experimental chemical shrinkage results shows that the Powers' model can be used to predict trends of filler-cement mixes when coarse fillers are used and when dilution effect is dominant. The results from this research show that Powers' model is not applicable to filler-cement mixtures where the filler modifies the cement hydration reaction due to heterogeneous nucleation. Comparing the data in Table 3.5, it can be observed that the experimental and Powers' model values of chemical shrinkage do not match, even if the standard deviation of the experimental results is considered, A trend is not evident between different filler-cement mixes or different dosages of the same filler. Thus, further research is required to predict

chemical shrinkage using Powers' model for filler-cement mixtures, and in particular to consider variations in cementitious mixture composition which may affect model accuracy, and also to modify Powers' model to include the effect of heterogeneous nucleation on cement hydration and chemical shrinkage.

3.4 Summary

The effect of nano and micro fillers of TiO_2 and limestone on the early age properties of cementitious materials was examined in this chapter. The conclusions for this part of the research are summarized below.

- High surface area inert particles (<3μm) can be used to accelerate and increase rate of cement hydration due to dominant heterogeneous nucleation effect. Larger inert particles (>3μm) can be used to maintain the rate of cement hydration due to dominant dilution effect.
- Chemical and autogenous shrinkage increases due to the addition of high surface area inert particles, but coarser inert fillers decreases shrinkage due to dilution effect.
- Apparent activation energy and hence temperature sensitivity of cementitious mixes increases due to the addition of nanoparticles. Activation energy increases with dosage, dispersion and surface area of nanoparticles.
- Powers' model can be used to model trends of filler-cement mixes when coarse inert fillers are used. But the Powers' model has to be modified to predict chemical shrinkage values and trends and the updated model should also consider modification of cement hydration in the presence of finer inert fillers

(heterogeneous nucleation effect) and the formation of additional products, including those not present in traditional portland cement binders but potentially formed in limestone-cement mixtures.

The results from the investigation of the early age properties of cementitious materials with nano and microparticles of TiO_2 and limestone demonstrate that inert fillers can be used to tailor early age properties. The effect of filler on early age properties (hydration rate, shrinkage and temperature sensitivity) depends on the particle size and dosage of filler and was not significantly affected by the type of inert filler used. Thus any inert filler could potentially cause similar effects on early age hydration. Hence, after selecting the particle size of the filler for modification of early age properties, any filler type could be selected based on expected impact on cost, modification of late age properties, novel properties (e.g. photocatalysis) and environmental impact due to the inclusion of the filler in cementitious materials.

CHAPTER 4

LONG TERM PROPERTIES OF CEMENTITIOUS MATERIALS WITH NANO AND MICROPARTICLE ADDITIVES

4.1 Introduction

Long-term properties of cementitious systems can be affected by addition of nano and microparticles to cement because of their potential to modify porosity, pore size distributions and permeability [9]. The long-term performance, especially strength and durability of cementitious materials could also impact sustainability of construction materials [85]. Thus, due to the increasing application of TiO_2 and limestone modified cementitious systems and their potential for environmental benefit, it is crucial that the long term performance of this emerging class of materials be examined more comprehensively.

In the previous chapter as well as in recent research (including that by the current author), TiO_2 nanoparticles and sub-micron sized limestone have been shown to accelerate cement hydration by providing additional surfaces causing heterogeneous nucleation of hydration products [53, 63, 140, 141]. Since cement hydration has a strong influence on the pore structure, the presence of fine fillers, which nucleates the growth of hydration product, could modify the pore structure and hence affect porosity and permeability.

In this chapter, the effects of the addition of several commercially available TiO_2 nanoparticles and limestone microparticles on the long term properties of cementitious materials are examined. In the long term tests, analysis of compressive strength

development, permeability, surface resistivity, and pore size distribution were conducted, all at varying percentages replacement of cement with TiO_2 and limestone. The overall aim of this section of the research was to better understand the influence of the TiO_2 and limestone fillers in the nano and microparticle size range on long term cementitious materials properties and to further tailor cementitious materials to possibly achieve desired long term properties.

4.2 Experimental Procedure

4.2.1 Materials

Commercially available TiO_2 and limestone powders, of different particle sizes and surface areas, were utilized for this research. Ordinary ASTM C 150 Type I portland cement (Lafarge) with median particle size of 10.08 μm was used and had a potential Bogue composition of 51.30% C_3S, 19.73% C_2S, 8.01% C_3A and 9.41% C_4AF and 0.40% Na_2O_{eq}. Table 3.1 lists the properties of the different fillers that were added to the cement and shows that the titanium dioxide powders' surface areas are greater and the particle size smaller than the limestone powders.

The effect of replacement of cement with TiO_2 and limestone at 5% and 10% on the hydration of ordinary portland cement at a constant water-to-solids ratio of 0.50 by mass was examined. Superplasticizers or other chemical admixtures were not added in any of the mixes because researchers have noticed that hydration reaction is affected by the presence of these additives [9].

Cement paste samples were used for the specific surface area analysis and strength tests and concrete samples were used for the chloride permeability and surface resistivity tests. The mixing procedure for cement pastes was conducted according to ASTM C 305 [129] and for concrete according to ASTM C 192 [142], with the following modification to mixing for the cement-filler mixes. In the cement mixes with fillers, the filler was initially added to the entire quantity of the water and mixed for 60 seconds using a handheld mixer at medium speed. This was followed by addition of cement and other materials (if any) and mixing according to the ASTM standard. The concrete mix design that was used for the rapid chloride permeability test and surface resistivity tests is listed in the Table 4.1.

Table 4.1 Concrete mix design used for chloride permeability and surface resistivity tests (for 1 cu. yd. concrete)

	0% filler mix (lbs)	5% filler mix (lbs)
Water	315	315
Cement	630	598.5
Coarse Aggregate	1746	1746
Fine Aggregate	1277	1277
Filler	0	31.5

4.2.2 Test Methodology

4.2.2.1 Strength Test

Compressive strength tests of cement pastes at different replacement rates of TiO_2 and limestone was determined using ½" (2.54cm) cement paste cubes. Samples were prepared according to ASTM C305 [143], cast in plastic cube molds and were vibrated in the molds for better compaction. The samples were demolded after 24 hours of curing at 100% RH, and stored in limewater at room temperature (23±2°C) until the compression testing. To ensure similar condition among all the samples at the time of the testing, the samples were maintained to be wet until just prior to testing. Samples were tested at 1, 3, 7, 14 and 28 days of age.

Tests were performed on samples of w/s=0.50 and at TiO_2 and limestone replacement rates of 10% dosage rates. A loading frame (Instron Satec Materials Testing Machine) with a capacity of 100kN (22kips) was used in a load controlled test. A loading rate of 500 lbs/min (226 kg/min) was used for the compressive strength tests. At least twelve samples were tested per sample type and age and results were averaged.

4.2.2.2 Pore Size Distribution

Nitrogen adsorption and desorption technique for porosity measurements was conducted using a Micromeretics ASAP® 2020 accelerated surface area and porosity analyzer. The relative pressure range used for the adsorption and desorption was from 0.002 - 0.995. Surface area was calculated using the BET [144] analysis method, over a relative pressure range of 0.05 – 0.30 on the adsorption isotherm. Total pore volume available to nitrogen (in the size range 3 – 40 nm pore radius), average pore width are pore size distribution were calculated using the Barrett, Joyner, Hallenda (BJH) [145] method using the data from the desorption isotherm.

Although researchers have noted that surface area measurements vary with technique, adsorbate and sample preparation [146], the use of nitrogen adsorption-desorption technique and comparison of results using BET surface area and pore size analysis using BJH desorption is regularly used for comparing among companion cement samples [147]. The variations due to sample preparation were minimized in this research by preparing samples using the same methodology. The samples used in this research were prepared similarly by curing at 100% relative humidity. Samples at 1, 3 and 28 days of curing and were freeze dried and stored under sealed conditions until further testing. The results from the 28-day cured samples could be used to compare long-term surface area and pore structure of the ordinary portland cement and filler-cement mixtures.

4.2.2.3 Rapid Chloride Permeability Test

The rapid chloride permeability test (RCPT) can be used to determine the relative permeability of concrete samples. The test is conducted according to ASTM C1202 [148], where the coulomb value of the total charge that passes through concrete is used as a measure of concrete permeability. The charge passed depends on the pore structure as well as the pore solution chemistry in concrete [149]. The charge passed correlates to the resistance of the concrete specimen to chloride ion penetration, an indirect indication of the permeability of concrete [150-152]. Research has shown that the charge passed in RCPT in a plain cement concrete was well correlated with the chloride penetration data obtained from a 90-day ponding test [153]. But researchers also note that the values may be inaccurate if the concrete is atypical – concrete with SCMs or chemical admixtures. Researchers have also raised concern about the ability of RCPT to determine the chloride

permeability of concrete mixtures containing mineral admixtures including silica fume, slag and fly ash [153], since the test measures the movement of all ions present and not just chloride ions. The movement of ions, especially in high permeability concrete can increase the temperature, which in turn can increase the charge passed [149].

In the current research, concrete cylindrical (4”x8”) samples were prepared at w/s=0.50 and stored in saturated lime water for 28 or 56 days before testing. The samples were then cut to 2” slices using a water cooled diamond saw to obtain 2 cut faces on each side. The cut samples were placed in a desiccation chamber and a vacuum less than 1mm Hg was applied for 3 hours using an electric pump. De-aerated water was introduced into the chamber while maintaining vacuum till all the samples were submerged and the pump was allowed to run for 1 hour. After the 4-hour desiccation and introduction of water, the vacuum was removed and the samples were allowed to return to atmospheric pressure and left submerged for 18 hours.

The fully saturated specimen was then subjected to a 60 V DC voltage for 6 hours, with one face exposed to a 3% sodium chloride (NaCl) solution and the other face exposed to a 0.3M sodium hydroxide (NaOH) solution. The RCP test procedure according to ASTM C 1202 was followed for the test [151].

4.2.2.4 Surface Resistivity Test

The surface resistivity test is a relatively new test which is being accepted and implemented in concrete research [152] and a provisional AASHTO test was also released recently (AASHTO TP 95). The surface resistivity test overcomes some of the inherent shortcoming of the RCP test (mentioned earlier), and the specimen conditioning

to be is less time and labor intensive. For concrete testing using surface resistivity, the Wenner array is used which utilizes four equally spaced surface contacts. A small alternating current is passed through the sample between the two outer contract points, and the potential difference between the two inner contact points is measured using a voltmeter. The resistance (R) is measured by dividing the voltage (V) by the current (I). The resistivity of the concrete sample can be obtained by multiplying the resistance with a cell conversion factor, called the cell constant [154]. In the current research, a 4-point Wenner probe (Proceq Resipod) with 1.5" probe spacing was used, and the reading of the resistivity value was directly displayed on the instrument.

Unlike the RCP test, the surface resistivity testing does not damage the sample and the same sample can be reused for testing at different ages. Hence, the surface resistivity testing was conducted every 2-3 days during the first 14 days of age and at least once every 7 days until 56 days of age. The samples were taken out of the curing tank and surface resistivity measurements were conducted under surface wet conditions after wiping off any excess surface water. The measurements were averaged using eight readings taken at 0°, 90°, 180° and 270° and repeated again at 0°, 90°, 180° and 270° along the circumference of the cylinder.

4.3 Results and Discussion

4.3.1 Strength Development

Compressive strength of cement and cement-filler paste samples containing 0% and 10% TiO_2 and limestone was measured at 1, 3, 7, 14 and 28 days of age at water-to-

solids ratio of 0.50. Figure 4.1 shows the strength development trend for ordinary portland cement and filler-cement mixes, depicted using average strength of at least 12 samples. By comparing average strength results, it was observed that during initial stages of hydration (1 day), T1, T3 and L3 had strength greater than or comparable to the ordinary portland cement mix, whereas at later ages (14 and 28 days), the strength of all the filler-cement mixes were lower than the ordinary portland cement mix. But, as observed by the error bars in Figure 4.1, the variation of strength data (standard deviation) associated with each data point was high. The smaller size of the test sample used as well as possible effect of imperfections could have increased the variation in strength data observed in Figure 4.1.

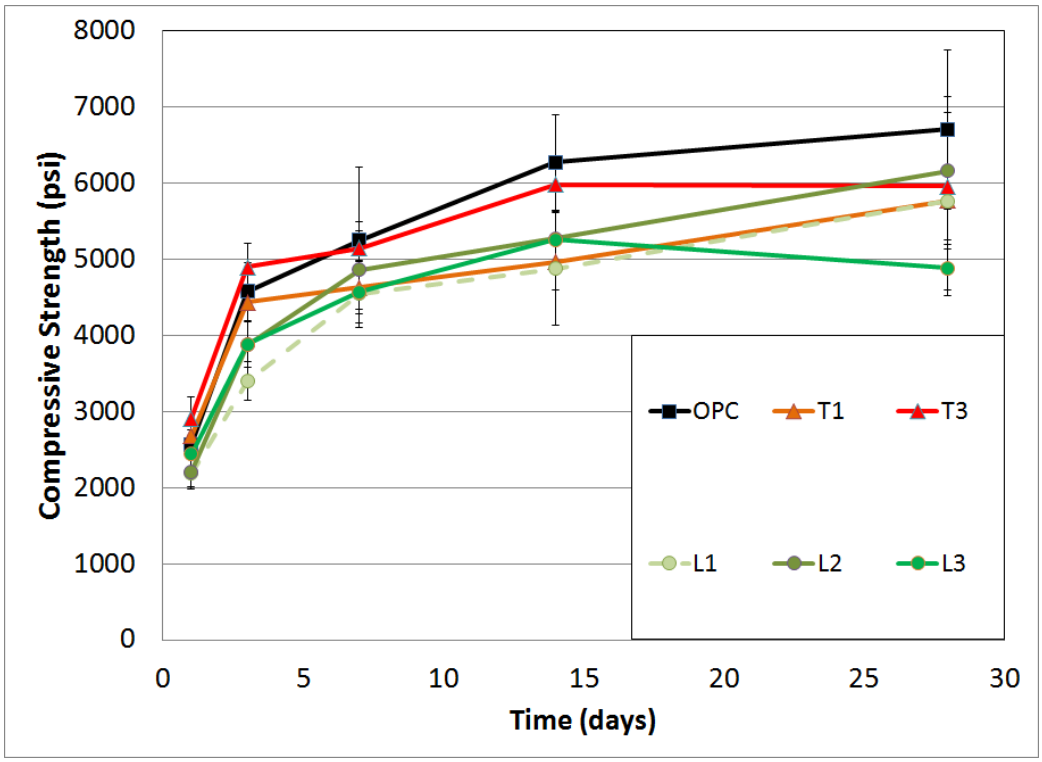

Figure 4.1. Strength test results for TiO_2 and limestone modified cements at 10% replacement rates and at a w/s=0.50

To better compare among the strength test data with high variability (standard deviation), a single factor analysis of variance (ANOVA) test was conducted using a 5% confidence interval. The strength of each individual filler-cement mix was compared with the plain cement mix and the results of the ANOVA test are given in Table 4.2. The results show that at 1 day, the strength of T1 and L3 filler-cement mixes can be considered the same as the strength of the plain cement paste mix. T3 (the smallest particle-sized filler tested) had a higher strength compared to plain cement paste, whereas L1 and L2 (the coarser limestone fillers) had lower strength compared to plain cement. The 28-day ANOVA results show that most of the filler-cement mixes (except for L2) had a strength value that was different from the ordinary portland cement mix. The lower average strength of all the filler-cement mixes, as shown in Figure 4.1, along with the ANOVA results demonstrates that the addition of fillers decreases the 28 day (long term) strength of filler-cement mixes.

Table 4.2. Results from analysis of variance (ANOVA) of strength data

		OPC-T1	**OPC-T3**	**OPC-L1**	**OPC-L2**	**OPC-L3**
P-value	1 day	0.24	0.004	0.0006	0.0009	0.18
	28 day	0.018	0.037	0.026	0.12	0.0004

Figure 4.1 shows that during the initial stages of hydration (1 day), T1, T3 and L3 cement-filler mixes had strength higher or comparable to the ordinary portland cement paste mix. The mix which showed greater initial strength than plain cement paste at both 1 and 3 day tests was the T3-cement mix. In the previous chapter on early age properties it was observed that the effect of heterogeneous nucleation was dominant during early

hydration, especially in the first 24 hours of hydration. It was also observed that T3 was the TiO_2 which increased the degree of hydration (total heat released) by the greatest amount in the isothermal calorimetry tests. Thus the higher strength of the TiO_2-cement mix in the 1 and 3 day tests was because of the higher degree of hydration caused by heterogeneous nucleation effect.

The strength of the filler-cement mixes was lower compared to the ordinary portland cement mix at later stages of testing (14 and 28 days). Comparing the 28 day average strength values, it was observed that the strength of the filler-cement mixes ranged from 73% to 92% of the ordinary portland cement mix. The lower strength of the filler-cement mixes could be due to the lower cement content in those mixes since 10% of the cement was replaced with fillers by maintaining a constant w/s. Thus with increasing cement hydration due to a diffusion controlled process [74, 155], the plain cement mix could have a higher content of hydrated cement compared to the filler-cement mixes. Hence at later ages, as more cement undergoes hydration, the total cement content and dilution effect could be the dominant factor which affects properties of cementitious systems. The lower strength of filler-cement mixtures could also be due to shrinkage which was observed to increase, especially with nanoparticle fillers. Shrinkage and shrinkage cracking could also result in a decrease of the strength of cementitious mixtures.

The compressive strength results obtained in this research is similar to that obtained by other researchers who studied the effect of replacement of cement with fillers. Some researchers observed that the replacement of cement with limestone resulted in marginal decrease of 28 day strengths at replacement rate of 15% [20] or even at 5%

replacement rate [156]. But other researchers have observed a marginal increase in 28 day strength for limestone cements with 5% limestone [157]. The increase in compressive strength observed in portland limestone cements is due to the additional grinding of limestone cement (during grinding of clinker) that results in finer cement grains and hence faster and higher degree of hydration and higher compressive strength. In the current research, blended cement was used where the limestone was added to water before mixing of cement with water and hence inter-grinding or reduction of cement fineness was not achieved. Further research is required to compare and understand the relative effects of blended limestone cement compared to inter-ground limestone cements.

4.3.2 Pore Size Distribution

Nitrogen adsorption and desorption technique for porosity measurements was conducted on cement paste sample at 1 and 28 days of age and the surface area was calculated using the BET analysis method and the pore volume and pore width was calculated using the BJH method using the data from the desorption isotherm.

Table 4.3. Results from specific surface area nitrogen adsorption-desorption experiments (28 day results)

	OPC	T1 - 5%	T2 - 5%	T3 - 5%	L3 - 5%
BET surface area (m^2/g)	18.45	22.00	24.35	24.48	23.55
BJH desorption pore volume (cm^3/g)	0.081	0.097	0.105	0.099	0.096
BJH desorption average pore width (nm)	12.68	12.16	12.41	10.84	11.53

Table 4.3 lists the results from the nitrogen adsorption-desorption tests conducted after 28 days of curing filler-cement paste samples at 100% relative humidity. The BET surface area, BJH desorption pore volume and BJH desorption average pore width are listed for the ordinary portland cement paste and the lab-blended cement pastes with TiO_2 particles (T1, T2 and T3) and limestone particle L3.

Compared to the ordinary portland cement paste mix, all the other mixes considered exhibited a higher surface area and pore volume. This could indicate the addition of the fine fillers encourages the formation of a higher surface area C-S-H. Similar increase in surface area was observed by Juenger and Jennings [147] when a chemical accelerator (calcium chloride) was added to cement paste. The larger surface area of the inert filler could also be contributing to an increase in the surface area of the filler-cement paste mix. The surface area results from 1 day and 28 can be compared to further distinguish between the effect of the filler surface area and additional surface area due to hydration product formed in the presence of fine fillers.

Figure 4.2 shows the relative surface area of the filler-cement mixes (at 1 and 28 days) normalized with respect to the surface area of the plain cement mix at that age. Comparing Figure 4.2a and 4.2b, it can be observed that the 28 day relative surface area for each filler-cement mix is greater than the 1 day relative surface area. This increase in relative surface area demonstrates that the higher surface area of filler-cement samples at later ages (28 days results) is not only because of the presence of fine fillers, but also because of increased cement hydration due to the presence of the fine filler. Thus the increase in surface area of the filler-cement mixes at 28 days shows that the fine fillers encourage the formation of hydration product.

The higher surface area observed in the filler-cement mixes in Figure 4.2b could also be due to the possible differences in the morphology of hydration product formed in the presence of fine inert fillers. Thomas et. al. [158] observed that C-S-H formed at higher temperatures had a different atomic packing density and porosity compared to samples cured at lower temperature. Heterogeneous nucleation in the presence of fine inert fillers could be compared to high temperature curing of cement, where both nucleation and higher temperature results in accelerated hydration of cement mixtures. Thus, the acceleration of cement hydration in the presence of fine inert filler could result in microstructural changes and the formation of a hydration product with a different morphology with greater surface area compared to plain cement mixes.

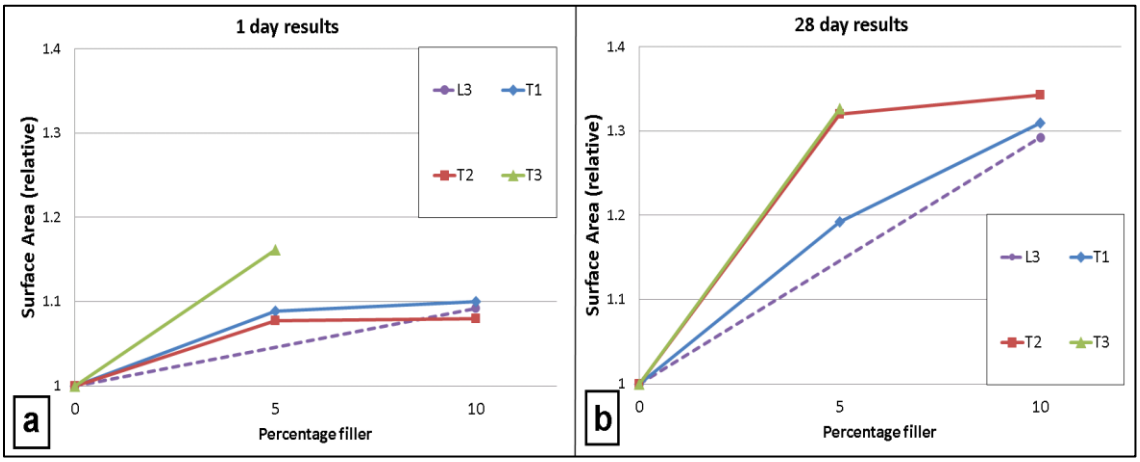

Figure 4.2. Relative specific surface areas of cement paste samples with 0%, 5% and 10% replacement of TiO_2 and limestone filler at (a) 1 day and (b) 28 days of hydration. (Notice that the y-axis scale on both the graphs is maintained equal for easy comparison. The line connecting data points are drawn as guides to the eye)

Results from Table 4.3 also shows that the presence of fine fillers increase the pore volume of cementitious materials. This should be examined more critically [159], as larger capillary pores (>50nm) can increase permeability and compromise durability [9].

It should be considered, for example, if the increase in effective water/cement ratio (since water to solids ratio was kept constant in the mixes) could contribute to an increased pore volume. But if the results of the pore width are examined in Table 4.3, it can be observed that the average pore diameter of the filler-cement mixes is lower than the plain cement mix. Thus, even though there is an increase in the pore volume in the filler-cement mixes, there is a decrease in the average pore width. This shows that a greater number of smaller pores are being formed in the microstructure and thus pore refinement is possibly occurring in the filler-cement mixes.

Figure 4.3 shows the relative pore diameter of filler-cement samples at 1 and 28 days with respect to the plain cement paste sample at the same age. If the results from 1 day and 28 day are analyzed, it can be observed that the pore diameter of the T3 sample is the lowest compared to all other samples. It was observed earlier that T3 causes greatest increase in hydration (Chapter 3 and [53]) among all the fillers tested in this research. In the 28 day results the decrease in pore diameter was also greater for higher percentage addition of fillers as well, indicating that greater dosage of fine inert filler results in greater reduction of average pore diameter. Thus, the higher degree of hydration, with formation of hydration products (e.g. C-S-H) with an intrinsic finer microstructure, could be resulting in the reduction of pore diameter of cementitious mixtures.

Figure 4.3b shows that all filler-cement mixes had a pore diameter lower than the plain cement paste. It was earlier observed in Figure 4.3b that the surface area increases with addition of fillers. These two results combined demonstrate that the pore spaces are being filled with cement hydration product (e.g., C-S-H) resulting in an increase in the

surface area and a decrease in average pore width which results in pore refinement. The pore size refinement shows that in the fine filler-cement mixes, lesser number of large capillary pores (>50nm) are possibly formed and greater number of smaller pores (<50nm) are formed. Researchers have earlier shown that the number of capillary pores larger than 50nm inversely affects permeability [89]. Thus, the lesser number of pores of size greater than 50nm possibly being formed in the filler-cement mixes could result in improved permeability properties.

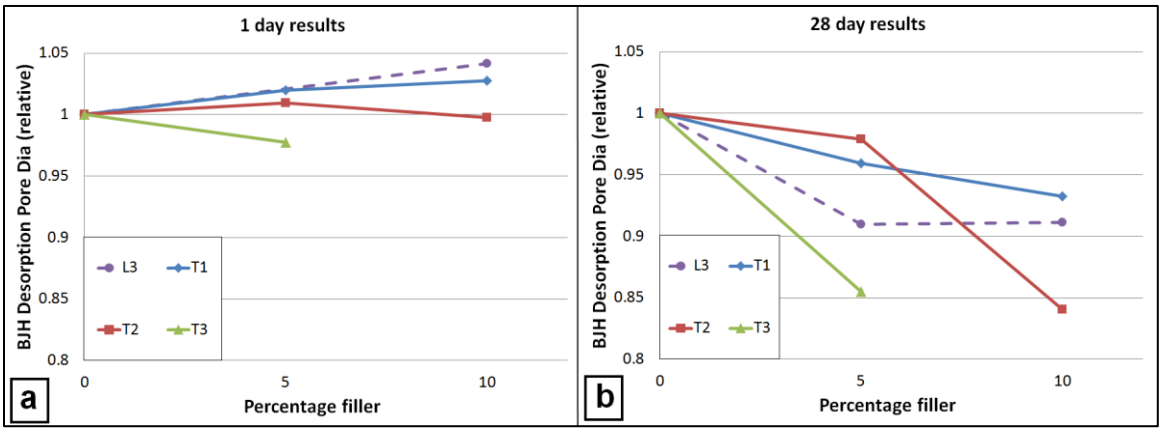

Figure 4.3. BJH desorption average pore diameter of cement paste samples with 0%, 5% and 10% replacement of TiO_2 and limestone filler at (a) 1 day and (b) 28 days of hydration (The line connecting data points are drawn as guides to the eye)

4.3.3 Rapid Chloride Permeability Test

The rapid chloride permeability test (RCPT) can be used to determine the relative permeability of concrete samples. The test was conducted according to ASTM C1202 [148], where the charge that passes through concrete measures the chloride ion permeability and the result is used as an indirect measure of concrete permeability.

Table 4.4 lists the results from the rapid chloride permeability test. All concrete mixes resulted in RCP test values greater than 4000C at 56 days indicating that the

chloride ion permeability for these mixes was high [148]. The high chloride ion permeability could be due to the higher water content (w/s = 0.50) in these mixes. But the results can be used for comparison between the filler-cement mixes with respect to the plain cement concrete mix. The results show that compared to the ordinary portland cement concrete mix, all the filler-cement mixes (except for L3 at 56 days) had a marginally higher amount of charge that passed through the concrete sample. This result shows that concrete mixtures made with limestone and titanium dioxide could have a marginally higher permeability. The concrete mixture with 5% replacement of cement with limestone L3 had RCPT results very similar to the ordinary portland cement mix. The 28 and 56 day results were within 2% of the result for ordinary portland cement. This shows that the use of fine limestone (with particle size 0.7μm) does not affect the RCPT result and possibly the permeability of concrete mixtures.

Table 4.4. Rapid chloride permeability test results for TiO_2 and limestone concrete mixes at 0% and 5% replacement rate

	28 day (C)	Average of 28 day results (C)	56 day (C)	Average of 56 day results (C)
OPC	5408	5408	5318	5318
L1	5765	5747	5490	5487
L2	5968		5743	
L3	5507		5228	
T1	5511	5791	5821	5984
T2	5963		6049	
T3	5898		6082	

There was no obvious trend for the RCP test result with respect to the particle size of the fillers that were used in this research. Thus the average of the limestone-cement mixtures and TiO_2-cement mixtures was compared with the ordinary portland cement

mix to broadly understand the effect of the type (chemistry) of these fillers on concrete permeability. The calculation of average RCPT results for all TiO_2-cement mixes and limestone-cement mixes was also justified because at later ages dilution effect would be dominant. The average 28 and 56 day RCPT results for the TiO_2-cement concrete mixes were greater than the ordinary portland cement mix by 6.2% and 12.5% respectively. Thus the replacement of cement with 5% TiO_2 increased the chloride ion penetration by a greater degree compared to the limestone-cement mixtures. The increase in RCPT result could be because of the effective increase in the w/c since in this research the w/s was maintained constant at 0.50. The increase in RCP result shows that the permeability of concrete mixtures with TiO_2 additives could be higher than ordinary portland cement mixes and warrants further investigation.

The average 28 and 56 day results of the limestone-cement mixture were only marginally higher (6.2% and 3.1% respectively) compared to the ordinary portland cement mix. Thus it can be concluded that the replacement of cement with 5% limestone does not change the permeability of concrete mixtures significantly, a result similar to that obtained by previous researchers [49]. In the current research, the limestone particles were added to cement immediately before mixing with water. But inter-grinding of limestone with cement, as usually conducted in the industry for producing portland-limestone cement (PLC), could result in an increase in cement fineness. In such inter-ground limestone-cement mixtures, the permeability of PLC concrete could be similar to ordinary portland cement because of possible higher degree of hydration due to the smaller cement particle size.

4.3.4 Surface Resistivity Test

The surface resistivity of filler-cement concrete samples prepared at 0% and 5% replacement of cement with filler and at w/s=0.50 was examined using a 4-point Wenner probe with 1.5" probe spacing.

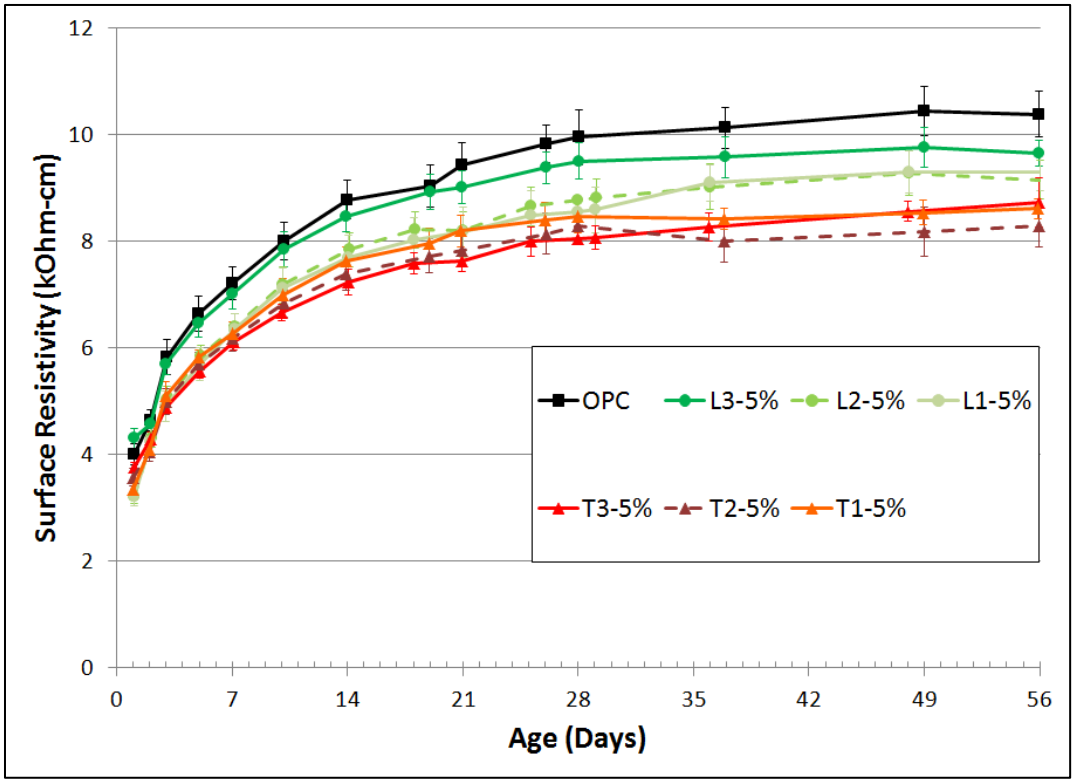

Figure 4.4. Surface resistivity of concrete samples with 0 and 5% titanium dioxide and limestone fillers

Figure 4.4 shows the results of the surface resistivity tests till 56 days of age, conducted on concrete samples stored in a saturated lime water bath at 23±2°C . It can clearly be observed from Figure 4.4 that the ordinary portland cement sample had a higher surface resistivity value than all the filler-cement concrete samples. This result shows that the concrete sample would have greater potential resistance to chloride and other deleterious ion ingress and lower permeability compared to filler-cement mixtures.

Similar to the RCPT results, the L3 limestone-cement concrete mix modified the resistivity value marginally compared to all other fillers used in this research. The 28 and 56 day surface resistivity measurement for the L3 mix was marginally lower than the control concrete mix by 4.5% and 7.1% respectively. This shows that the use of fine limestone (with particle size 0.7μm) does not change the resistivity of concrete significantly, even though there is a dilution of the cement content by 5% (or an effective increase in the w/c in the filler-cement concrete).

The surface resistivity results for L1 and L2 was similar, but both were lower than the control mix by approximately 10-14% at 28 and 56 days of testing. Thus the use of coarser limestone particles (of sizes 3μm and 20μm in this research) resulted in a decrease of the resistivity below the 5% dilution effect. Replacement of cement with TiO_2 decreased the resistivity measurement significantly (for example 5% T2-cement mix reduced the resistivity by 20.2% at 56 days). The drastic reduction of resistivity or increase in conductivity in the TiO_2-cement mixtures could be due to the semiconductor nature of TiO_2. This warrants further investigation with different types of semiconductors and conductors to understand the impact of these materials on the surface resistivity test. Further tests would also help ascertain whether the surface resistivity test can be used as a technique to measure permeability of concrete samples with conductors and semiconductors additives.

4.4 Summary

The effect of nano and micro fillers of TiO_2 and limestone on the long term properties of cementitious materials was examined in this chapter. The conclusions for this section of the research are summarized below.

- Initial strength of filler-cement mixtures was greater than ordinary portland cement mix due to increased degree of hydration because of heterogeneous nucleation effect. When cement was replaced with fillers, dilution effect was dominant at later ages, and the strength of the ordinary portland cement mix was greater than the filler-cement mixtures.
- Surface area and pore size distribution analysis conducted on cement mixtures with nano-TiO_2 and fine limestone (L3) demonstrates that total surface area and pore volume increases when compared to ordinary portland cement mix. Pore size refinement was also evident by the decrease in the average pore width of the filler-cement mixtures tested. Pore size refinement shows a possible reduction in larger porosity (>50nm) as well as disconnected porosity, which can result in decreased permeability of filler-cement mixes.
- The use of fine limestone (0.7μm in this research) did not significantly affect the RCP and surface resistivity of concrete. Thus the permeability of concrete made with limestone could be comparable to ordinary portland cement mixture. The use of TiO_2 increased the RCPT result and reduced the surface resistivity. Thus concrete made with TiO_2 could have higher chloride ion permeability compared to ordinary portland cement mixes.

The results from investigation of the long-term properties of cementitious mixtures with nano and microparticles of TiO_2 and limestone demonstrate that fine fillers can modify the cementitious materials properties by refining pores within the microstructure. The use of fine limestone fillers results in pore refinement as well as concrete permeability comparable to control mixtures. Thus fine limestone can be used as a filler in cementitious mixtures to obtain long term properties comparable to plain cement mixtures, but also effectively reduce cement clinker usage thereby contributing to sustainability.

CHAPTER 5

PHOTOCATALYTIC PROPERTIES

5.1 Introduction

Anatase phase of TiO_2 is photocatalytic and can be used for removal of organic and inorganic pollutants, photo-degradation of pathogenic organisms [94] and self-cleaning and anti-fogging applications [34]. The photoreactivity of TiO_2 is due to the formation of highly oxidizing electron pair holes and hydroxyl radicals which are indiscriminate oxidizing agents [96], with only fluorine exceeding the oxidizing potential of this radical. Research has demonstrated that ultraviolet (UV) illuminated TiO_2 can be used for degradation of nitrogen oxides [160], volatile organic compounds (VOC's) [96] and sulfur oxides in the air [18].

Atmospheric nitrogen oxides or "NO_X" (NO and NO_2) are predominantly responsible for production of ozone in the troposphere and urban smog by reaction with hydrocarbons which are environmental irritants to humans [18, 100]. Moreover, NO_X, together with SO_2 and SO_3, produce acid rain, which can be harmful for vegetation (e.g., forests, crops) as well as aquatic life [97] and the built environment [98, 99]. Thus, decreases in NO_X concentration has been a major focus area for environmental regulatory agencies across the world. In a recent proposal United States Environmental Protection Agency (US EPA) increased the standards for air quality and proposed a new one-hour NO_2 standard at a level of 100 parts per billion (ppb) [161]. Similar air quality standards directives have been proposed in other parts of the world including Japan and Europe [162, 163]. The US EPA also proposes setting up new air monitoring systems in urban

areas near major roads where maximum concentrations are expected. Due to these potential new standards, new technologies will be required for the reduction of NO_X in the atmosphere, especially in urban environments.

There is much interest surrounding the introduction of photocatalytic properties to cement-based materials or other construction materials to address increasing standards on NO_X levels in the air. The inclusion of TiO_2 to construction materials could thus be used as a method to decrease pollutant NO_X gases. The photocatalytic oxidation of NO_X in a steady state by TiO_2 can be represented by [101]:

$$NO + \bullet OH \longleftrightarrow HNO_2 + \bullet OH \longleftrightarrow NO_2 + H_2O \tag{5.1}$$

$$NO_2 + \bullet OH \xleftrightarrow{h\nu} HNO_3 \tag{5.2}$$

For cement or concrete, photocatalytic particles can be intermixed in the bulk material as additive [109] or used in surface coating [164]. Some research has shown effectiveness of such materials to address NO_X levels, especially if the materials are used on or near major roads and in urban areas [39, 95], while other studies have demonstrated that all TiO_2 surfaces might not be effective in photocatalysis in field applications [31, 165]. Variability in lab and field studies on the capabilities of photocatalytic materials suggest a need for review of test methods related to this growing class of cement-based materials.

The surface and near-surface structure and properties of cement-based materials can vary widely with mix proportions, age, finishing operations and curing techniques used during construction, as well as changes during service. Since photocatalysis is

predominantly a surface reaction which occurs in the presence of near-UV and UV radiation [18], the surface properties of the material are expected to affect the test results. In addition, changes in surface and near-surface properties due to hydration or environmental interactions have been shown to measurably affect the rate and efficiency of the photocatalytic reaction on cement-based materials [30, 31, 102].Thus, the surface properties of the material being tested should be considered when characterizing the photocatalytic properties of cement-based or other construction materials, so that comparisons can be conducted between inter-laboratory tests and to ensure reproducibility between different tests.

For example, as discussed in greater detail in a subsequent section, the existing standard test methods [103-105] have to be modified for assessment of photocatalytic efficiency in cementitious materials to consider the distributed pore structure and varying surface characteristics which could affect the photocatalytic properties, as well as intrinsic adsorption of NO_X [166]. Since the cost of TiO_2 is much higher than ordinary portland cement, construction materials typically have low concentrations of TiO_2 which could result in a lower photocatalytic efficiency compared to ceramics or coatings. Hence, any proposed procedures for testing these should also allow for discrimination among materials with relatively low photocatalyst addition rates. Specifically, it is proposed that lower gas concentrations, slower flow rates, longer residence times, and longer test durations are needed to produce data with the fidelity necessary to better discern among myriad potential variations in cementitious materials.

Thus, due to this need for an appropriate standard procedure for characterizing the photocatalytic efficiency of cementitious materials used for reducing NO_X, the main

objective of this section of the research is to propose and evaluate a test method that can be used by researchers as well as field engineers for testing and quantifying photocatalytic activity of cement-based materials. Stemming from this, a new photocatalytic efficiency factor is defined which could be used to characterize and quantify the photocatalytic activity of any photoactive surface. As demonstration, the proposed experimental procedure was used to evaluate various commercially available TiO_2 powders incorporated at different replacement rates in cement paste and the photocatalytic efficiency for these mixtures was measured and compared.

Table 5.1. Comparison of testing, sample and analysis parameters of various tests for testing NO_X conversion performance of photocatalytic materials

		ISO 22197-1	**JIS R 1701-1**	**UNI 11247**	**Proposed test**
Testing parameters	Test gas	NO	NO	NO and NO_2	NO
	Test gas concentration (ppb)	1000ppb	1000ppb	400ppb NO + 150ppb NO_2	500ppb
	Gas flow rate (l/min)	3	3	3	1
	Test duration (hour)	5	5	1	5
	UV light intensity (W/m^2)	10	10	20	10
Sample parameters	Sample area (cm^2)	49.25	49.25	65	Variable
	Sample curing	–	–	–	14 days lime water curing
	Surface preparation	–	–	–	Grinding and polishing
Analysis parameters		η_{ads} (equation 5.3)	Q_{ads} (equation 5.3)	NO_X reduction percentage	PEF or PEF_{RN} (equation 5.4, 5.5)

As discussed earlier, several organizations describe standard test procedures for examination of the air purification capabilities of fine ceramics and other inorganic materials [103-105]. These test methods have begun to be used for the examination of cement-based materials, as well. Table 5.1 lists key features of the existing tests for photocatalytic NO_X conversion as well as the proposed procedure. The rationale and details of the proposed variations in test parameters for assessment of photocatalytic cement-based materials are given in the subsequent sections of this chapter.

5.2 Methodology

The test method that is proposed here is applicable for testing the photocatalytic properties of any cement-based materials which could be in the form of a mixture of a photocatalytic material (for example TiO_2) and cement or a photocatalytic material applied as a top coat to cement-based construction materials. The test method and PEF are demonstrated by comparing performance of cement-based materials containing varying types and amounts of commercially available photocatalytic TiO_2 particles and also by comparison with a photocatalytic ceramic tile.

5.2.1 Materials

Cement paste samples were prepared using a commercially available Type I cement (Lafarge in Atlanta, Georgia, USA) with a Bogue potential composition of 51.30% C_3S, 19.73% C_2S, 8.01% C_3A and 9.41% C_4AF and 0.40% Na_2O_{eq} and commercially available photocatalytic TiO_2 powders. Properties of the photocatalytic TiO_2 examined are shown in Table 5.2. The anatase form of TiO_2 generally demonstrates

a greater potential for photocatalytic activity compared to rutile [92], but there are a few studies which report that a mixture of anatase (70-75%) and rutile (30-25%) is more active than pure anatase [167]. TiO_2 was used in the cement paste mixes as obtained from the manufacturers. Deionized water was used for preparing all the paste samples and no other admixtures were used in the mixes.

Table 5.2. Properties of TiO_2 added to cement, as provided by manufacturers

	Manufacturer	Crystal Size (nm)	Agglomerate Size (μm)	Surface Area (m^2/g)	Purity (%)	Structure
T1	Cristal	20-30	1.5	45-55	>97	100% Anatase
T2	Cristal	15-25	1.2	75-95	>95	100% Anatase
T3	Evonik	21	0.58	50±15	99.5	80% Anatase 20% Rutile
T4	Tayca	30	1.5	52	95-99	100% Anatase
T5	Cristal	67-75	1-2	8-12	>99	100% Anatase

5.2.2 Specimen Preparation

Samples with TiO_2 were prepared at a water-to-solids ratio of 0.50. TiO_2 was used at 5, 10 or 15% of the mass of cement to the mixes for testing photocatalytic activity. Each TiO_2 powder was initially dispersed in deionized water and mixed thoroughly for one minute using a handheld mixer. No special technique or chemicals were used for dispersing the TiO_2 particles to replicate conditions as close as possible to field application. Cement was then added and mixing continued for another 3 minutes.

The pastes were cast in molds to form 5mm thick samples with 50mm x 100mm dimensions and were initially cured at 100% relative humidity at 23±2°C. After 2 days of curing the samples were demolded and immersed in a saturated calcium hydroxide

solution 23±2°C and cured until reaching 14 days of age. In addition to the samples that were prepared using the procedure given above, a set of commercially available TiO_2 coated ceramic samples (denoted "TC") was also tested for comparison.

It should be noted that other convenient dimensions could be used for the samples, but the thickness should be maintained as 5mm to avoid photocatalytic reaction occurring on the sides of the sample during NO_X tests. If samples of other area dimensions are used, the photocatalytic activity should be normalized per unit exposed area. The area of the sample is considered in a photocatalytic efficiency factor, which is defined later in the chapter.

Sample surface characteristics are very important for the surface-initiated photocatalytic reaction. For example, as the surface roughness (roughness number) increases, more effective surface area would be exposed to the gases and UV light. Thus it is paramount to maintain a constant roughness of surfaces in the test samples between various mixes. Hence after 14 days of curing, one flat surface of the samples was polished to obtain uniform surface roughness between different samples and mixes. This procedure also has the effect of minimizing any variations in finishing operations. Once removed from the curing solution the samples were immediately ground/polished using grinding papers #400, #600 and #1000 and finally using a suspension of a grit size 5μm.The polished samples were cleaned with deionized water to remove any residual material from the polishing step and then dried in an oven at 40°C for 2 days, until the mass change was less than 0.5%. This was done to minimize variation in moisture content among the samples. The dry samples were stored under sealed conditions, to avoid carbonation, and away from any light source until further testing.

5.2.3 NO_X Exposure Chamber

The test setup including the reaction flow cell and chemiluminescent NO_X analyzer for studying the photocatalytic activity and measuring the photocatalytic efficiency of cement-based materials is shown in Figure 5.1.

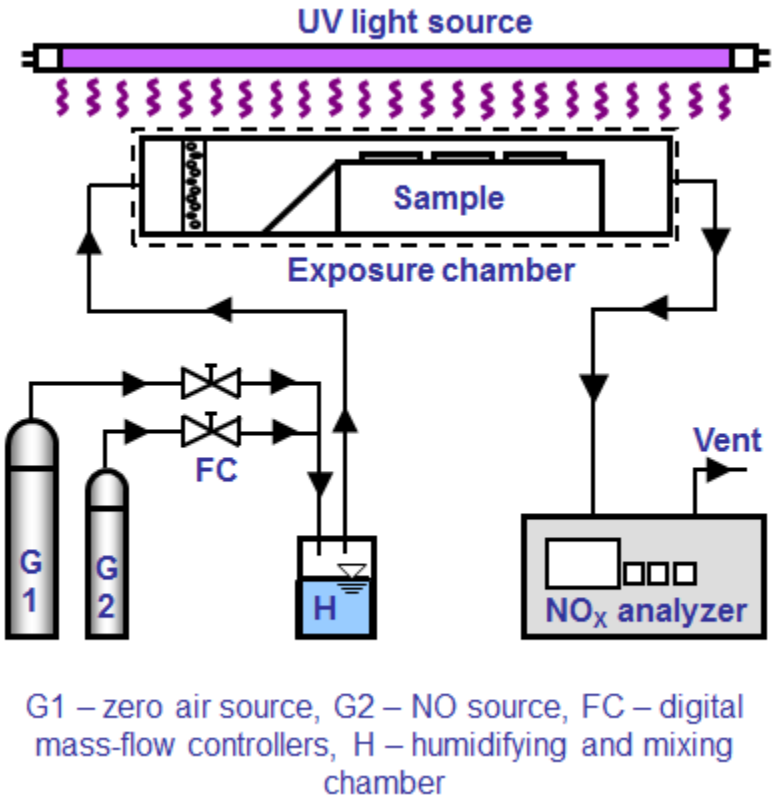

Figure 5.1. Experimental setup for testing photocatalytic activity of cement

A flow cell was specially designed and built for the NO_X exposure tests. The flow cell was designed as a 100cm long, 8cm wide and 5cm high chamber and the top surface was made with UV transparent poly-methyl methacrylate (PMMA) plate. The samples were placed inside the exposure chamber such that there was a gap of 5mm between the top surface of the samples and the bottom surface of the PMMA plate. The gas was allowed to pass only through this 5mm gap to ensure interaction between the gas and the

sample. The ends of the flow cell were sealed to ensure that there is no gas loss due to leakages. The absence of leaks was ensured by connecting digital flow meters at the entrance and exit of the flow cell before the experiments. The various components of the test setup were connected using 6.35 mm (¼") PTFE tubing and corresponding fittings (UltraTorr). Two 1219 mm (48 in.) 40-W UV fluorescent lamps (GE) with peak emission at 368nm were used to produce the UV light. The power of the UV light inside the flow cell at the plane of the samples was maintained at 10W m^{-2}, as measured using a digital UV meter (UVX Radiometer, UVP) attached with a 365nm sensor.

5.2.4 Concentration and Flow Rate of NO_X

NO gas was used as the pollutant gas for tests conducted as a part of this research. It should be noted that either NO or NO_2 gas can be used for the same test parameters in these tests [166]. A similar test procedure could be used for testing the photocatalytic activity of other pollutant gases such as VOCs. But the test parameters such as gas concentration and flow rate would have to be changed and optimized based on expected air pollution concentrations and expected outdoor residence time respectively.

The value of 1000ppb NOx concentration suggested in the ISO 22197-1 standard could be too high for realistic assessments of field performance of cement-based materials. First, the current annual average NO_2 level according to US EPA is only 53ppb and NO_X concentrations, particularly near urban roadways, can have values in hundreds of ppb's depending on atmospheric conditions [161]. Also, when considering cement-based materials specifically, the photocatalyst dosage rate is in this class of materials is, due to economy and constraints on plastic behavior, typically smaller than used in

ceramics and coatings on impervious materials. Further, even when twice the recommended value of sample surface area was used, it was found that 1000ppb gas concentration was not necessary for assessing cement-based materials nor discriminating among different material compositions. Also, for improving the precision of measurements made by the NO_X analyzer, the gas concentration range to be measured by the analyzer should be maintained at a minimum value.

On the other hand, the input gas concentration should not be too low since if all the NO_X is absorbed by a certain material, then differentiation of such a material surface and other surfaces with greater or lesser photocatalytic efficiency would not be possible. For optimizing input gas concentrations, test samples were cast and tested at 15% cement replacement by mass with various photocatalytic TiO_2 particles. Based upon these tests, the optimum input gas concentration was found to be 500 ppb.

A flow rate of 1 l/min for the gas mixture was selected for the tests to decrease the velocity of the gases passing over the samples and thus to increase the residence time (240 sec in these tests) of the gas in the exposure chamber. The higher flow rate that is specified in the ISO standard results in a lower residence time of the gas over the samples and greater percentage of the gas not interacting with the samples and merely flowing in the region above the interaction volume of the samples. The decreased flow rate allows sufficient time for interaction and reaction of gases on the TiO_2-cement surface.

For the experiments conducted in this research, NO gas at 100ppm (balance Nitrogen) concentration was mixed with ultrapure zero air at a ratio of 1:200 to obtain the desired concentration of 500ppb directly upstream of the samples. The gas flows were regulated using digital mass flow controllers (Tylan). The resultant mixture of NO and

zero air was passed through a humidifying chamber containing deionized water, which increased the relative humidity of the gas mixture. The relative humidity of the gas was maintained at 50% and was regularly checked using a digital humidity meter. The gas entering the flow cell first passed through a flow straightener which ensured a laminar flow over the samples. Following ISO 22197-1-2007, the gap between the samples and the bottom surface of the PMMA plate was maintained at 5mm using a height adjusting plate facilitate contact with the samples.

For each set of experiments, the samples were placed in the flow cell and the gas was allowed to stabilize for at least 30 minutes before the samples were exposed to UV light. The UV light was turned on at least 30 minutes before exposure of samples to UV light, to allow enough time for the lamp to warm up. During this time period the samples and exposure chamber were not exposed to the UV light. The photocatalytic activity of the cement samples was studied by measuring the variation of NO, NO_2 and NO_X concentrations over a period of 5 hours when the samples were exposed to UV light, similar to the ISO and JIS standard. The duration of the test was extended beyond the 1-hour duration specified in the UNI tests because, as reported in the Results section, the NO_X gases could take longer than one hour to stabilize after the test is started.

The concentration of NO, NO_2 and NO_X gas were measured at the outlet of the flow cell using a chemiluminescent $NO/NO_2/NO_X$ analyzer (Teledyne Instruments), with an accuracy of 5ppb. At the end of 5 hours the UV light was turned off, and the concentration of gases was allowed to return back to initial levels.

5.2.5 Characterization of Photocatalytic Efficiency

During the photocatalytic reaction of NO at the surface of samples, NO_2 gas can be produced as a by-product as shown in Equation 5.1. Since the total decrease of NO and NO_2 due to photocatalysis on the sample surface is of interest, the variation of the NO_X, rather than the variation of NO, was analyzed in determining the photocatalytic activity of TiO_2-cement samples.

Various experimentally measured or derived parameters can be used to characterize the activity of photocatalytic materials. For example, the initial decrease in the concentration of NO_X or the maximum difference between inlet and outlet concentration can be used as a measure of photocatalytic activity. While these values a measure of NOx binding at particular instants during the test, each measure does not represent the overall behavior of the photocatalytic surface over the entire test duration.

The ISO 22197-1-2007 and JIS R 1701-1 standards describes a measure of the total amount of NO_X adsorbed by the test piece, η_{ads} and Q_{ads} respectively in μmol, for characterizing photocatalytic materials by [103, 104]:

$$\eta_{ads} = Q_{ads} = (f / 22.4) \cdot \left\{ \int_0^T ([NO_X]_{in} - [NO_X]_{out}) dt \right\} \tag{5.3}$$

where f = air-flow rate converted to that at the standard state (0 °C,101,3 kPa, and dry gas basis) (l/min), $[NO_x]_{in}$ = supply volume concentration of NO_X before UV light is turned on (μl/l or ppm), $[NO_x]_{out}$ = outlet concentration of NO_X after UV light is turned on (μl/l or ppm) where the integration is conducted over time period 0 to T, expressed in minutes. The term that is integrated denotes the total NO_X gas that is absorbed (in ppm)

during the entire duration of the test. The factor 22.4 is used to convert from volume units to molar units, using the ideal gas law which states that one mole of an ideal gas at standard temperature and pressure occupies 22.4 liters.

However, the approach in equation 5.3 for representing the photocatalytic effectiveness of surfaces fails to take into consideration the decrease in concentration of NO_X will be directly related to the exposed area of the test material. The presumption with each of the three standard tests is that the sample surfaces are flat and impervious, which may be reasonable for fired ceramics, but not necessarily for cement-based materials. In addition, for cement-based materials, the photocatalytic efficiency has also been shown also to decrease with extended exposure to pollutant gases and with increasing age and even carbonation of cement surface [109], among other potential factors considered previously in this chapter. For cement-based materials, the method of curing and age at testing should be specified and treatment of the sample surfaces should be prescribed; here it is proposed that samples be cured in a saturated calcium hydroxide solution for 14 days and ground/polished using grinding papers #400, #600 and #1000 followed by polishing using an abrasive of grit size 5μm.

Thus, to incorporate the exposure area of the samples when characterizing photocatalytic surfaces and to include a normalizing factor for time of irradiation, a new photocatalytic efficiency parameter is proposed which facilitates comparison among various types of photocatalytic surfaces.

$$PEF = \frac{f}{22.4 \cdot A \cdot T}\left\{\int_0^T ([NO_X]_{in} - [NO_X]_{out})dt\right\} \quad (5.4)$$

where PEF = Photocatalytic Efficiency Factor in units of moles.time^{-1}.area^{-1}, $[NO_x]_{ave}$ = instantaneous concentration of the gas above the samples which could be considered as the average of the input and output gas concentration at any particular time during the test, A = sample surface area (m^2) and the other variables are the same as defined for equation 5.3. By normalizing the efficiency factor per unit area of the exposed photocatalytically active surface, researchers can use (if required) samples of different dimensions and/or different number of samples but still compare the results across tests that used different area of exposure. The input concentration at which the test is conducted should also be specified in the results, as the decrease in the pollutant level does not vary directly with increasing input gas concentration, as will be shown in the Results section.

For samples which are not plane or smooth, the roughness of the surface can also be incorporated into the equation. Because as the roughness increases, surface reactions would be expected to increase since more area is exposed to the NO_X and UV light. The roughness of a surface can be quantified as a roughness number (RN) defined by:

$$RN = \frac{\sum A_i}{\sum A_{pi}} \quad (5.5)$$

where A_i = area of a triangulated surface and A_{pi} = nominal area of the surface under consideration.

The roughness number of a surface can be determined through quantitative imaging of the surface, such as through confocal microscopy [168]. The effect of the surface roughness on photocatalytic activity can be considered by measuring the RN value for the surface being analyzed and incorporating the value into the calculations of photocatalytic activity. If a direct correlation between the surface area of the sample and the photocatalytic activity is assumed, the equation for PEF can be normalized by RN to consider difference in roughness between surfaces:

$$PEF_{RN} = \frac{f \cdot RN}{22.4 \cdot A \cdot T} \left\{ \int_0^T ([NO_X]_{in} - [NO_X]_{out}) dt \right\} \tag{5.6}$$

Further research is required to accurately obtain the relationship between the roughness properties and photocatalytic surface reactivity. In the current research, the roughness number was not considered because similar surface roughness was achieved for all the samples by sample surface polishing that was performed before the NO_X exposure tests, as previously described.

5.3 Results and Discussion

The proposed method was examined, both as a proof-of-concept by comparing among behavior of various sample compositions but also to validate the exposure conditions selected. A summary of the test conditions is provided in Table 5.1.

5.3.1 Photocatalytic Activity of TiO_2-Cement Paste Samples

Figure 5.2 shows the NO, NO_2 and total NO_X concentrations measured using the chemiluminescent analyzer when the control cement paste samples without any TiO_2 was tested using the proposed procedure; this was done to verify the air tightness of the chamber and the nonreactivity of the materials composing the chamber and samples. It can be observed that there was no meaningful change in the concentration of NO and NO_X nor was there any increase in the NO_2 when the ordinary (i.e. non-photocatalytic) samples are exposed to UV light, as expected. Minor fluctuations observed in the concentrations can be attributed to variations in the pressure and temperature due to the building ventilation system and because of the use of a mass flow controller to regulate concentration of gases. The mass flow controller assumes an ideal pressure and temperature and since there could be variations in these in the testing environment, the concentrations of the gases were observed to fluctuate marginally. This result demonstrates that neither the neat cement paste samples nor the reaction cell walls or PTFE tubes act as photocatalytic material during these tests. Thus any photocatalytic activity that is measured in other TiO_2-cement paste samples would solely be a result of the photocatalytic activity of the TiO_2 added to cement.

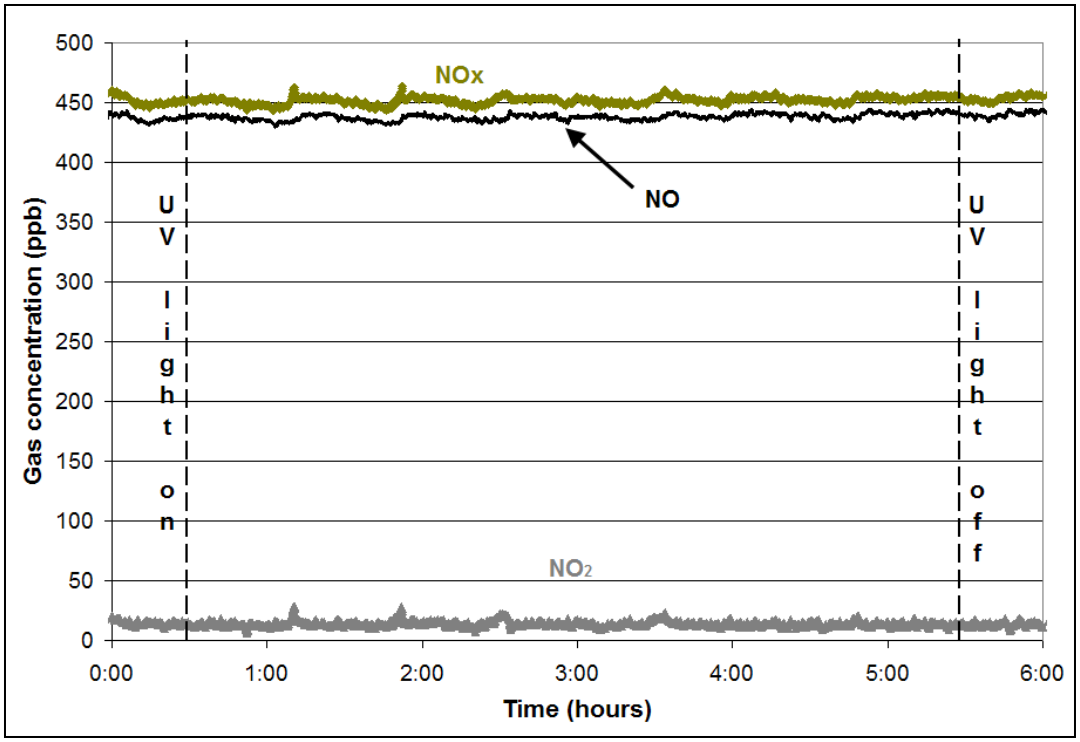

Figure 5.2. Variation of NO, NO_X and NO_2 gas during the test for photocatalytic properties of control cement samples

As further proof-of-concept, testing was performed on a variety of TiO_2-containing samples using the same chamber and exposures. As an example of these results, Figure 5.3a and 5.3b shows a typical pattern of variation of NO, NO_2 and NO_X - gas for cement-TiO_2 (T1) cement samples at 5% replacement rates and TiO_2 coated commercial ceramic tile, respectively. Note that when the UV light is turned on, as shown in Figure 5.3, photocatalysis is expected to initiate. For these tests the pollutant gas used was NO and hence the initial concentration of NO_2 can be observed to negligible. (The tests could also be conducted with NO_2 gas as the pollutant gas, which is not described in the ISO standard test but has been examined by this group and presented elsewhere [166, 169].) For the 5% T1 sample, during the first 30 minutes of the test when the samples were not exposed to UV light, the gas concentrations remained constant at a

value of ~450ppb for NO and NO_X and ~0ppb for NO_2. As soon as the samples were exposed to UV light, the concentration of the NO and NO_X gas decreased to ~380ppb and ~395ppb and NO_2 increased to ~15ppb, which corresponds to a 12.2% decrease in NO_X concentration. The NO_2 concentration increases because of the conversion of NO to NO_2 because of the photocatalytic reaction (see Equation 5.1). Comparing Figures 5.2 and 5.3, it can be concluded that the addition of TiO_2 to cement imparts photocatalytic properties to cement-based materials, as has been well-demonstrated in the literature [31, 34].

The change in concentration of the gases for the other sample compositions tested followed similar trends, and for this reason are not presented here but can be found in [170]. In general, the extent of decrease in NO and NO_X and increase in NO_2 concentration varying with dosage and type of TiO_2 used. That is, greater decreases were observed with greater TiO_2 addition rates and with more dispersible TiO_2 particles, as previously reported [31, 166].

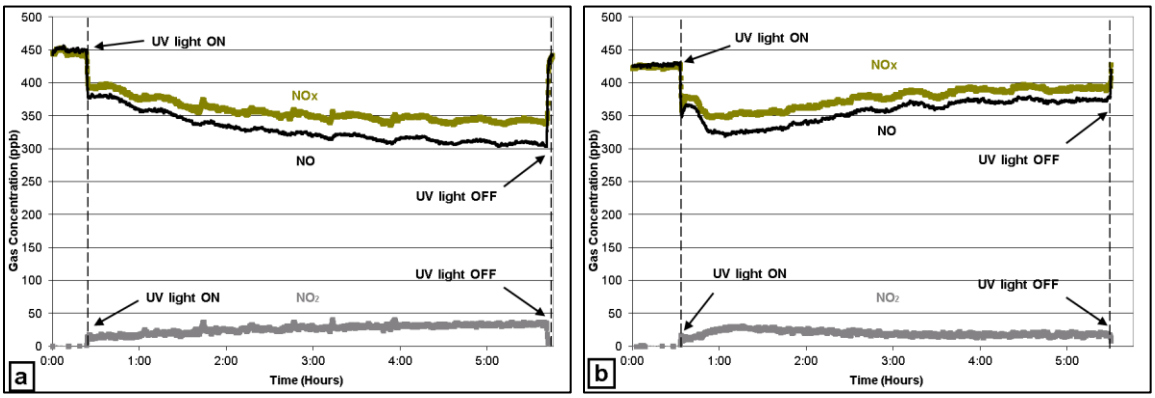

Figure 5.3. Variation of NO, NO_X and NO_2 gas during the test for photocatalytic properties of a)TiO_2- cement samples (5% T1 type TiO_2) and b) TiO_2 coated commercial ceramic tile (TC)

From Figure 5.3a it can also be observed that during the 5 hours of UV exposure the concentration of NO and NO_X decreased continuously, which suggests ongoing

oxidization of the gas via surface photocatalysis. The final concentration of the gases at 5 hours of exposure was ~305ppb, ~340ppb and ~35ppb for NO, NO_X and NO_2 respectively, which corresponds to a 24.4% decrease in the NO_X concentration. Moreover, there is a gradual increase in the NO_X conversion in the case of 5% T1 sample. The percentage (or absolute) reduction of the NO_X concentration at the end of the 5 hour testing period approximately doubled compared to the decrease in concentration at beginning of the test. And, the absolute reduction in NO_X concentration, when compared to the initial concentration was 70ppb at 1 hour compared to 106ppb at 5 hours. From Figure 5.3b it can be observed that there is a gradual decrease in NO_X conversion for the TiO_2-coated ceramic tile. The absolute reduction in NO_X concentration, when compared to the initial concentration was 70ppb at 1 hour compared to 34ppb at 5 hours. Thus it can be observed that it takes more than 1 hour for the NO_X conversion to stabilize, based on the tile used. Thus, it appears the 5 hour test duration is more appropriate for testing photocatalytic samples compared to the 1 hour test duration as specified by the UNI test [105].

The continuous decrease of the NO_X and NO gas concentration in the case of 5% T1 sample during the five hour test (Figure 5.3a) demonstrates that the surface has not yet saturated with the reaction products and that removal of gases by photocatalytic activity may continue in the presence of UV light. With continued exposure, the rate of the photocatalysis could decrease, and saturation would eventually occur. In that case, the photocatalytic activity of samples can be regenerated by simple washing with water in the laboratory and by any form of precipitation in field applications [18, 95].

Thus, descriptive parameters of photoactivity should consider time of exposure. Hence, a parameter which is normalized with the total testing duration should be used to compare among various photocatalytic materials. This further justifies the use of the Photocatalytic Efficiency Factor (PEF) which normalizes the photocatalytic activity of the TiO_2-cement surface with respect to the test duration.

5.3.2 Effect of Variation of Input Gas Concentration on Photocatalytic Activity

To better understand the influence of input gas concentration, the photocatalytic activity of various cement samples were tested at input test gas concentrations of 100, 200, 500, 1000 and 1400ppb while keeping all the other test parameters the same, as stated earlier. The variation of the decrease in concentration of gas with change in input gas concentration for T1 added to cement at 15% replacement rate is shown in Figure 5.4. Figure 5.4 shows that as the input gas concentration is increased, the NO_X binding capability also increases. This behavior is expected since at a higher input gas concentration, more pollutant gas interacts with the TiO_2 surface, resulting in increased photocatalytic NO_X binding, particularly for relatively short exposure durations. The increase in NO_X binding will continue until a saturation limit is reached [18].

But, it can be seen that there is not a linear relationship between the various input concentrations and the change in concentration of pollutant gas. With increasing input gas concentration, the NO_X binding capability (conversion efficiency) was observed to decrease, as demonstrated by the decrease in slope of the graphs in Figure 5.4. Thus, whenever the photocatalytic activity of a material is specified the input gas concentration

should also be specified, since the relative decrease in pollutant gas concentration depends on input gas concentration.

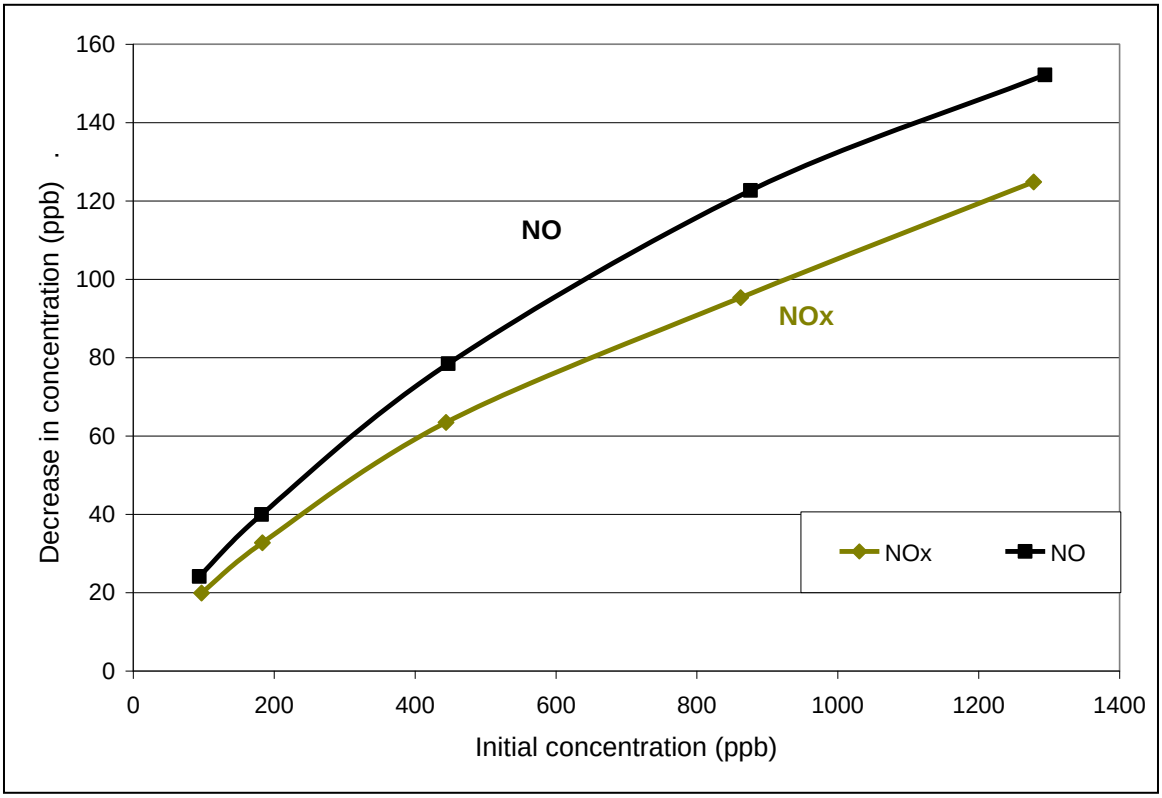

Figure 5.4. Variation of change in concentration with input gas concentration for T1 at 15% replacement rate

In the proposed test method, an input gas concentration of 500ppb was selected, based upon behavior observed in Figure 5.4 and also due to other experimental constraints. For example, at higher input gas concentrations, the accuracy of the measurements is decreased due to limitations on the resolution of the chemiluminescent NO_X analyzer used as the detection equipment. Also, at higher gas concentrations, as noted previously, the relationship defined in Figure 5.4 becomes non-linear even for relatively highly photocatalytic cement-based materials, suggesting saturation. It is

validating that the recently proposed UNI method also uses a similar input gas concentration of 550ppb, lower than the 1000ppb in the ISO and JIS methods.

5.3.3 Photocatalytic Efficiency Factor (PEF) for TiO_2-Cement Mixes

Figure 5.5 shows the variation of the NO_X concentration of samples made T1 used at 5, 10 and 15% replacement rates by mass of cement. It can be seen that as the dosage of TiO_2 is increased in the samples, the photocatalytic conversion of NO_X increases, with the 15% mix showing the greatest decrease in the NO_X concentration, as expected.

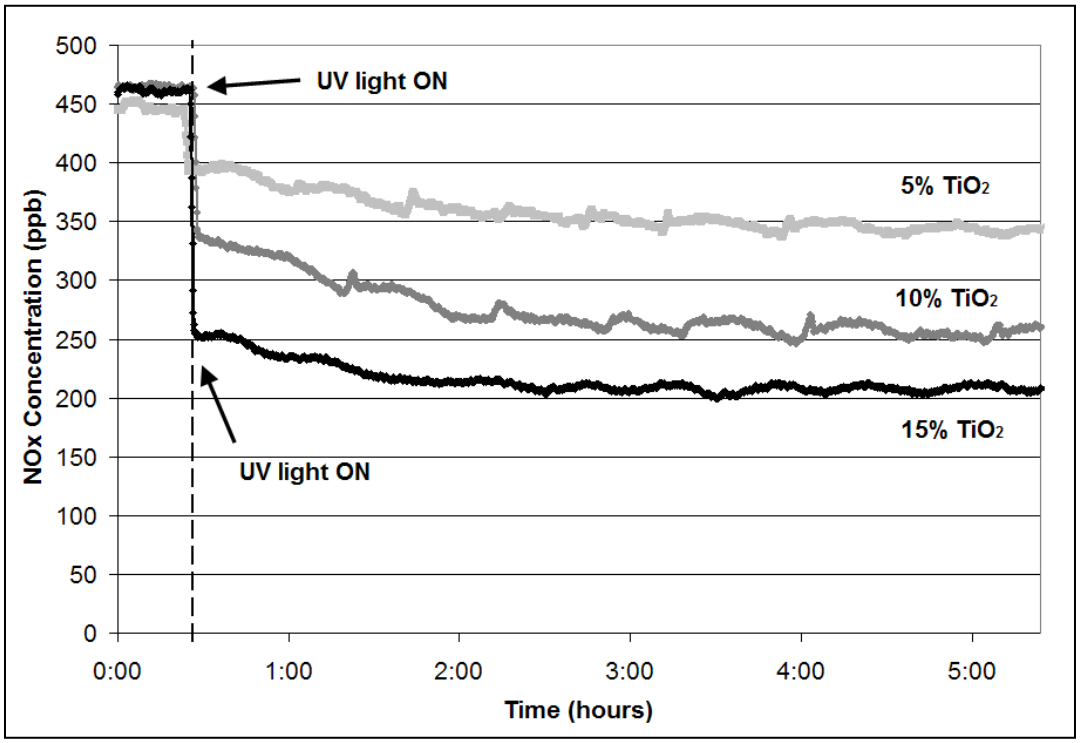

Figure 5.5. Variation of NO_X during the test for photocatalytic properties of TiO2-cement samples with 5, 10 and 15% dosage rates of T1

To demonstrate how the proposed test and PEF can be used to compare among photocatalytic materials, the PEF values for these materials were calculated and are

shown in Figure 5.6. The PEF values obtained for these three mixes were 18.96, 40.35 and 51.55 $\mu mol \cdot hr^{-1} \cdot m^{-2}$ respectively. Thus, it can be concluded that the photocatalytic activity of the TiO_2-cement paste mixes increases with increases dosages of TiO_2 powder addition, within the range of dosages examined. It also appears that there are "diminishing returns" when the photocatalyst dosage is increased beyond 10% by mass of cement.

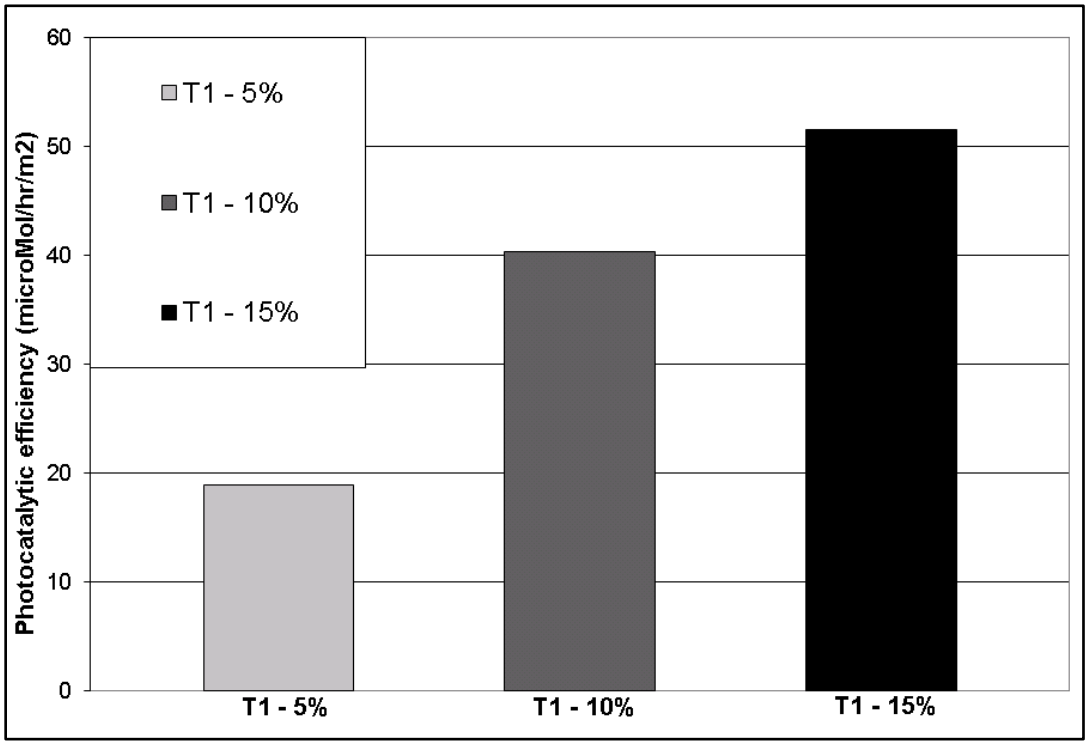

Figure 5.6. PEF for cement-TiO_2 samples made with 5, 10 and 15% percentage replacement by T1

To further demonstrate how PEF can be used to compare among different materials, Figure 5.7 shows the variation of PEF for the various commercially available TiO_2 particles with cement paste at 5% by mass TiO_2 as well as TiO_2 coated commercial ceramic tiles (TC). The photocatalytic activity and, hence, the PEF for the control mix is

almost negligible, as expected. That a non-zero value was measured for the control mix could be an artifact of the minor fluctuations in the NO_X concentration observed during the test, NO_X binding to the hydrated cement or flow into the pore structure of the sample. Compared to the control sample the PEF of the TiO_2-cement mixtures were significantly higher. A wide range of photocatalytic activity was observed for the different TiO_2 samples tested, with PEF values ranging from 8.404 $\mu mol \cdot hr^{-1} \cdot m^{-2}$ for T4 to 21.747 $\mu mol \cdot hr^{-1} \cdot m^{-2}$ for T3. Thus T3 - a mixture of 80% anatase and 20% rutile TiO_2 - was observed to be the most photocatalytically active among all the different TiO_2 samples that were tested. Similar observations were made by other researchers studying the photocatalytic activity of various commercially available TiO_2 powders [171]. The photocatalytic activity for the TiO_2 coated ceramic tile, as measured using PEF, was 7.88 $\mu mol \cdot hr^{-1} \cdot m^{-2}$.

No direct correlation is evident in these data between the mean particle or crystal size or surface area (obtained from the manufacturer) of the TiO_2 used in the mixes and the photocatalytic efficiency of the TiO_2-cement samples tested in the research. Though T2 had the highest surface area as a powder (75-95 m^2/g) it was observed that the PEF for the cement mix made with T2 was lower than the PEF for various other mixes. T5 had the lowest surface area as a powder but the PEF for T5 was much higher than several other mixes. Another interesting observation is that the surface areas of T1, T3 and T4 were similar but photocatalytic efficiency obtained for cement mixes produced with T4 had the lowest PEF among all the TiO_2-cement mixes and T1 and T3 were on the other end of the spectrum with highest PEF values. This could be because of dispersibility of the TiO_2 in the cement mix as TiO_2 agglomerates were observed in some of the mixes in

the current research. Further research is required to study the effect of dispersion of TiO_2 and also the effect of TiO_2 particle size on the photocatalytic efficiency of TiO_2-cement mixes.

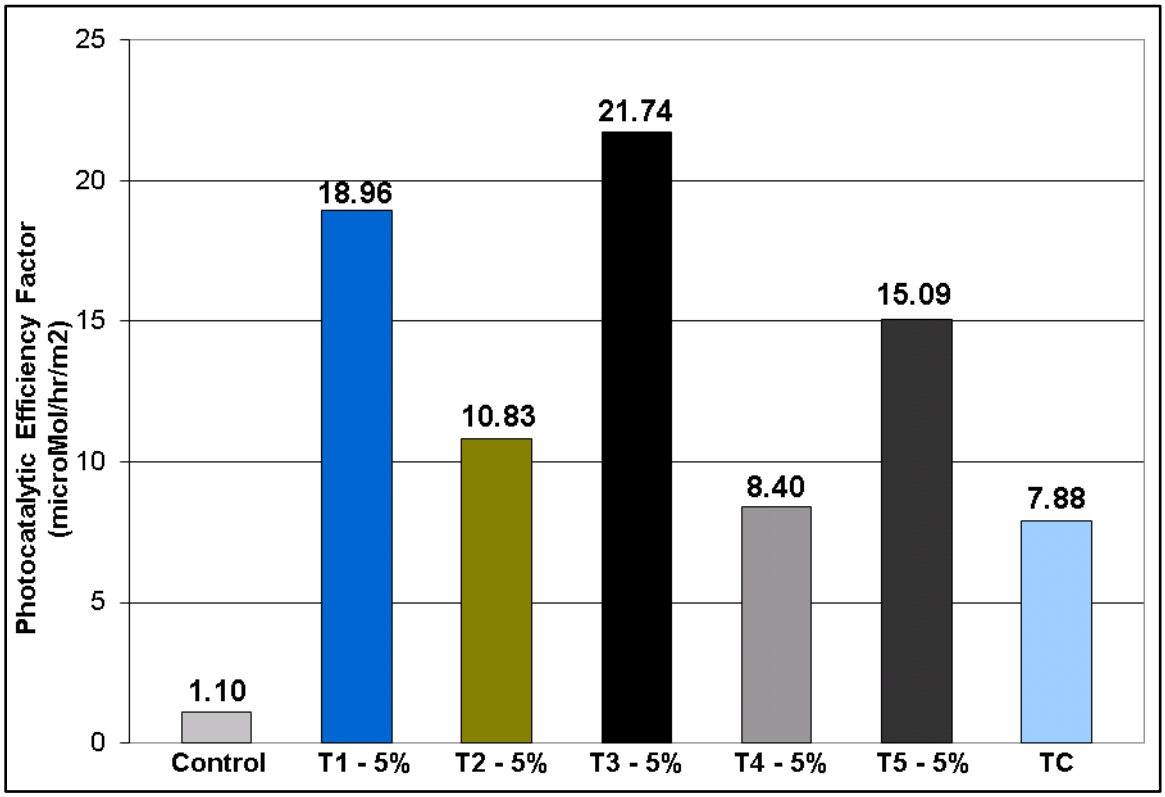

Figure 5.7. Photocatalytic efficiency factor of various TiO_2-cement mixes at 5% replacement levels by TiO_2

5.4 Conclusions

The applicability of current standard tests for photocatalytic activity of ceramics was examined for the assessment of cement-based materials and was found to have shortcomings in terms of not considering the composition of photocatalytic cementitious materials, their anticipated rate and variation in photocatalytic behavior, nor the surface characteristics of the material. Modifications for sample preparation techniques, test

parameters (i.e., input gas concentration, test duration, flow rate) and normalized measurement variables were suggested to make such tests appropriate for cement-based materials. The proposed changes are tabulated and the rationale for selection of testing parameters, based upon experimental evaluation is provided. A new photocatalytic efficiency factor (PEF), which addresses potential variations in test sample surface area and roughness and variations in test duration, was defined which could be used to obtain the photocatalytic activity of any cement-based material surface or construction material.

The addition of TiO_2 to cement introduced photocatalytic properties to the cement surface as observed in the experiments conducted in this research. The photocatalytic efficiency was found to be proportional to the addition rate of TiO_2 to the cement, with higher dosages decreasing the concentration of NO_X gases at a higher rate and hence increasing the photocatalytic efficiency. The PEF values for cement paste samples made with 5, 10 and 15% replacement of cement with T1 was calculated to be 18.96, 40.35 and 51.55 $\mu mol \cdot hr^{-1} \cdot m^{-2}$ respectively when the input test gas concentration was 500ppb. The input gas concentration and the change in gas concentration due to photocatalytic reaction were observed to be non-linear and thus it is proposed that the input gas concentration should be specified in any test which reports the photocatalytic activity of a material.

The photocatalytic activity of five different commercially available TiO_2 mixed with cement at 5% replacement rate was compared using the proposed photocatalytic efficiency parameter (PEF). The PEF values of the different TiO_2 that were tested ranged from 8.40 $\mu mol \cdot hr^{-1} \cdot m^{-2}$ for T4 to 21.75 $\mu mol \cdot hr^{-1} \cdot m^{-2}$ for T3 when tested at 500ppb input gas concentration. T3 was observed to be the most photocatalytically active among all the commercially available TiO_2 samples that were tested in this research.

The PEF parameter defined can be used for comparisons of different mixes and between inter-laboratory specimens, even when cement paste or mortar samples of different surface areas or roughness are used. This developed procedure and test parameters could also be used to test photocatalytic activity of TiO_2-cement mixes or other construction materials in the presence of other pollutants such as toluene, acetaldehyde and chloramines, with minor modifications of the test parameters.

CHAPTER 6

SUSTAINABILITY OF CEMENT MIXTURES WITH TITANIUM DIOXIDE AND LIMESTONE PARTICLE ADDITIVES

6.1 Introduction

The construction industry, like other science and engineering fields, is examining developments in nanotechnology to identify potential applications. In particular, the use of nanoparticles in construction materials is of increasing interest. The use of nanoparticles can not only modify properties of cement-based materials by potentially enhancing strength [172-174] and durability [175, 176] but also by introducing new functionality, including photocatalytic (self-cleaning, pollution reduction and anti-microbial ability) [109], anti-fogging [34] and self-sensing capabilities [177].

While the use of nanoparticles could increase in the construction industry [12], such materials, especially when engineered and manufactured, can be energy-intensive to produce and thus direct economic costs and environmental impacts could be high [125]. With an increasing emphasis on sustainable development in many sectors including the construction industry [115], it is important to understand the costs and benefits associated with the use of nanomaterials when compared to relatively less energy-intensive microparticles. However, while the potential improvements in performance and functionality of nanoparticle modified cementitious composites have been increasingly examined, relatively little effort has been put toward understanding the potential implications of these technologies on sustainability.

Particles considered in this research include fillers which are largely non-reactive in the presence of portland cement (TiO_2 and limestone powder); as a result, the effect of particle size and dosage of the filler can be isolated. TiO_2 production is a highly energy intensive process in both the sulfate process and chloride process of extraction [18]. Limestone production, contrarily, is a relatively less energy intensive process, even when compared to cement clinker production [49]. The effect of these two fillers of such varied energy intensity of production on the sustainability of cementitious mixtures needs further analysis. Moreover recent research studies have shown that nanoparticles could be released into the environment during the life cycle of a structure and could results in adverse biological and toxicological effects [125, 178, 179]. The life cycle costs due to unforeseen environmental and human health impacts of nanomaterials have not yet been fully quantified [178] and hence are not included in this research.

An analyses of the potential environmental impact of cementitious materials with TiO_2 and limestone replacement is conducted through a life cycle analysis (LCA) [115]. Although the NO_X binding ability of photocatalytic TiO_2 is a potential environmental benefit [95], a comprehensive investigation that includes all factors including total embodied energy, emissions including CO_2 and NO_X among other factors associated with the production of both of these particles, is required to evaluate the impact (especially on the environment) of their usage.

6.2 Methodology Used in Life Cycle Analysis

6.2.1 Scope and Functional Unit of LCA

LCA is a technique that incorporates environmental impact and considers all energy and emissions of the various stages of a product or process from raw material production stage through end of life disposal or recycling (cradle-to-grave approach) [121]. In the current research, SimaPro LCA analysis software was used along with BEES (developed by NIST) [123, 180] and EcoIndicator 99(E) for impact assessment, with a primary goal of providing data for comparing the relative impacts of TiO_2 and limestone particle additions. It should be noted that processing techniques and hence environmental impacts of materials vary with each individual product and manufacturer. But LCA analysis is typically conducted utilizing databases compiled with data from several material manufacturers. Thus LCA analysis can provides an overall impact, especially suitable for a comparison – rather than an absolute measure - of the environmental impact of different classes of materials.

In the current research, a process-based LCA was conducted, where all the inputs and outputs including materials and disposals are analyzed by using a process flow analysis. The other alternative, which uses economic input-output (EIO) data, is an EIO-LCA. The EIO-LCA uses national averages of industry data [115] and hence is not applicable for LCA of specific products as required in this research. Thus the process-based LCA was conducted in this research using SimaPro LCA software.

A functional unit of 1000kg of the cementitious mixture was used for all of the analysis. A generalized processing of TiO_2 and limestone based on data obtained from the respective manufacturers were considered for the material manufacturing in this research.

TiO_2 manufactured using the sulfate process, milled loose limestone, ordinary portland cement and tap water were the other inputs for the LCA analysis. The mixes with a w/s of 0.50 and addition rate of 5% of TiO_2 and limestone were considered for the LCA analysis and compared with the ordinary portland cement paste.

Table 6.1. Environmental impact factors considered in the BEES model

Environmental Impact Factor	**Reference substance/unit**
Acidification	Hydrogen ion
Criteria air pollutants	Disability-adjusted life year (DALY)
Ecotoxicity	2,4-dichlorophenoxy-acetic acid
Eutrophication	Nitrogen
Fossil fuel depletion	Joules surplus
Global warming	Carbon dioxide
Habitat alteration	Threatened & Endangered (T&E) species count
Human health (cancer)	Benzene
Human health (noncancer)	Toluene
Indoor air quality	Total Volatile Organic Compound (TVOC)
Ozone depletion	CFC-11
Smog	Nitrogen Oxide
Water intake	Liters water

Table 6.2. Environmental impact factors considered in the EcoIndicator 99(E) model

Environmental Impact Factor	**Reference substance/unit**
Carcinogens	Disability-adjusted life year (DALY)
Respiratory organics	DALY
Respiratory inorganics	DALY
Climate change	DALY
Radiation	DALY
Ozone layer	DALY
Ecotoxicity	Potentially Disappeared Fraction (PDF*m^2yr) of species
Acidification/ Eutrophication	PDF*m^2yr
Land use	PDF*m^2yr
Minerals	MJ surplus
Fossil fuels	MJ surplus

6.2.2 Stages of Life Cycle Analysis

Mix design data for the different materials were input into the SimaPro LCA software, which conducted the life cycle impact analysis that includes classification, characterization, normalization and weighting steps. The analysis conducted in this research considered only the materials production, including raw material acquisition and processing of the components used in the cementitious mixes and was thus a "cradle-to-gate" approach. The LCA considers the energy and emissions due to the manufacturing and production of cement, titanium dioxide, water, limestone. The LCA does not consider the energy and emissions due to production of the equipment used for the production of fuels, cement, TiO_2 or limestone. The toxicological impact on nanoparticles is a research area under investigation [124], and hence was not included in this research, but could be included when the data are available. The performance of the cementitious mixture

during use in a structure (including durability, strength and thermal properties) was not considered in the LCA analysis. The system boundary for the LCA analysis was fixed at second order, which includes the material and energy flows including operations for all the products.

The Life Cycle Inventory (LCI) analysis accounts for all individual material, energy and emissions inventory and flows to and from the product under consideration. The inventory data and environmental impact due to the various materials in this research were obtained by utilizing databases embedded in LCA software suite used in this research, SimaPro. In the classification step of LCA, BEES and EcoIndicator 99(E) assessment methods categorized the impact of the materials into the categories given in the tables below (Table 6.1 and Table 6.2).

The cumulative impact of all the inventory items on each impact category was calculated based on the potential effect (damage) of each inventory item on that impact category. For example, the global warming potential of all the components would generate a single index in grams of carbon dioxide produced per functional unit of a product. The global warming index is calculated based on the following equation:

$$\text{Global warming potential} = \Sigma(m_i \cdot P_i) \tag{6.1}$$

where m_i = mass of harmful emissions i produced per functional unit and P_i = conversion factor from one gram of harmful emission i to its equivalent of carbon dioxide. Thus each emission is converted to the common unit according to the P_i conversion factor. The conversion factors for each functional unit are provided by the BEES or EcoIndicator

99(E) model based on research conducted by the U.S. EPA and PRé Consultants. A similar approach is used for each environmental impact category listed in Table 6.1 and 6.2 for the two impact assessment methods utilized.

In the last stage of the LCA (interpretation stage), each of the impact factor results could be normalized based on set of weights to achieve a single impact score that can be used to compare the alternative products or processes under consideration [121, 123]. At this stage of the LCA, key areas could be identified for potential change of the energy and emissions to reduce effect on the environment.

Also, further investigation was performed to account for the NO_X binding capability of TiO_2-cement, which could offset a part of the environmental impact of the production of the TiO_2 nanoparticles. The time required to offset the initial NO_X emissions from material was also estimated.

6.3 Life Cycle Analysis Results

The four stages of LCA are (a) define scope and boundary, (b) life cycle inventory analysis, (c) life cycle impact assessment, and (d) interpretation. The scope and boundary of the LCA was defined in the previous section of this chapter. The life cycle inventory analysis accounts for all the individual material, energy and emissions inventory, and flows to and from the product under consideration. The impact assessment was conducted using SimaPro software based on the scope and boundary of the products under comparison.

6.3.1 Life Cycle Inventory Analysis Results

The extensive inventory results for the individual products under consideration (ordinary cement paste, 5% TiO_2-cement paste, 5% limestone-cement paste) are given in Appendix A. The results include all the material, energy and emissions due to all the components that are used in the cement paste mix and the filler-cement mixes.

6.3.2 Life Cycle Impact Assessment Results

The results from the third stage of the LCA, impact assessment, are given in Tables 6.3 and Table 6.4 when using the BEES and EcoIndicator impact assessment methods respectively. In all the impact categories it was observed that the TiO_2-cement mix had a higher environmental impact compared to the plain cement mix. For example, the fossil fuel usage by TiO_2-cement mix was 571.76 MJ surplus compared to 294.15 MJ surplus for the plain cement paste, which is a 94.38% higher value. Thus the total environmental impacts due to the usage of TiO_2-cement mix are expected to be higher. On the other hand, the environmental "costs" due to the usage of limestone-cement mix was lower than the plain cement mix. The fossil fuel usage by limestone-cement mix was 280.14, which is a 4.73% decrease compared to the plain cement mix. Thus the use of limestone in cementitious materials decreases the environmental impacts and thus improves sustainability.

Table 6.3. Life cycle impact assessment results based on BEES impact assessment

Impact category	**Unit**	**LS-cement paste**	**TiO_2-cement paste**	**Plain cement paste**
Global warming	g CO_2 eq	9.43E+05	1.19E+06	9.92E+05
Acidification	H^+ moles eq	1.49E+05	2.73E+05	1.57E+05
HH cancer	g C_6H_6 eq	7.67E+02	1.14E+03	8.06E+02
HH noncancer	g C_7H_7 eq	1.47E+06	2.28E+06	1.53E+06
HH criteria air pollutants	microDALYs	2.38E+01	8.73E+01	2.45E+01
Eutrophication	g N eq	1.93E+02	3.04E+02	2.03E+02
Ecotoxicity	g 2,4-D eq	4.00E+03	6.00E+03	4.21E+03
Smog	g NOx eq	2.51E+03	3.43E+03	2.64E+03
Natural resource depletion	MJ surplus	1.89E+02	7.30E+02	1.98E+02
Indoor air quality	kg TVOC eq	0.00E+00	0.00E+00	0.00E+00
Habitat alteration	T&E count	3.80E-14	1.62E-11	4.43E-15
Water intake	liters	4.70E+05	8.00E+05	4.49E+05
Ozone depletion	g CFC-11 eq	7.05E-02	7.58E-02	7.41E-02

Table 6.4. Life cycle impact assessment results based on EcoIndicator impact assessment

Impact category	**Unit**	**LS-cement paste**	**TiO_2-cement paste**	**Plain cement paste**
Carcinogens	DALY	3.39E-05	4.69E-05	3.56E-05
Respiratory organics	DALY	2.91E-07	4.44E-07	3.06E-07
Respiratory inorganics	DALY	2.62E-04	6.15E-04	2.74E-04
Climate change	DALY	1.98E-04	2.50E-04	2.08E-04
Radiation	DALY	1.91E-06	2.58E-06	2.00E-06
Ozone layer	DALY	9.90E-08	1.26E-07	1.04E-07
Ecotoxicity	PDF*m^2yr	3.94	7.46	4.13
Acidification/ Eutrophication	PDF*m^2yr	12.72	19.40	13.36
Land use	PDF*m^2yr	4.20	6.10	4.41
Minerals	MJ surplus	0.74	8.29	0.75
Fossil fuels	MJ surplus	280.14	571.76	294.15

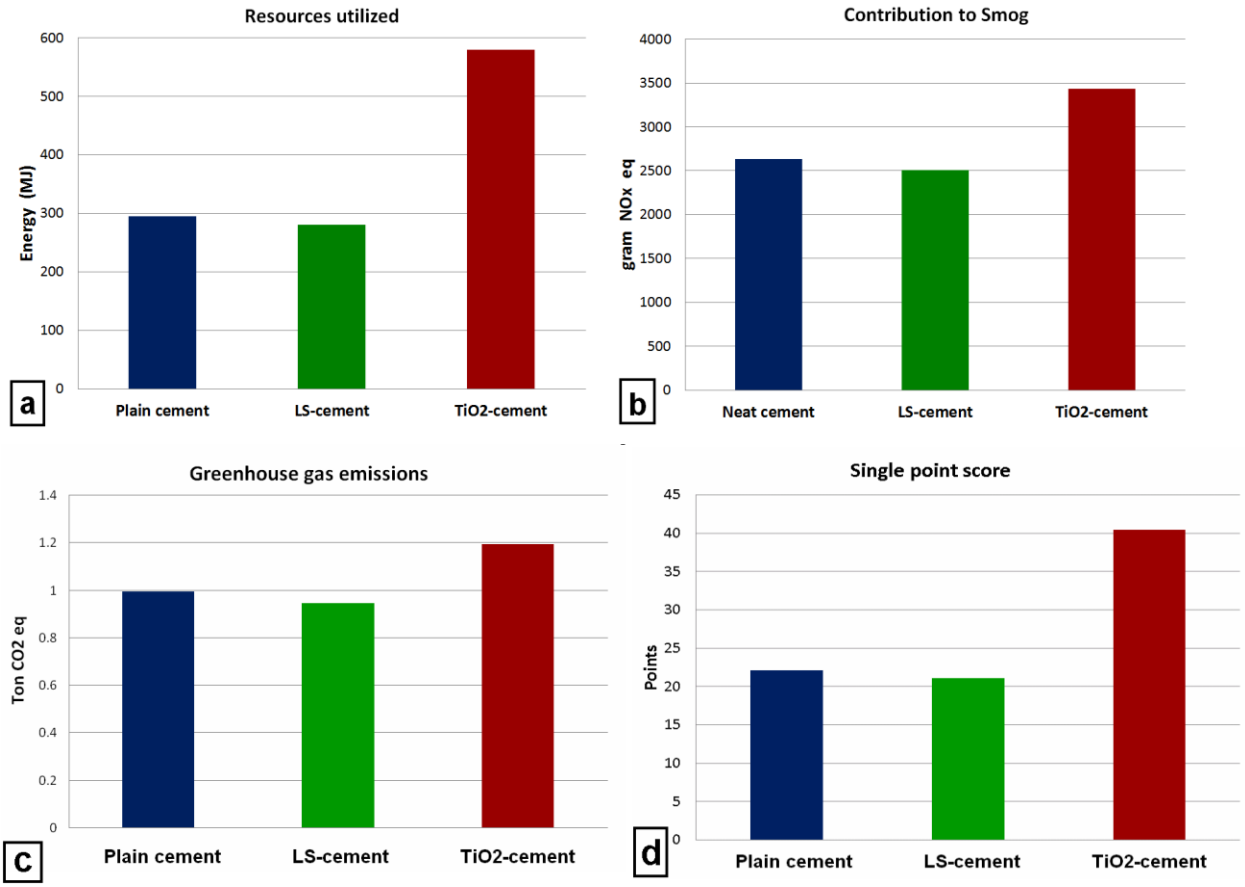

Figure 6.1. LCA results showing (a) utilized resources (energy) and (b) contribution to smog (due to NO_X emissions) (c) greenhouse gas emissions (d) single point score, by ordinary portland cement paste and cement-filler mixes with 5% addition of filler

Figure 6.1 shows some of the salient results from the LCA impact assessment for ordinary portland cement and cement containing 5% TiO_2 or 5% limestone filler. The total utilized resources and smog creation due to the use of 1000kg (functional unit) of ordinary portland cement paste and cement-filler mixes with 5% addition of limestone and titanium dioxide is shown in Figure 6.1a and 6.1b respectively. Figure 6.1c and 6.1d shows the results of the greenhouse gas emissions and single point score for the ordinary portland cement and the TiO_2 and limestone filler. This analysis considers only the materials production, including raw material acquisition and processing of the

components used in the cementitious mixes. It is clearly evident that limestone-cement mixes have a lower environmental impact compared to plain cement paste mix, whereas TiO_2-cement mixes have considerably higher environmental impacts ("costs"). The source of the greater environmental impact by the TiO_2-cement mix is because of the significantly higher energy and emissions "costs" of TiO_2 manufacturing process compared to cement production [119, 124].

By comparing the environmental "costs" of the ordinary portland cement mix and limestone-cement mixture, it can be observed that the addition of 5% limestone results in almost a 5% decrease in the various impact categories, as might be expected. This suggests that compared to ordinary portland cement, the energy and emissions of limestone powder is negligible. This can partly be explained due to the fact that limestone is used as a raw material in cement production and most of the energy and emissions from the cement production is due to the clinkering and grinding processes [119]. Hence, the replacement of cement with a lower embodied energy filler, such as limestone powder, is one pathway to enhance sustainability of the construction industry, as has been recognized in the industry [49, 86].

6.3.3 Life Cycle Analysis – Interpretation – Results

The results from the final step of the LCA, interpretation, are given in Table 6.5. The results show that the TiO_2-cement paste had a single point score that was 82.6% greater than the plain cement paste mix. The results also show the high impact due to the respiratory organics and respiratory inorganics released into the atmosphere as emissions, as well as the high impact due to fossil fuel consumption. The scores for the TiO_2-cement

paste was almost double compared to the plain cement paste, in all three of the impact categories which had the highest impact on the single point score. If reducing the fossil fuel dependency and total environmental impact of the product under consideration are of concern, reducing the amount of material required of these inputs or reducing the fossil fuels required to produce the material through innovation are pathways of reducing fossil fuel contribution to environmental impact.

Table 6.5. Single point score considering the EcoIndicator 99(E) impact assessment categories

Impact category	**Unit**	**LS-cement**	**TiO2-cement**	**Plain cement**
Total	Pt	21.10	40.47	22.14
Carcinogens	Pt	0.66	0.91	0.69
Respiratory organics	Pt	0.01	0.01	0.01
Respiratory inorganics	Pt	5.09	11.94	5.32
Climate change	Pt	3.84	4.86	4.04
Radiation	Pt	0.04	0.05	0.04
Ozone layer	Pt	0.00	0.00	0.00
Ecotoxicity	Pt	0.38	0.73	0.40
Acidification/ Eutrophication	Pt	1.24	1.89	1.30
Land use	Pt	0.41	0.59	0.43
Minerals	Pt	0.03	0.28	0.03
Fossil fuels	Pt	9.41	19.21	9.88

The single point score of the limestone cement paste is shown to be lower than the plain cement paste mix and is lower than the plain cement mix for all the impact assessment categories considered in the EcoIndicator 99(E) method. The value of single point score for the limestone-cement mix was 4.7% lower than the plain-cement mix, demonstrating that the limestone fillers have a much lower embodied energy compared to

the portland cement. Thus the use of lower embodied energy materials in cementitious mixtures is a pathway for improving sustainability in the construction industry.

6.4 Pathways for Use of Nano and Micro Particles - Do We Need Nano Particles?

The potential benefits associated with nanoparticle addition should not be set aside completely based upon LCA [181]; here, some pathways for sustainable nanoparticle utilization are proposed. First, for example, fine particles which are naturally occurring or are by-products of industrial or commercial processes potentially would have significantly lower environmental cost than manufactured nanoparticles and should be examined for applications in cement and concrete. The advantage of using such nano, or even fine microparticle fillers, would be that the environmental impacts as well as economic costs would be extremely low, when compared to processed and manufactured nanoparticles. Thus, toward attaining sustainability by reducing environmental "costs", the utilization of naturally-occurring or by-product nano and finer microparticles should be the subject of further examination. Further extensive research is needed to optimize the potential benefits for the construction industry from using natural nanoparticles in cementitious materials.

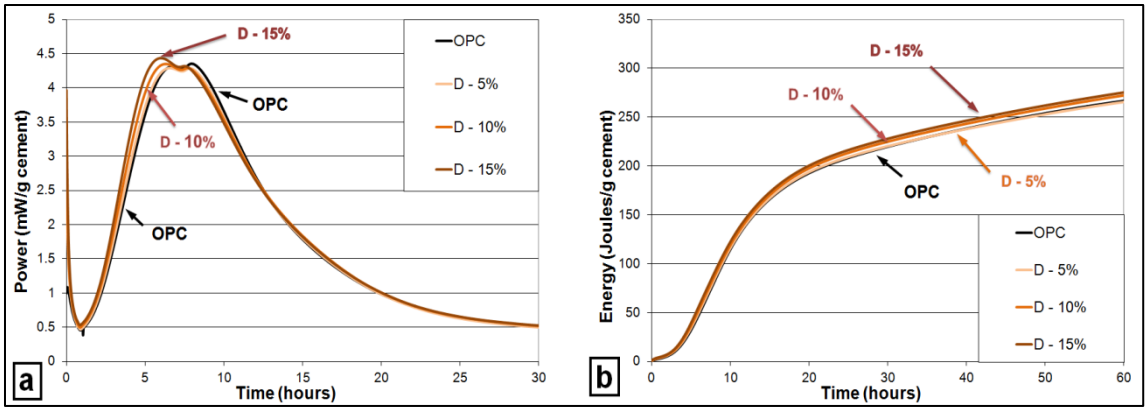

Figure 6.2. (a) Rate of heat release and (b) total heat release by 5, 10 and 15% mixture of diatomaceous earth and cement.

One such naturally-occurring, nanostructured material, and one which may become a widely available is a bio-energy by-product [182, 183] – diatomaceous earth (DE), the silicon-rich remains of certain forms of algae. To examine whether DE could be used effectively in cements in a manner similar to the other particles assessed here, preliminary isothermal calorimetry experiments were conducted (Figure 6.2) to understand the effect of this filler on early age properties. Commercially available flux-calcined diatomaceous earth (CAS# 68855-54-9) with an average particle size of 3µm was used for these tests. From Figure 6.2 it can be observed that the replacement of cement with 10 and 15% of diatomaceous earth only subtly increased the rate of cement hydration and accelerated the reaction marginally compared to the ordinary portland cement paste. While these results are not satisfactory for acceleration of early age hydration, other naturally occurring fine fillers, for example a finer diatomaceous earth, should be examined. Such particles, when identified, could increase the rate of cement hydration possibly even similar to the extent observed with the TiO_2 particles used in this

research. As demonstrated below, cement-savings could be the net result of the acceleratory effects observed with nano and fine microparticle addition.

The LCA results of the TiO_2 blended cements shows that the environmental costs due to TiO_2 addition is significantly higher than ordinary cement paste. But interestingly, the results from calorimetry (Figure 3.3 and 3.4) show that 5% addition of TiO_2 filler to cement increases the cumulative heat evolved in significant excess of this addition rate - by 21% at 48 hours of hydration. Similar acceleratory effects have been measured during cement replacement with titania nanoparticles [53]. Since the increase in total energy evolved can directly be related to degree of hydration, these results suggest that nanoparticles could effectively replace a higher percentage of cement than that tested in this research, while achieving a similar degree of hydration as that of ordinary portland cement paste. The use of supplementary cementitious materials (SCM's) along with nanoparticles could also result in higher degrees of hydration, especially at later ages of hydration.

Combining this concept with the notion that inert filler materials can be selected such that the life cycle cost of the filler is negligible compared to the cement or TiO_2 suggests that identification of an "optimum" inert filler material, from both particle size and embodied energy perspectives, should be the subject of further investigation. If such a filler were added to TiO_2-blended cements to reach similar degrees of hydration as ordinary portland cement at 48 hours, the maximum replacement rate is calculated to be approximately 17%. For such a mix, the total environmental impact could be much lower compared to the TiO_2-cement mix.

Now, if the capability of TiO_2 to bind pollutant gases (e.g. NO_X, SO_X and VOC's) is considered, a part of the impacts – (e.g. the NO_X emissions) - can be offset with time. Further analysis was performed based on the conditions in Atlanta, USA to calculate the time required to offset the NO_X from TiO_2 production. Atlanta, USA with an average sunshine per day of 7.25 hours was selected because of the location where this research was conducted as well as its relevance to urban environmental conditions. The annual NO_2 concentration in Atlanta was reported 17.0 ppb in 2004 [184]. When 5% of TiO_2 was used as an additive to cement by mass and 5mm thick surface layer is used, 2.12 years (776 days) are required to offset the initial NO_X emissions by the TiO_2-cement mixture. If the surface is frequently washed, as with rainfall or dew, as expected during the life of TiO_2-cement surfaces, the photocatalytic activity could be renewed and hence these surfaces could perform well throughout the life of the structure.

The results from the analytical calculations for the TiO_2-modified cement shows that pollutant gas (NO_X) concentration is reduced, urban air quality improved and smog creation reduced, if TiO_2-containing cementitious materials are used in these localities. Thus in the long term, TiO_2 modified cement could be beneficial to decrease the initial higher environmental impact because of production "costs". Further research and development of TiO_2 with enhanced efficiency for pollutant gas binding (e.g. by doping TiO_2 with transition metal ions [18, 185]) is required. Lower energy use for production of photocatalytic TiO_2 [186] could also make these nanoparticles more favorable from an environmental impact perspective. The use/production of nanoparticles with a lower embodied energy and emissions could result in increased nanoparticle usage in the construction industry even when considering life-cycle costs. Thus the introduction and

optimization of additional functionalities such as photocatalytic properties (binding pollutant gases, antimicrobial effect, self-sensing capability) and development of lower-embodied energy nanoparticles could enhance sustainability and result in a sustainable construction product.

The results from the LCA and photocatalytic properties analysis demonstrate that there are various pathways for enhancing sustainability in construction materials. The use of natural or by-product nanoparticles or a filler with lower embodied energy and lower emissions (such as limestone) is one such potential pathway to attain greater sustainability. The use of microparticles (with size near 1μm) can impart similar properties as that of non-dispersed nanoparticles and cause significant increase in the rate and degree of hydration, especially in the first day of cement hydration. Thus, the use of highly dispersed nanoparticles might not be required for significant increase in the rate and degree of hydration as shown by the use of the submicron sized limestone powder (L3) in this research. The introduction of additional functionalities to cementitious materials, which decreases the environmental impact of construction materials, is another pathway to increase sustainability. The introduction of TiO_2 powder with photocatalytic properties such as pollutant gas binding, anti-microbial properties and self-cleaning capability has the potential to thus improve the sustainability of construction materials. Potential improvement of photocatalytic efficiency and development of lower-energy production processes through ongoing research will also significantly enhance the environmental sustainability index of TiO_2-cement composites [187].

6.5 Economic Cost Analysis

Since photocatalytic TiO_2 is a technology that is being introduced as a technique for achieving sustainability, the economic impact of this material should also be considered. In the construction industry, decisions about materials selected for use are often based on cost. Thus an analysis of the cost of such technology if used in concrete was conducted. The average price of ultrafine and nanoparticles of TiO_2 is \$15/kg [123]. If a 5mm thick layer of TiO_2 is used on the surface (as a thin cladding element, coating or whitetopping) for photocatalytic application, the structure incurs an additional cost of \$3.11/m^2 of surface mix. The increase in cost of concrete with a TiO_2 surface can also be calculated. If concrete cost is estimated to be \$250/m^3 (according to current truckload costs) and concrete is placed with a thickness of 10"(254mm), the additional cost due to the use of a TiO_2 surface would be \$4.68/m^3 of concrete placed. This additional construction cost could be reduced if more TiO_2 is used by the construction industry and also with better efficiency in production techniques for TiO_2 which would reduce manufacturing cost.

6.6 Summary of Life Cycle Analysis

The effect of TiO_2 and limestone fillers on the sustainability of cementitious mixtures was examined in this chapter using a life cycle analysis methodology. The conclusions for this part of the research are summarized below.

- Inclusion of TiO_2 fillers in cement increased the environmental impact of the cementitious mixtures significantly when compared to plain cement mixtures. The

high environmental impact of the TiO_2-cement mixture is due to the higher energy and emissions of TiO_2 manufacturing process compared to cement clinker production.

- Limestone filler decreased the environmental impact of the limestone-cement mixtures compared to plain cement mix. The use of natural or by-product nanoparticles or a filler with lower embodied energy and lower emissions (such as limestone) is one potential pathway to attain greater sustainability for cementitious mixtures.
- The introduction of nanosized TiO_2 powder with photocatalytic properties such as pollutant gas binding, anti-microbial properties and self-cleaning capability has the potential to improve the sustainability of cement-based construction materials. Thus, the introduction of additional functionalities to cementitious materials is another pathway to increase sustainability in the construction industry.

Based on the results from the life cycle analysis of cementitious mixtures with TiO_2 and limestone fillers, the environmental impact of cementitious materials is reduced by replacing cement with fillers which have lower environmental "costs" of production as well as fillers which can positively impact the environment during the life of the structure. Natural submicron or nanosized particles with lower environmental impact could be used as an alternative to manufactured nanoparticles for tailoring properties and reducing environmental impact of cementitious materials. However, before extensive use of nanoparticles in the construction industry, further research is needed to understand the

biological and toxicological impacts on the environment due to natural and manufactured nanoparticles.

CHAPTER 7

CONCLUSIONS AND FUTURE RESEARCH

7.1 Conclusions

The main objective of this research was to understand the effect of addition of commercially available micro and nanoparticles of TiO_2 and limestone on the properties of cementitious materials. Based on the literature review in Chapter 2, the effects of these inert fillers on early age, long term and photocatalytic properties and life cycle costs were investigated. The following sections present the key conclusions of this research.

7.1.1 Early Age Hydration Studies

Due to an increasing interest in the use of TiO_2 and limestone fillers in cementitious mixtures, the effect of these materials of varying particle sizes (up to maximum 20μm particle size) and dosages (up to 15%) on the early age properties of cementitious mixtures was studied, and the following were concluded:

- Replacement of cement with finer inert particles (particle size < 3μm) modifies cement hydration by a dominant heterogeneous nucleation effect. Heterogeneous nucleation effect accelerates hydration reaction, increases the rate of hydration, decreases setting time, but also decreases flow characteristics (workability) and increases chemical and autogenous shrinkage.
- Larger inert fillers (particle size >3 μm) can maintain the rate of cement hydration due to a dominant dilution effect. Large inert particles decrease chemical shrinkage of cementitious mixtures. Setting time and flow characteristics of

cementitious mixtures are not significantly modified due to the replacement of cement with coarse inert fillers.

- Apparent activation energy and temperature sensitivity of cementitious mixtures increases due to the addition of fine inert particles. The activation energy increases with increasing dosage, dispersion and surface area of the nanoparticles used.
- For the compositions examined here, Powers' model can be used to model hydration of filler-cement mixes when coarse inert fillers are used. Powers' model has to be modified to predict chemical shrinkage values and trends in the presence of fine fillers, by incorporating changes to cement hydration due to heterogeneous nucleation effect. Powers' model also has to be modified to consider additional reaction products potentially formed in limestone-cement mixtures, which modifies cement hydration.

7.1.2 Long Term Properties

The long term properties (28- and 56-day strength, permeability and pore structure) of filler-cement mixes with nano and microparticle fillers were investigated, and the following were concluded:

- Strength of ordinary portland cement mix is greater than filler-cement mixes at later ages due to a dominant dilution effect. But initial strength, particularly at ages up to 3 days, can be increased by using fine inert particles due to increased degree of hydration by heterogeneous nucleation effect.

- Total surface area and pore volume increases and pore size decreases by the addition of fine inert fillers. A pore size refinement is thus possible due to the replacement of cement with fine inert fillers.
- Fine limestone (with particle size 0.7µm) does not affect the chloride permeability and surface resistivity of cementitious mixtures. Thus permeability comparable to ordinary portland cement can achieved by using fine limestone fillers. TiO_2 increased the RCPT result and reduced the surface resistivity, indicating that TiO_2-cement mixtures can result in higher permeability when the mineral is used as a partial replacement for cement.

7.1.3 Photocatalytic Properties of TiO_2-Cement

The photocatalytic properties of TiO_2-cement mixtures were studied and the applicability of current standard test methods for NO_X conversion by cement-based materials was investigated, and the following were concluded:

- Due to a lack of an appropriate procedure for characterizing photocatalytic efficiency of cementitious mixtures for reducing NO_X, a new standardized procedure and NO_X conversion efficiency factor is proposed. Modifications for sample preparation techniques and test parameters (i.e., input gas concentration, test duration, flow rate) are suggested to make NO_X conversion tests appropriate for cement-based materials.
- A new photocatalytic efficiency factor (PEF), which considers potential variations in test sample surface area, sample surface roughness and variations in test duration, was defined. The PEF metric can be used to characterize the

photocatalytic activity of any cement-based material or other construction material.

- The inclusion of TiO_2 to cementitious mixtures introduced photocatalytic properties to construction materials. Photocatalytic NO_X conversion efficiency increased with increasing dosage of TiO_2.
- The photocatalytic efficiency of various commercially available TiO_2 mixed with cement was compared using the proposed photocatalytic efficiency factor (PEF). The PEF values of various TiO_2 tested ranged from 8.40 $\mu mol \cdot hr^{-1} \cdot m^{-2}$ for T4 to 21.75 $\mu mol \cdot hr^{-1} \cdot m^{-2}$ for T3 when tested at 500ppb input gas concentration.

7.1.4 Sustainability of cementitious mixtures with TiO_2 and limestone

The effect of TiO_2 and limestone fillers on the sustainability and life cycle costs of cementitious mixtures were examined. The major conclusions based on the life cycle analysis of filler-cement mixtures are summarized below:

- Inclusion of TiO_2 fillers increases the environmental impact of the cementitious mixtures significantly when compared to plain cement. The high environmental impact of the TiO_2-cement mixture is due to the higher energy and emissions of TiO_2 manufacturing process compared to cement clinker production.
- Limestone filler decreases the environmental impact of cementitious mixtures compared to plain cement mix. The use of natural or by-product fillers or fillers with lower embodied energy and emissions is a potential pathway to improve sustainability for cementitious mixtures.

- The introduction of TiO_2 filler with photocatalytic properties (binding pollutant gases, anti-microbial properties and self-cleaning capability) improves sustainability on one metric by offsetting initial emissions of construction materials.

7.2 Recommendations

7.2.1 Early Age Properties

Based on the results from the present study, particle size and dosage of inert fillers can be selected to obtain desired early age properties. For applications where an increased rate of reaction and/or apparent activation energy is required, fine inert fillers (particle size < 3μm) are recommended. In applications where shrinkage is of concern, a coarser microparticle ((particle size > 3μm)) is recommended as the filler. Due to the increased apparent activation energy observed in the presence of nanoparticles, it is recommended that fine inert particles be used to obtain a faster setting and strength gain for cementitious mixtures produced at higher ambient temperatures.

The results from this section of the research show that the effect on early age hydration depends on the particle size and dosage and not significantly on the type of inert filler used. Thus, cement clinker usage by the construction industry could be reduced by the replacement of cement with various inert fillers (including limestone and TiO_2) with simultaneous tailoring of early age properties based on dosage and particle size of inert filler.

7.2.2 Long Term Properties

The results from the present study demonstrate that chloride ion permeability of filler-cement mixtures increases, except in the case of fine limestone filler, when inert fillers are used as partial replacements for cement. The higher RCPT value shows that the permeability could be higher and hence such concrete mixes could have durability issues. Thus, it is recommended that for achieving desirable long term properties, supplementary cementitious materials (SCMs) could be used along with inert fillers. The use of SCMs in filler-cement mixes would increase the strength and decrease permeability. Further research is required on such ternary cementitious mixtures with inert fillers and SCMs.

The lower value of resistivity observed in the TiO_2-cement mixes could be because of the semiconductor nature of TiO_2. This behavior warrants further investigation with different types of additives (e.g. chemicals, SCMs) in concrete to understand the impact of such materials on the surface resistivity test. Since resistivity test is a relatively new test, further research would also help ascertain whether the surface resistivity test can be used as an effective technique to predict and compare permeability of various types of concrete mixtures.

7.2.3 Photocatalytic Properties

Based on the literature review as well as experiments conducted in the present study, it was concluded that the current test methods is not be appropriate for testing photocatalytic efficiency of cementitious materials. It is recommended that the modifications for sample preparation techniques and test parameters (i.e., input gas concentration, test duration, flow rate) and the proposed photocatalytic efficiency factor

be used for all future testing and comparison of photocatalytic NO_X conversion by cement-based materials. It is also recommended that the surface conditioning techniques suggested in the present research (Section 5.2.2) be followed for photocatalytic testing of other pollutant gases or other photocatalytic properties (e.g. self-cleaning, anti-microbial properties) of TiO_2-cement surfaces.

7.2.4 Sustainability of TiO_2 and Limestone Cement Mixes

The replacement of cement with inert fillers was proposed due to the high energy use and emissions from cement clinker production. But sustainability can be improved in filler-cement mixes only if the life cycle cost of such mixes is equal to or lower than plain cement mixes. Although the use of TiO_2 enhanced early age and photocatalytic properties, the environmental impact of cementitious materials increased due to the addition of TiO_2. Thus it is recommended that before widespread use of any filler, a life cycle analysis of the filler-cement composite should be conducted to characterize the environmental impact for achieving sustainability. Based on the result from the present study, fillers with lower embodied energy (naturally occurring fillers or fillers with low production "costs") or fillers which contribute to sustainability due to additional functionalities (e.g. photocatalysis) are recommended to be used in cementitious materials for improving sustainability. For reducing environmental impact if TiO_2 will be used, it is recommended that the TiO_2 be utilized as surface coatings or in thin coating materials such as "whitetopping" overlays, stuccos or plastering cements.

7.3 Future research

The current study investigated the effect of inert nano and microparticles of TiO_2 and limestone on early age, long term and photocatalytic properties and sustainability of cementitious mixtures. However, much further research will be necessary to further optimize the properties of cementitious mixtures for widespread application of such inert fillers. Some key topics that require additional research are listed below:

- The current research used commercially available limestone that was blended with portland cement during preparation of the cementitious mix. But in commercially available portland limestone cement (PLC), limestone and cement are inter-ground during the cement manufacturing process. Such inter-ground PLC could have a lower cement particle size which could increase hydration rate and modify properties compared to laboratory prepared blended limestone-cements. A comparative analysis of early age and term properties and life-cycle costs of blended and inter-ground limestone-cement mixtures should be conducted.
- European standards for portland limestone cements allow up to 35% replacement of cement with limestone [48]. Although ASTM and Canadian standards currently approve the use of limestone only up to 15% [45, 46], there is a possibility that higher percentages of limestone could be approved and used in future construction. Thus the properties of cementitious materials with higher volume replacement (>15%) of cement with limestone (and possibly other inert fillers) needs further research.

- The results from the present research show that the use of inert fillers decreases long term properties of cementitious mixtures. But supplementary cementitious materials (SCMs) added to inert filler-cement mixes could enhance strength, reduce permeability and hence improve long term properties of cementitious materials. The inclusion of SCMs in inert filler-cement mixtures could also modify early age properties and improve sustainability. Thus the combined use of inert nano and microparticles and SCMs in cementitious mixtures needs further research.
- The RCPT and surface resistivity test results from this research indicate that permeability of filler-cement mixtures could be higher than plain cement concrete. But RCPT and surface resistivity tests are indirect tests for measuring permeability. Thus, direct measurement of transport of water and ions through the matrix of filler-cement mixtures could be conducted using long term tests such as salt ponding test and bulk diffusion test. Results from these tests could be used to further understand transport properties.
- Research has shown that effectiveness of fillers increases at lower w/s, when cement is not able to undergo complete hydration [51]. Thus, the effect of variation of w/s (or w/c) on the properties of cementitious mixtures with TiO_2 and limestone should be examined. Variation of w/s of filler-cement mixes could affect properties including early age hydration, shrinkage, strength, resistivity and permeability and hence warrants further research.
- The photocatalytic tests in the current research were conducted in the presence of UV light. But new TiO_2 based materials are being developed which are

photocatalytic in the presence of visible light [18, 188]. These TiO_2-based materials could be used in construction materials that can be placed in the interior of a building without the requirement for UV light. The photocatalytic activity of cement mixtures with these new TiO_2 materials needs further research.

- Photocatalytic tests of TiO_2-cement surfaces should be conducted under field conditions, so that this technology can be effectively utilized for decreasing pollution, especially in urban environments. Pollution reduction, self-cleaning and anti-microbial properties of TiO_2-cement surfaces should be examined simultaneously, to truly characterize the benefits of the use of these materials in field applications.
- Further research is needed to address the environmental impacts associated with the manufacture of photocatalytic nanoparticles and other manufactured nanoparticles. The life cycle impact of manufactured nanoparticles including toxicity and environmental impact could be quantified and included in life cycle analysis.
- The possibility of release of nanoparticles into the environment from construction materials during the life or at end-of-life-disposal needs further research. The nanoparticles could enter the food cycle of humans and animals and can result in accumulation of nanoparticles. The long term effect of such accumulated nanoparticles on ecology and impact on life cycle costs needs further analysis.
- Improvement of early age properties, long term properties and sustainability could not be simultaneously achieved with the inert fillers tested. Further research is necessary to obtain improved or satisfactory properties when addressing multiple

properties. Future research should consider TiO_2, limestone as well as other inert fillers, including natural or by-product fillers of varying sizes to simultaneously optimize multiple properties of cementitious materials.

APPENDIX A

EFFECT OF PARTICLE DISPERSION ON HYDRATION

A challenge in the use of nanoparticles in the construction industry is effective dispersion, which is required due to the tendency of nanomaterials to form agglomerates [176]. Poor dispersion can result in the formation of defects and also decrease the efficacy of the nanomaterial in the material matrix [189]. With an objective of obtaining effective dispersion, different mixing procedures were examined to assess the influence of TiO_2 nanoparticle dispersion on early age hydration reactions. The techniques that were tested and compared in this study include pre-dispersion of TiO_2 in the mixing water using the following techniques: use of a handheld mixer, dispersing agent (superplasticizer) and ultrasonication. Ultrasonication of powders in water is considered to be a good technique for dispersing agglomerates, especially for nanoparticles [179].

All cementitious mixes were prepared at w/s of 0.50, with the same TiO_2 (T2), at 10% TiO_2 but were dispersed using different methods. The dispersing agent (surfactant) used in the current research was a polycarboxylate based superplasticizer, ADVA 140 (Grace Construction Products) and was used at an addition rate of 10 mL/1 kg of cement. The following are the different types of dispersion techniques investigated in this study:

- D1 – TiO_2 dispersed in water using a handheld mixer for 1 minute before mixing with cement
- D2 – Superplasticizer added to water and stirred. TiO_2 was then added to the water-super plasticizer mixture and dispersed using a handheld mixer for 1 minute before mixing with cement

- D3 – Super plasticizer added to water and stirred and the TiO_2 was then added to the water-super plasticizer mixture. The beaker with the solution was then immersed in an ultrasonic bath (Branson 1510R-DTH) for 30 minutes. The ultrasonication was conducted at a frequency of 42±2.5 kHz and at a power output of 70W. The mixture was then blended using a handheld mixer for 1 minute before mixing with cement.

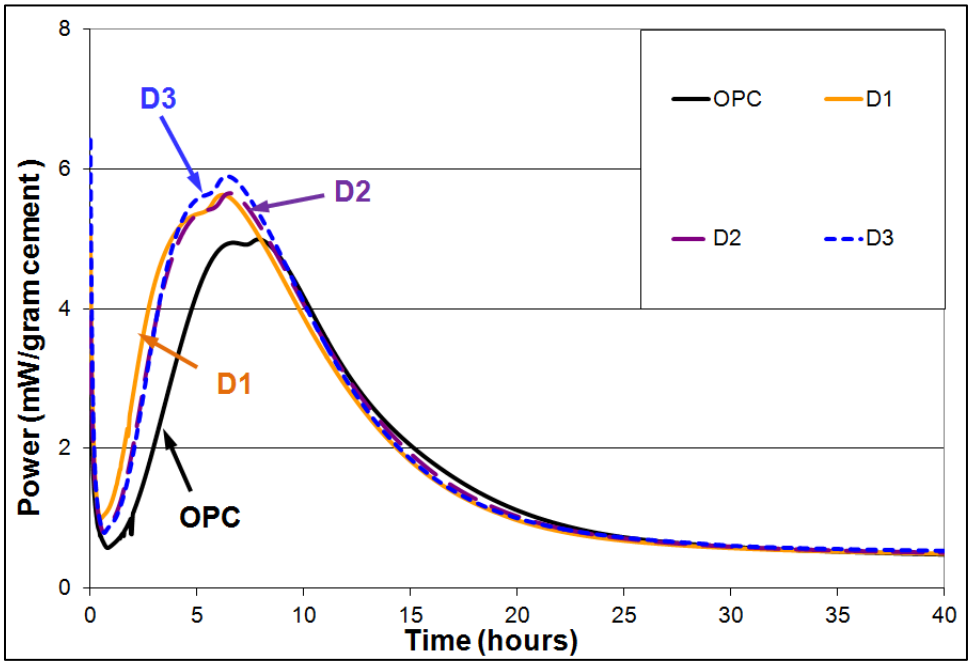

Figure A.1. Heat of hydration curves for TiO_2 cement mixes when different techniques were used for dispersing TiO_2 particles

Figure A.1 shows the rate of heat evolution data for the different mixes D1, D2 and D3 in which various dispersion techniques were used. The two mixes in which the TiO_2 was dispersed using the superplasticizer (D2 and D3) showed a marginal retardation of the cement hydration reaction, as observed in the accelerating region of the hydration curve, when compared to mix D1. The hydration curve for mixing technique D3 resulted

in a higher peak of the hydration graph compared to D1 and D2. This shows that the use of a combination of dispersing agent, ultrasonic bath and handheld mixer used to disperse the nanoparticles could be beneficial for dispersion. But for further clarification the cumulative heat of hydration curves of the different mixes was compared in Figure A.2.

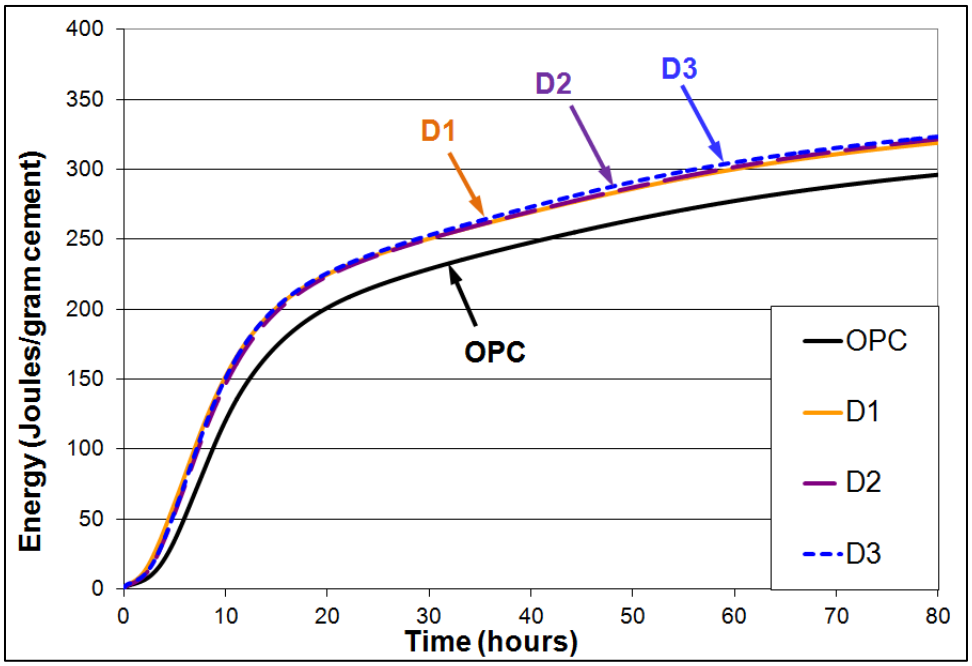

Figure A.2. Cumulative heat of hydration curves for TiO_2 cement mixes when different techniques were used for dispersing TiO_2 particles

Figure A.2 shows the cumulative heat of hydration curve for the different mixes tested for the effect of dispersion. It was observed that during the testing period the difference between the cumulative heats of hydration graphs was minimal for all the mixes with TiO_2 addition. Thus in the current research, mixing of the nanoparticle with water using a handheld mixer was found to be as effective as the use of dispersing agents and ultrasonication. Since the difference between the hydration behaviors was minimal, it is suggested that other forms of effective dispersion could be necessary to utilize the true

nanosize of the TiO_2 particles when used in cementitious materials. Some previous researchers have observed that the use of ultrasonication techniques and surfactants increases dispersion of nanoparticles [176]. Thus, further research is required for effective dispersion of commercially available nanoparticles, using possibly different sonication methods (e.g. immersion type sonication, high powered sonication) as well as other dispersing agents.

APPENDIX B

LIFE CYCLE INVENTORY DATA

The Life cycle inventory data for ordinary portland cement mix as well as limestone-cement and TiO_2-cement mix where cement was replaced with 5% filler, as obtained from the life cycle analysis is listed in Table B.1.

Table B.1. Life cycle inventory data for plain cement and filler-cement mix with 5% filler

No	Substance	Compartment	Unit	LS-cement	TiO2-cement	Plain cement
1	Aluminium, 24% in bauxite, 11% in crude ore, in ground	Raw	g	6.76E-01	8.76E+01	3.41E-01
2	Anhydrite, in ground	Raw	µg	3.19E+00	5.79E+02	1.58E+00
3	Barite, 15% in crude ore, in ground	Raw	g	6.89E-01	1.63E+02	2.26E-02
4	Baryte, in ground	Raw	g	8.75E+01	8.75E+01	9.21E+01
5	Basalt, in ground	Raw	g	2.18E-02	1.77E+01	4.28E-03
6	Bauxite, in ground	Raw	g	5.49E+01	5.49E+01	5.78E+01
7	Borax, in ground	Raw	µg	9.15E+00	2.31E+02	1.95E+00
8	Cadmium, 0.30% in sulfide, Cd 0.18%, Pb, Zn, Ag, In, in ground	Raw	mg	3.18E-02	2.49E+01	9.67E-03
9	Calcite, in ground	Raw	lb	1.10E+02	6.10E+01	6.66E-02
10	Carbon dioxide, in air	Raw	oz	6.91E-01	7.53E+01	5.13E-01
11	Carbon, in organic matter, in soil	Raw	mg	1.04E+00	6.29E+01	1.17E-02
12	Cerium, 24% in bastnasite, 2.4% in crude ore, in ground	Raw	pg	x	9.62E-02	x
13	Chromium, 25.5% in chromite, 11.6% in crude ore, in ground	Raw	g	1.65E-01	5.18E+01	2.56E-02
14	Chromium, in ground	Raw	g	2.33E+00	2.33E+00	2.45E+00
15	Chrysotile, in ground	Raw	mg	8.49E-03	3.56E+02	3.24E-03
16	Cinnabar, in ground	Raw	mg	9.74E-04	3.27E+01	4.87E-04
17	Clay, bentonite, in ground	Raw	g	2.95E+01	8.17E+01	3.08E+01
18	Clay, unspecified, in ground	Raw	kg	2.66E+02	2.72E+02	2.80E+02
19	Coal, 18 MJ per kg, in ground	Raw	kg	1.48E+02	1.48E+02	1.56E+02
20	Coal, brown, 8 MJ per kg, in ground	Raw	kg	1.79E+01	1.79E+01	1.88E+01
21	Coal, brown, in ground	Raw	oz	1.69E+00	5.01E+02	4.78E-01
22	Coal, hard, unspecified, in ground	Raw	oz	1.76E+00	3.97E+02	5.04E-01
23	Cobalt, in ground	Raw	µg	1.40E+01	1.01E+02	1.05E+01
24	Colemanite, in ground	Raw	mg	2.25E+00	4.42E+02	1.91E+00
25	Copper, 0.99% in sulfide, Cu 0.36% and Mo 8.2E-3% in crude ore, in ground	Raw	g	1.48E-02	5.35E+00	2.58E-03

Table B.1 (Continued)

No	Substance	Compartment	Unit	LS-cement	TiO2-cement	Plain cement
26	Copper, 1.18% in sulfide, Cu 0.39% and Mo 8.2E-3% in crude ore, in ground	Raw	g	8.22E-02	2.94E+01	1.43E-02
27	Copper, 1.42% in sulfide, Cu 0.81% and Mo 8.2E-3% in crude ore, in ground	Raw	g	2.18E-02	7.80E+00	3.79E-03
28	Copper, 2.19% in sulfide, Cu 1.83% and Mo 8.2E-3% in crude ore, in ground	Raw	g	1.08E-01	3.91E+01	1.88E-02
29	Copper, in ground	Raw	g	1.48E+01	1.48E+01	1.56E+01
30	Diatomite, in ground	Raw	µg	4.27E-02	6.36E+00	1.16E-02
31	Dolomite, in ground	Raw	g	3.74E-02	8.14E+00	5.00E-03
32	Energy, gross calorific value, in biomass	Raw	MJ	2.03E-01	2.18E+01	1.55E-01
33	Energy, gross calorific value, in biomass, primary forest	Raw	kJ	7.18E-02	4.36E+00	8.13E-04
34	Energy, kinetic (in wind), converted	Raw	MJ	2.69E-02	5.86E+00	7.09E-03
35	Energy, potential (in hydropower reservoir), converted	Raw	MJ	8.45E+01	1.27E+02	8.44E+01
36	Energy, solar, converted	Raw	kJ	8.23E-01	8.44E+01	1.94E-01
37	Feldspar, in ground	Raw	µg	2.50E+01	5.29E+01	2.50E+01
38	Fluorine, 4.5% in apatite, 1% in crude ore, in ground	Raw	mg	6.19E-01	2.67E+02	5.87E-02
39	Fluorine, 4.5% in apatite, 3% in crude ore, in ground	Raw	mg	2.84E-01	1.19E+02	2.66E-02
40	Fluorspar, 92%, in ground	Raw	g	3.20E-02	8.07E+00	4.65E-03
41	Gallium, 0.014% in bauxite, in ground	Raw	ng	2.36E+00	2.40E+02	5.56E-01
42	Gas, mine, off-gas, process, coal mining/kg	Raw	g	9.06E+02	9.06E+02	9.54E+02
43	Gas, mine, off-gas, process, coal mining/m3	Raw	dm3	5.01E-01	1.13E+02	1.48E-01
44	Gas, natural, 35 MJ per m3, in ground	Raw	m3	5.77E+00	5.77E+00	6.07E+00
45	Gas, natural, in ground	Raw	cu.yd	3.55E-02	9.72E+01	6.36E-03
46	Gas, petroleum, 35 MJ per m3, in ground	Raw	m3	1.24E+00	1.24E+00	1.30E+00
47	Gold, Au 1.1E-4%, Ag 4.2E-3%, in ore, in ground	Raw	µg	3.28E-02	3.06E+02	1.04E-02
48	Gold, Au 1.3E-4%, Ag 4.6E-5%, in ore, in ground	Raw	µg	6.01E-02	5.61E+02	1.90E-02
49	Gold, Au 1.4E-4%, in ore, in ground	Raw	µg	7.20E-02	6.72E+02	2.28E-02
50	Gold, Au 2.1E-4%, Ag 2.1E-4%, in ore, in ground	Raw	mg	1.10E-04	1.03E+00	3.48E-05

Table B.1 (Continued)

No	Substance	Compartment	Unit	LS-cement	TiO2-cement	Plain cement
51	Gold, Au 4.3E-4%, in ore, in ground	Raw	µg	2.72E-02	2.54E+02	8.63E-03
52	Gold, Au 4.9E-5%, in ore, in ground	Raw	µg	6.53E-02	6.09E+02	2.07E-02
53	Gold, Au 6.7E-4%, in ore, in ground	Raw	µg	1.01E-01	9.43E+02	3.20E-02
54	Gold, Au 7.1E-4%, in ore, in ground	Raw	mg	1.14E-04	1.06E+00	3.61E-05
55	Gold, Au 9.7E-4%, Ag 9.7E-4%, Zn 0.63%, Cu 0.38%, Pb 0.014%, in ore, in ground	Raw	µg	6.83E-03	6.37E+01	2.16E-03
56	Granite, in ground	Raw	ng	2.18E+01	2.25E+02	8.36E-02
57	Gravel, in ground	Raw	kg	9.51E+00	4.27E+01	9.96E+00
58	Gypsum, in ground	Raw	mg	1.36E-01	1.13E+01	8.05E-03
59	Helium, 0.08% in natural gas, in ground	Raw	µg	1.19E-02	1.21E+00	2.80E-03
60	Indium, 0.005% in sulfide, In 0.003%, Pb, Zn, Ag, Cd, in ground	Raw	µg	6.42E-01	4.26E+02	1.87E-01
61	Iron, 46% in ore, 25% in crude ore, in ground	Raw	oz	6.78E-01	1.23E+02	1.88E-01
62	Iron, in ground	Raw	g	9.23E+02	9.23E+02	9.72E+02
63	Kaolinite, 24% in crude ore, in ground	Raw	mg	3.16E+01	3.11E+02	4.39E-01
64	Kieserite, 25% in crude ore, in ground	Raw	mg	8.87E-02	2.15E+00	7.12E-03
65	Land use II-III	Raw	m2a	5.69E+00	5.69E+00	5.99E+00
66	Land use II-III, sea floor	Raw	m2a	1.39E+00	1.39E+00	1.46E+00
67	Land use II-IV	Raw	m2a	7.70E-01	7.70E-01	8.10E-01
68	Land use II-IV, sea floor	Raw	m2a	1.43E-01	1.43E-01	1.51E-01
69	Land use III-IV	Raw	m2a	5.60E-01	5.60E-01	5.89E-01
70	Land use IV-IV	Raw	cm2a	3.60E+01	3.60E+01	3.79E+01
71	Lanthanum, 7.2% in bastnasite, 0.72% in crude ore, in ground	Raw	pg	x	2.54E-01	x
72	Lead, 5.0% in sulfide, Pb 3.0%, Zn, Ag, Cd, In, in ground	Raw	g	7.35E-03	1.39E+00	1.26E-03
73	Lead, in ground	Raw	g	4.44E+00	4.44E+00	4.67E+00
74	Magnesite, 60% in crude ore, in ground	Raw	g	3.39E-01	5.15E+01	1.40E-01
75	Magnesium, 0.13% in water	Raw	mg	4.97E-03	1.49E+00	1.38E-03
76	Manganese, 35.7% in sedimentary deposit, 14.2% in crude ore, in ground	Raw	g	1.57E-01	6.38E+00	4.99E-03
77	Manganese, in ground	Raw	mg	9.29E+02	9.29E+02	9.78E+02
78	Marl, in ground	Raw	tn.lg	1.08E+00	1.08E+00	1.13E+00

Table B.1 (Continued)

No	Substance	Compartment	Unit	LS-cement	TiO2-cement	Plain cement
79	Metamorphous rock, graphite containing, in ground	Raw	mg	5.27E-01	1.22E+02	3.87E-02
80	Molybdenum, 0.010% in sulfide, Mo 8.2E-3% and Cu 1.83% in crude ore, in ground	Raw	mg	2.01E+00	7.26E+02	3.49E-01
81	Molybdenum, 0.014% in sulfide, Mo 8.2E-3% and Cu 0.81% in crude ore, in ground	Raw	mg	2.86E-01	1.02E+02	4.98E-02
82	Molybdenum, 0.022% in sulfide, Mo 8.2E-3% and Cu 0.36% in crude ore, in ground	Raw	g	5.51E-02	2.21E+00	1.63E-03
83	Molybdenum, 0.025% in sulfide, Mo 8.2E-3% and Cu 0.39% in crude ore, in ground	Raw	mg	1.05E+00	3.75E+02	1.82E-01
84	Molybdenum, 0.11% in sulfide, Mo 4.1E-2% and Cu 0.36% in crude ore, in ground	Raw	g	1.11E-01	4.46E+00	3.29E-03
85	Molybdenum, in ground	Raw	µg	8.59E+00	8.59E+00	9.04E+00
86	Neodymium, 4% in bastnasite, 0.4% in crude ore, in ground	Raw	pg	x	5.37E-02	x
87	Nickel, 1.13% in sulfide, Ni 0.76% and Cu 0.76% in crude ore, in ground	Raw	mg	5.17E-01	5.90E+01	4.93E-02
88	Nickel, 1.98% in silicates, 1.04% in crude ore, in ground	Raw	g	7.14E-01	1.54E+02	7.58E-02
89	Nickel, in ground	Raw	g	1.29E+00	1.29E+00	1.36E+00
90	Occupation, arable, non-irrigated	Raw	cm2a	5.54E-01	5.31E+01	3.13E-02
91	Occupation, construction site	Raw	cm2a	4.92E-01	3.19E+02	2.30E-01
92	Occupation, dump site	Raw	m2a	1.19E-03	2.89E-01	2.56E-04
93	Occupation, dump site, benthos	Raw	cm2a	4.83E-01	2.17E+02	2.04E-02
94	Occupation, forest, intensive	Raw	m2a	4.14E-04	5.58E-01	1.90E-05
95	Occupation, forest, intensive, normal	Raw	m2a	1.32E-02	2.49E+00	9.98E-03
96	Occupation, forest, intensive, short-cycle	Raw	cm2a	1.80E-01	1.09E+01	2.04E-03
97	Occupation, industrial area	Raw	m2a	6.98E-03	1.17E-01	6.49E-03
98	Occupation, industrial area, benthos	Raw	mm2a	4.13E-01	2.06E+02	1.99E-02
99	Occupation, industrial area, built up	Raw	m2a	2.22E-04	1.41E-01	4.99E-05
100	Occupation, industrial area, vegetation	Raw	cm2a	9.25E-01	4.86E+02	5.19E-01
101	Occupation, mineral extraction site	Raw	m2a	5.07E-03	1.05E-01	5.64E-04

Table B.1 (Continued)

No	Substance	Compartment	Unit	LS-cement	TiO2-cement	Plain cement
102	Occupation, permanent crop, fruit, intensive	Raw	cm2a	2.62E-01	1.55E+01	2.89E-03
103	Occupation, shrub land, sclerophyllous	Raw	cm2a	3.05E-01	1.81E+02	2.07E-01
104	Occupation, traffic area, rail embankment	Raw	cm2a	4.00E-01	5.59E+02	9.97E-02
105	Occupation, traffic area, rail network	Raw	cm2a	4.43E-01	6.18E+02	1.10E-01
106	Occupation, traffic area, road embankment	Raw	cm2a	1.48E+00	4.59E+02	1.02E+00
107	Occupation, traffic area, road network	Raw	m2a	5.18E-04	2.47E-01	1.96E-04
108	Occupation, urban, discontinuously built	Raw	mm2a	1.46E-01	8.55E+00	3.31E-03
109	Occupation, water bodies, artificial	Raw	m2a	1.02E-03	1.70E-01	3.13E-04
110	Occupation, water courses, artificial	Raw	cm2a	4.77E+01	4.23E+02	2.24E+00
111	Oil, crude, 42.6 MJ per kg, in ground	Raw	kg	1.81E+01	1.81E+01	1.90E+01
112	Oil, crude, in ground	Raw	oz	5.64E+00	4.11E+02	1.65E-01
113	Olivine, in ground	Raw	µg	2.40E+00	2.47E+02	1.14E+00
114	Palladium, in ground	Raw	µg	4.09E+00	4.09E+00	4.31E+00
115	Pd, Pd 2.0E-4%, Pt 4.8E-4%, Rh 2.4E-5%, Ni 3.7E-2%, Cu 5.2E-2% in ore, in ground	Raw	µg	1.66E-01	8.27E+01	6.76E-03
116	Pd, Pd 7.3E-4%, Pt 2.5E-4%, Rh 2.0E-5%, Ni 2.3E+0%, Cu 3.2E+0% in ore, in ground	Raw	µg	4.00E-01	1.99E+02	1.62E-02
117	Peat, in ground	Raw	g	1.66E-03	1.19E+00	3.09E-04
118	Phosphorus, 18% in apatite, 12% in crude ore, in ground	Raw	mg	3.05E+01	5.08E+02	2.95E+01
119	Phosphorus, 18% in apatite, 4% in crude ore, in ground	Raw	g	2.48E-03	1.07E+00	2.35E-04
120	Platinum, in ground	Raw	µg	4.77E+00	4.77E+00	5.02E+00
121	Pt, Pt 2.5E-4%, Pd 7.3E-4%, Rh 2.0E-5%, Ni 2.3E+0%, Cu 3.2E+0% in ore, in ground	Raw	µg	9.63E-03	6.21E+00	1.52E-03
122	Pt, Pt 4.8E-4%, Pd 2.0E-4%, Rh 2.4E-5%, Ni 3.7E-2%, Cu 5.2E-2% in ore, in ground	Raw	µg	3.45E-02	2.22E+01	5.46E-03
123	Rh, Rh 2.0E-5%, Pt 2.5E-4%, Pd 7.3E-4%, Ni 2.3E+0%, Cu 3.2E+0% in ore, in ground	Raw	ng	4.12E+00	5.77E+02	2.28E-01
124	Rh, Rh 2.4E-5%, Pt 4.8E-4%, Pd 2.0E-4%, Ni 3.7E-2%, Cu 5.2E-2% in ore, in ground	Raw	µg	1.29E-02	1.81E+00	7.15E-04

Table B.1 (Continued)

No	Substance	Compartment	Unit	LS-cement	TiO2-cement	Plain cement
125	Rhenium, in crude ore, in ground	Raw	µg	5.89E-03	1.79E+00	1.74E-04
126	Rhenium, in ground	Raw	µg	3.95E+00	3.95E+00	4.16E+00
127	Rhodium, in ground	Raw	µg	4.38E+00	4.38E+00	4.61E+00
128	Sand, unspecified, in ground	Raw	g	1.94E+02	1.94E+02	2.04E+02
129	Shale, in ground	Raw	mg	9.05E-03	1.64E+00	4.46E-03
130	Silver, 0.007% in sulfide, Ag 0.004%, Pb, Zn, Cd, In, in ground	Raw	mg	9.80E-04	6.78E+00	2.90E-04
131	Silver, 3.2ppm in sulfide, Ag 1.2ppm, Cu and Te, in crude ore, in ground	Raw	mg	7.02E-04	4.83E+00	2.07E-04
132	Silver, Ag 2.1E-4%, Au 2.1E-4%, in ore, in ground	Raw	µg	6.46E-02	4.46E+02	1.91E-02
133	Silver, Ag 4.2E-3%, Au 1.1E-4%, in ore, in ground	Raw	mg	1.48E-04	1.02E+00	4.36E-05
134	Silver, Ag 4.6E-5%, Au 1.3E-4%, in ore, in ground	Raw	µg	1.45E-01	9.99E+02	4.27E-02
135	Silver, Ag 9.7E-4%, Au 9.7E-4%, Zn 0.63%, Cu 0.38%, Pb 0.014%, in ore, in ground	Raw	µg	9.55E-02	6.59E+02	2.82E-02
136	Silver, in ground	Raw	mg	5.64E+01	5.64E+01	5.94E+01
137	Sodium chloride, in ground	Raw	oz	3.78E+00	4.38E+02	3.96E+00
138	Sodium nitrate, in ground	Raw	ng	2.01E-01	1.91E+02	1.02E-01
139	Sodium sulphate, various forms, in ground	Raw	g	4.62E-03	2.07E+00	3.35E-04
140	Stibnite, in ground	Raw	ng	4.43E+00	6.61E+02	1.21E+00
141	Sulfur, in ground	Raw	mg	7.50E-01	7.79E+01	3.65E-01
142	Sylvite, 25 % in sylvinite, in ground	Raw	mg	3.22E+00	5.06E+02	5.91E-01
143	Talc, in ground	Raw	mg	7.75E+00	2.58E+02	4.50E+00
144	Tantalum, 81.9% in tantalite, 1.6E-4% in crude ore, in ground	Raw	mg	7.35E-04	5.35E+00	2.19E-04
145	Tellurium, 0.5ppm in sulfide, Te 0.2ppm, Cu and Ag, in crude ore, in ground	Raw	µg	1.05E-01	7.25E+02	3.11E-02
146	Tin, 79% in cassiterite, 0.1% in crude ore, in ground	Raw	mg	1.02E+01	2.62E+02	3.35E-02
147	Tin, in ground	Raw	mg	3.14E+01	3.14E+01	3.30E+01
148	TiO2, 54% in ilmenite, 2.6% in crude ore, in ground	Raw	lb	3.39E-05	1.27E+02	4.81E-06
149	TiO2, 95% in rutile, 0.40% in crude ore, in ground	Raw	µg	5.27E-02	4.25E+01	1.79E-02
150	Transformation, from arable	Raw	mm2	6.64E-01	6.18E+01	2.22E-01
151	Transformation, from arable, non-irrigated	Raw	cm2	1.02E+00	9.79E+01	5.79E-02

Table B.1 (Continued)

No	Substance	Compartment	Unit	LS-cement	TiO2-cement	Plain cement
152	Transformation, from arable, non-irrigated, fallow	Raw	mm2	8.20E-02	1.06E+01	4.14E-02
153	Transformation, from dump site, inert material landfill	Raw	mm2	1.84E+00	3.69E+02	4.08E-01
154	Transformation, from dump site, residual material landfill	Raw	cm2	6.57E-03	3.22E+01	1.23E-03
155	Transformation, from dump site, sanitary landfill	Raw	mm2	3.60E+00	1.34E+01	3.60E+00
156	Transformation, from dump site, slag compartment	Raw	mm2	5.70E-03	1.23E+00	3.19E-03
157	Transformation, from forest	Raw	cm2	5.04E+00	3.14E+02	5.97E-02
158	Transformation, from forest, extensive	Raw	cm2	9.45E-01	2.38E+02	6.78E-01
159	Transformation, from forest, intensive, clear-cutting	Raw	mm2	6.43E-01	3.91E+01	7.28E-03
160	Transformation, from industrial area	Raw	mm2	1.57E+00	4.18E+02	3.41E-01
161	Transformation, from industrial area, benthos	Raw	mm2	5.75E-04	2.35E+00	1.41E-04
162	Transformation, from industrial area, built up	Raw	mm2	8.84E-04	3.79E-01	8.38E-05
163	Transformation, from industrial area, vegetation	Raw	mm2	1.51E-03	6.47E-01	1.43E-04
164	Transformation, from mineral extraction site	Raw	cm2	3.47E+00	2.91E+01	1.62E-01
165	Transformation, from pasture and meadow	Raw	cm2	3.87E-01	6.40E+01	7.74E-02
166	Transformation, from pasture and meadow, intensive	Raw	mm2	8.30E-02	7.98E+00	4.72E-03
167	Transformation, from sea and ocean	Raw	cm2	4.88E-01	2.17E+02	2.05E-02
168	Transformation, from shrub land, sclerophyllous	Raw	cm2	3.46E-01	3.83E+01	5.37E-02
169	Transformation, from tropical rain forest	Raw	mm2	6.43E-01	3.91E+01	7.28E-03
170	Transformation, from unknown	Raw	cm2	2.03E+00	2.14E+02	1.62E+00
171	Transformation, to arable	Raw	cm2	3.77E-02	4.54E+01	1.15E-02
172	Transformation, to arable, non-irrigated	Raw	cm2	1.02E+00	9.80E+01	5.79E-02
173	Transformation, to arable, non-irrigated, fallow	Raw	mm2	1.41E-01	3.48E+01	8.82E-02
174	Transformation, to dump site	Raw	cm2	8.22E-02	1.49E+01	1.14E-02
175	Transformation, to dump site, benthos	Raw	cm2	4.83E-01	2.17E+02	2.04E-02
176	Transformation, to dump site, inert material landfill	Raw	mm2	1.84E+00	3.69E+02	4.08E-01

Table B.1 (Continued)

No	Substance	Compartment	Unit	LS-cement	TiO2-cement	Plain cement
177	Transformation, to dump site, residual material landfill	Raw	cm2	6.57E-03	3.22E+01	1.23E-03
178	Transformation, to dump site, sanitary landfill	Raw	mm2	3.60E+00	1.34E+01	3.60E+00
179	Transformation, to dump site, slag compartment	Raw	mm2	5.70E-03	1.23E+00	3.19E-03
180	Transformation, to forest	Raw	cm2	3.50E+00	5.48E+01	1.94E-01
181	Transformation, to forest, intensive	Raw	cm2	2.76E-02	3.72E+01	1.27E-03
182	Transformation, to forest, intensive, clear-cutting	Raw	mm2	6.43E-01	3.91E+01	7.28E-03
183	Transformation, to forest, intensive, normal	Raw	cm2	9.04E-01	1.98E+02	6.70E-01
184	Transformation, to forest, intensive, short-cycle	Raw	mm2	6.43E-01	3.91E+01	7.28E-03
185	Transformation, to heterogeneous, agricultural	Raw	cm2	8.13E-02	1.52E+01	2.84E-03
186	Transformation, to industrial area	Raw	cm2	9.58E-01	1.55E+01	9.30E-01
187	Transformation, to industrial area, benthos	Raw	mm2	5.34E-01	1.93E+01	2.40E-03
188	Transformation, to industrial area, built up	Raw	cm2	5.67E-02	2.92E+01	1.34E-02
189	Transformation, to industrial area, vegetation	Raw	cm2	2.36E-02	1.03E+01	1.30E-02
190	Transformation, to mineral extraction site	Raw	cm2	5.63E+00	3.68E+02	5.92E-01
191	Transformation, to pasture and meadow	Raw	mm2	9.36E-02	3.51E+02	2.22E-02
192	Transformation, to permanent crop, fruit, intensive	Raw	mm2	3.68E-01	2.18E+01	4.07E-03
193	Transformation, to sea and ocean	Raw	mm2	5.75E-04	2.35E+00	1.41E-04
194	Transformation, to shrub land, sclerophyllous	Raw	cm2	6.10E-02	3.61E+01	4.13E-02
195	Transformation, to traffic area, rail embankment	Raw	mm2	9.32E-02	1.30E+02	2.32E-02
196	Transformation, to traffic area, rail network	Raw	mm2	1.02E-01	1.43E+02	2.55E-02
197	Transformation, to traffic area, road embankment	Raw	mm2	9.63E-01	2.87E+02	6.67E-01
198	Transformation, to traffic area, road network	Raw	cm2	6.00E-02	2.70E+01	1.61E-02
199	Transformation, to unknown	Raw	mm2	1.85E+00	4.40E+02	5.50E-01
200	Transformation, to urban, discontinuously built	Raw	mm2	2.91E-03	1.70E-01	6.60E-05

Table B.1 (Continued)

No	Substance	Compartment	Unit	LS-cement	TiO2-cement	Plain cement
201	Transformation, to water bodies, artificial	Raw	cm2	1.99E-01	3.26E+01	1.26E-01
202	Transformation, to water courses, artificial	Raw	mm2	5.82E+01	4.96E+02	2.67E+00
203	Ulexite, in ground	Raw	mg	4.99E-02	1.34E+01	1.31E-02
204	Uranium, 560 GJ per kg, in ground	Raw	g	1.22E+00	1.22E+00	1.28E+00
205	Uranium, in ground	Raw	mg	1.30E+01	5.93E+02	2.87E+00
206	Vermiculite, in ground	Raw	mg	9.78E+01	9.96E+01	9.77E+01
207	Volume occupied, final repository for low-active radioactive waste	Raw	cm3	2.67E-02	1.22E+00	5.92E-03
208	Volume occupied, final repository for radioactive waste	Raw	mm3	6.01E+00	3.07E+02	1.34E+00
209	Volume occupied, reservoir	Raw	m3y	1.78E+00	2.62E+00	1.85E+00
210	Volume occupied, underground deposit	Raw	cm3	1.37E-02	4.62E+00	3.87E-03
211	Water, cooling, unspecified natural origin/m3	Raw	gal*	1.47E+00	6.39E+02	3.98E-01
212	Water, lake	Raw	dm3	9.03E+01	9.22E+01	9.03E+01
213	Water, river	Raw	dm3	2.70E+02	5.64E+02	2.66E+02
214	Water, salt, ocean	Raw	dm3	5.64E-01	9.55E+01	1.22E-01
215	Water, salt, sole	Raw	cu.in	6.86E+00	5.35E+02	1.86E-01
216	Water, turbine use, unspecified natural origin	Raw	m3	4.67E+02	7.88E+02	4.45E+02
217	Water, unspecified natural origin/kg	Raw	tn.lg	3.12E+00	3.12E+00	3.29E+00
218	Water, unspecified natural origin/m3	Raw	cuft	4.24E-02	1.98E+02	1.62E-02
219	Water, well, in ground	Raw	dm3	2.11E+02	2.80E+02	2.09E+02
220	Wood, dry matter	Raw	kg	1.11E+00	1.11E+00	1.17E+00
221	Wood, hard, standing	Raw	cm3	1.27E+01	3.86E+02	1.14E+01
222	Wood, primary forest, standing	Raw	mm3	6.66E+00	4.05E+02	7.54E-02
223	Wood, soft, standing	Raw	cu.in	2.62E-01	1.12E+02	6.21E-02
224	Wood, unspecified, standing/m3	Raw	mm3	2.64E-01	4.52E+00	1.32E-01
225	Zinc, 9.0% in sulfide, Zn 5.3%, Pb, Ag, Cd, In, in ground	Raw	g	5.20E-02	2.49E+01	3.73E-02
226	Zinc, in ground	Raw	mg	1.32E+02	1.32E+02	1.39E+02
227	Zirconium, 50% in zircon, 0.39% in crude ore, in ground	Raw	mg	8.08E-04	7.33E+00	2.54E-04
228	1-Propanol	Air	µg	1.07E-02	1.09E+00	2.52E-03
229	1,4-Butanediol	Air	µg	2.15E-04	1.78E+00	6.60E-05
230	2-Propanol	Air	mg	3.55E-03	3.33E+01	1.12E-03
231	Acenaphthene	Air	ng	3.73E-01	1.00E+02	1.03E-01
232	Acetaldehyde	Air	mg	2.82E+01	1.03E+02	2.96E+01
233	Acetic acid	Air	mg	1.27E+02	2.03E+02	1.33E+02

Table B.1 (Continued)

No	Substance	Compartment	Unit	LS-cement	TiO2-cement	Plain cement
234	Acetone	Air	mg	2.80E+01	8.10E+01	2.94E+01
235	Acetonitrile	Air	µg	6.99E-01	4.25E+01	7.92E-03
236	Acrolein	Air	µg	5.73E+00	2.40E+01	3.79E+00
237	Acrylic acid	Air	µg	9.22E-03	8.61E+01	2.92E-03
238	Actinides, radioactive, unspecified	Air	mBq	2.56E-01	1.22E+01	5.72E-02
239	Aerosols, radioactive, unspecified	Air	mBq	3.45E+00	2.56E+02	7.88E-01
240	Aldehydes, unspecified	Air	mg	9.82E-01	1.74E+00	1.02E+00
241	Aluminum	Air	g	1.64E+00	4.25E+00	1.10E+00
242	Americium-241	Air	mBq	9.37E+00	9.37E+00	9.86E+00
243	Ammonia	Air	g	8.18E-01	4.72E+00	6.07E-01
244	Ammonium carbonate	Air	µg	2.76E-01	2.00E+01	6.02E-02
245	Antimony	Air	mg	8.96E-01	4.20E+00	9.36E-01
246	Antimony-124	Air	µBq	1.38E+02	1.40E+02	1.45E+02
247	Antimony-125	Air	µBq	2.16E+01	3.76E+01	1.97E+01
248	Argon-41	Air	kBq	1.09E+00	1.23E+00	1.15E+00
249	Arsenic	Air	mg	1.95E+01	4.52E+01	2.05E+01
250	Arsine	Air	ng	7.35E-05	1.00E+00	x
251	Barium	Air	mg	1.63E+01	2.25E+01	1.71E+01
252	Barium-140	Air	mBq	2.21E+00	3.25E+00	2.13E+00
253	Benzal chloride	Air	pg	x	4.90E+00	x
254	Benzaldehyde	Air	µg	2.32E+00	8.72E+00	1.30E+00
255	Benzene	Air	mg	2.74E+02	7.78E+02	2.87E+02
256	Benzene, ethyl-	Air	mg	1.09E+02	1.25E+02	1.15E+02
257	Benzene, hexachloro-	Air	µg	2.95E-01	3.34E+01	1.63E-01
258	Benzene, pentachloro-	Air	µg	1.88E-01	1.58E+00	1.97E-01
259	Benzo(a)pyrene	Air	mg	1.19E-01	1.05E+00	1.20E-01
260	Beryllium	Air	µg	1.83E+02	2.40E+02	1.93E+02
261	Boron	Air	g	6.96E-01	1.06E+00	7.32E-01
262	Boron trifluoride	Air	pg	x	7.49E+00	x
263	Bromine	Air	mg	7.27E+01	1.13E+02	7.65E+01
264	Butadiene	Air	ng	1.72E-01	9.87E+02	4.31E-02
265	Butane	Air	g	1.57E+00	3.00E+00	1.64E+00
266	Butanol	Air	ng	6.66E-04	5.51E+00	2.05E-04
267	Butene	Air	mg	9.08E+01	1.06E+02	9.53E+01
268	Butyrolactone	Air	ng	6.22E-02	5.15E+02	1.91E-02
269	Cadmium	Air	mg	7.17E+00	1.63E+01	7.53E+00
270	Calcium	Air	g	1.11E+00	1.19E+00	1.17E+00
271	Carbon-14	Air	Bq	7.79E+02	1.82E+03	8.00E+02
272	Carbon dioxide	Air	kg	9.16E+02	9.16E+02	9.64E+02
273	Carbon dioxide, biogenic	Air	oz	5.47E-01	7.64E+01	3.86E-01
274	Carbon dioxide, fossil	Air	lb	1.53E+00	4.94E+02	1.64E-01
275	Carbon dioxide, land transformation	Air	g	2.01E-02	3.56E+00	2.94E-03
276	Carbon disulfide	Air	mg	4.13E+00	6.05E+02	3.41E-01
277	Carbon monoxide	Air	kg	1.12E+00	1.12E+00	1.18E+00

Table B.1 (Continued)

No	Substance	Compartment	Unit	LS-cement	TiO2-cement	Plain cement
278	Carbon monoxide, biogenic	Air	g	4.25E-01	7.28E+00	3.99E-01
279	Carbon monoxide, fossil	Air	g	1.26E+00	4.26E+02	1.88E-01
280	Cerium-141	Air	µBq	1.04E+02	3.56E+02	6.12E+01
281	Cerium-144	Air	mBq	9.98E+01	9.98E+01	1.05E+02
282	Cesium-134	Air	mBq	3.56E+02	3.56E+02	3.75E+02
283	Cesium-137	Air	mBq	6.87E+02	6.87E+02	7.23E+02
284	Chlorine	Air	mg	2.42E-01	2.50E+02	4.83E-02
285	Chloroform	Air	µg	3.31E+01	1.18E+02	3.45E+01
286	Chlorosilane, trimethyl-	Air	µg	1.66E-04	1.55E+00	5.24E-05
287	Chromium	Air	mg	1.03E+02	2.85E+02	1.08E+02
288	Chromium-51	Air	mBq	1.77E+00	1.79E+00	1.86E+00
289	Chromium VI	Air	mg	1.38E-02	4.49E+00	2.02E-03
290	Cobalt	Air	mg	8.84E+00	1.52E+01	9.29E+00
291	Cobalt-57	Air	nBq	8.62E+02	8.62E+02	9.07E+02
292	Cobalt-58	Air	mBq	1.43E+01	1.43E+01	1.50E+01
293	Cobalt-60	Air	mBq	2.13E+01	2.15E+01	2.24E+01
294	Copper	Air	mg	8.48E+01	1.85E+02	8.55E+01
295	Cumene	Air	mg	2.68E-02	8.95E+00	3.89E-03
296	Curium-242	Air	nBq	4.93E+01	4.93E+01	5.19E+01
297	Curium-244	Air	nBq	4.47E+02	4.47E+02	4.71E+02
298	Curium alpha	Air	mBq	1.48E+01	1.48E+01	1.56E+01
299	Cyanide	Air	mg	3.54E-01	4.79E+00	3.61E-01
300	Dinitrogen monoxide	Air	g	3.20E+00	1.66E+01	3.34E+00
301	Dioxins, measured as 2,3,7,8-tetrachlorodibenzo-p-dioxin	Air	ng	1.59E+02	2.12E+02	1.67E+02
302	Ethane	Air	g	1.43E+00	1.41E+01	1.50E+00
303	Ethane, 1,1-difluoro-, HFC-152a	Air	µg	3.06E-01	3.11E+01	7.19E-02
304	Ethane, 1,1,1-trichloro-, HCFC-140	Air	ng	2.47E+00	1.18E+02	5.52E-01
305	Ethane, 1,1,1,2-tetrafluoro-, HFC-134a	Air	µg	6.25E-01	3.45E+01	1.89E-01
306	Ethane, 1,1,2-trichloro-1,2,2-trifluoro-, CFC-113	Air	µg	4.38E-04	4.08E+00	1.39E-04
307	Ethane, 1,2-dichloro-	Air	mg	5.40E-03	2.19E+00	2.25E-03
308	Ethane, 1,2-dichloro-1,1,2,2-tetrafluoro-, CFC-114	Air	mg	1.02E+01	1.06E+01	1.07E+01
309	Ethane, dichloro-	Air	mg	1.23E+00	1.23E+00	1.29E+00
310	Ethane, hexafluoro-, HFC-116	Air	mg	6.05E-01	2.84E+00	6.29E-01
311	Ethanol	Air	mg	5.62E+01	7.45E+01	5.91E+01
312	Ethene	Air	g	2.01E+00	2.12E+00	2.11E+00
313	Ethene, chloro-	Air	mg	2.05E-01	1.65E+00	2.14E-01
314	Ethene, tetrachloro-	Air	ng	5.56E+00	2.93E+02	1.25E+00
315	Ethyl acetate	Air	mg	1.75E-02	1.54E+02	5.45E-03
316	Ethyl cellulose	Air	µg	3.34E-02	3.12E+02	1.06E-02
317	Ethylene diamine	Air	ng	2.96E+00	4.57E+01	7.87E-02
318	Ethylene oxide	Air	µg	3.85E-01	2.06E+02	1.21E-01

Table B.1 (Continued)

No	Substance	Compartment	Unit	LS-cement	TiO2-cement	Plain cement
319	Ethyne	Air	mg	7.81E+00	1.33E+01	8.19E+00
320	Fluorine	Air	mg	2.42E-02	3.97E+00	2.45E-03
321	Fluosilicic acid	Air	mg	9.77E-03	2.30E+00	6.62E-04
322	Formaldehyde	Air	mg	2.31E+02	4.52E+02	2.38E+02
323	Formic acid	Air	µg	4.70E+00	4.77E+02	5.95E-02
324	Furan	Air	µg	1.33E+00	8.07E+01	1.50E-02
325	Heat, waste	Air	MWh	1.19E+00	2.09E+00	1.25E+00
326	Helium	Air	g	1.25E+00	1.29E+00	1.31E+00
327	Heptane	Air	mg	3.29E+02	4.81E+02	3.44E+02
328	Hexane	Air	g	6.92E-01	1.13E+00	7.23E-01
329	Hydrocarbons, aliphatic, alkanes, cyclic	Air	µg	9.99E-01	1.22E+02	3.09E-01
330	Hydrocarbons, aliphatic, alkanes, unspecified	Air	g	5.82E-01	1.86E+00	6.08E-01
331	Hydrocarbons, aliphatic, alkenes, unspecified	Air	mg	9.19E+01	9.19E+01	9.67E+01
332	Hydrocarbons, aliphatic, unsaturated	Air	mg	3.84E-01	9.59E+01	1.04E-01
333	Hydrocarbons, aromatic	Air	mg	1.47E+01	5.28E+02	1.47E+01
334	Hydrocarbons, chlorinated	Air	mg	6.85E-03	1.84E+00	2.17E-03
335	Hydrogen	Air	g	1.56E-03	3.97E+00	4.47E-04
336	Hydrogen-3, Tritium	Air	kBq	7.86E+00	1.38E+01	8.19E+00
337	Hydrogen chloride	Air	g	1.59E+01	1.93E+01	1.68E+01
338	Hydrogen fluoride	Air	g	1.42E+00	2.07E+00	1.49E+00
339	Hydrogen peroxide	Air	µg	2.54E-02	2.31E+02	7.99E-03
340	Hydrogen sulfide	Air	g	1.49E-01	2.03E+00	1.56E-01
341	Iodine	Air	mg	3.24E+01	5.38E+01	3.41E+01
342	Iodine-129	Air	Bq	2.70E+00	3.74E+00	2.82E+00
343	Iodine-131	Air	Bq	6.71E-01	5.27E+01	4.09E-01
344	Iodine-133	Air	mBq	1.67E+02	1.69E+02	1.75E+02
345	Iodine-135	Air	mBq	2.49E+02	2.52E+02	2.62E+02
346	Iron	Air	mg	7.35E+02	8.11E+02	7.73E+02
347	Iron-59	Air	µBq	1.95E+01	1.95E+01	2.05E+01
348	Isocyanic acid	Air	µg	5.05E+00	8.31E+02	1.17E+00
349	Isoprene	Air	µg	6.16E-02	3.74E+00	6.98E-04
350	Krypton-85	Air	kBq	4.61E+04	4.61E+04	4.85E+04
351	Krypton-85m	Air	Bq	5.96E+01	8.12E+01	5.98E+01
352	Krypton-87	Air	Bq	2.56E+01	3.39E+01	2.63E+01
353	Krypton-88	Air	kBq	2.18E+00	2.18E+00	2.29E+00
354	Krypton-89	Air	Bq	1.80E+01	2.02E+01	1.86E+01
355	Lanthanum	Air	µg	4.65E+02	4.65E+02	4.89E+02
356	Lanthanum-140	Air	mBq	1.26E+00	1.35E+00	1.31E+00
357	Lead	Air	mg	1.23E+02	2.12E+02	1.29E+02
358	Lead-210	Air	Bq	8.88E+00	1.47E+01	9.32E+00
359	m-Xylene	Air	mg	5.64E-03	1.34E+00	1.61E-03
360	Magnesium	Air	mg	3.69E+02	4.07E+02	3.88E+02
361	Manganese	Air	mg	4.79E+01	6.58E+01	5.04E+01

Table B.1 (Continued)

No	Substance	Compartment	Unit	LS-cement	TiO2-cement	Plain cement
362	Manganese-54	Air	µBq	5.12E+02	5.20E+02	5.37E+02
363	Mercury	Air	mg	3.21E+01	4.82E+01	3.38E+01
364	Methane	Air	kg	1.12E+00	1.12E+00	1.18E+00
365	Methane, biogenic	Air	g	9.05E-02	3.39E+00	8.57E-02
366	Methane, bromo-, Halon 1001	Air	pg	x	1.12E+00	x
367	Methane, bromochlorodifluoro-, Halon 1211	Air	mg	9.98E-04	3.79E+00	2.41E-04
368	Methane, bromotrifluoro-, Halon 1301	Air	mg	7.01E+00	7.43E+00	7.37E+00
369	Methane, chlorodifluoro-, HCFC-22	Air	mg	9.71E-02	1.35E+01	9.81E-02
370	Methane, chlorotrifluoro-, CFC-13	Air	µg	5.21E+01	5.21E+01	5.48E+01
371	Methane, dichloro-, HCC-30	Air	µg	5.14E+01	5.62E+01	5.40E+01
372	Methane, dichlorodifluoro-, CFC-12	Air	µg	8.29E+01	1.07E+02	8.72E+01
373	Methane, dichlorofluoro-, HCFC-21	Air	mg	1.62E+01	1.62E+01	1.71E+01
374	Methane, fossil	Air	g	8.46E-01	9.51E+02	1.32E-01
375	Methane, monochloro-, R-40	Air	µg	6.57E-02	3.21E+00	1.48E-02
376	Methane, tetrachloro-, CFC-10	Air	µg	2.98E+02	5.48E+02	3.13E+02
377	Methane, tetrafluoro-, CFC-14	Air	mg	5.44E+00	2.30E+01	5.66E+00
378	Methane, trichlorofluoro-, CFC-11	Air	µg	3.86E+02	3.86E+02	4.06E+02
379	Methane, trifluoro-, HFC-23	Air	µg	6.14E-02	8.66E+00	5.97E-02
380	Methanol	Air	mg	5.86E+01	9.31E+01	6.15E+01
381	Methyl acrylate	Air	µg	1.05E-02	9.76E+01	3.31E-03
382	Methyl amine	Air	ng	2.24E-02	1.86E+02	6.89E-03
383	Methyl borate	Air	pg	x	3.30E+01	x
384	Methyl ethyl ketone	Air	mg	1.75E-02	1.54E+02	5.45E-03
385	Methyl formate	Air	ng	4.04E-02	3.79E+02	1.28E-02
386	Molybdenum	Air	mg	3.63E+00	5.12E+00	3.82E+00
387	Monoethanolamine	Air	mg	2.65E-03	4.74E+00	5.76E-04
388	Neptunium-237	Air	nBq	4.90E+02	4.90E+02	5.16E+02
389	Nickel	Air	mg	2.33E+02	3.97E+02	2.45E+02
390	Niobium-95	Air	µBq	9.05E+01	9.15E+01	9.50E+01
391	Nitrate	Air	µg	2.70E+01	1.41E+02	1.46E-01
392	Nitrogen	Air	g	1.52E+00	1.52E+00	1.60E+00
393	Nitrogen oxides	Air	kg	1.98E+00	2.71E+00	2.08E+00
394	NMVOC, non-methane volatile organic compounds, unspecified origin	Air	g	2.07E+02	3.06E+02	2.17E+02
395	Noble gases, radioactive, unspecified	Air	kBq	1.80E+02	1.02E+04	4.03E+01
396	Ozone	Air	mg	8.53E+00	3.71E+02	4.51E+00
397	PAH, polycyclic aromatic hydrocarbons	Air	mg	2.76E+00	2.22E+01	2.78E+00

Table B.1 (Continued)

No	Substance	Compartment	Unit	LS-cement	TiO2-cement	Plain cement
398	Paraffins	Air	ng	8.86E-02	5.31E+01	1.71E-02
399	Particulates, < 10 um (mobile)	Air	g	5.52E+00	5.52E+00	5.81E+00
400	Particulates, < 10 um (stationary)	Air	g	2.00E+01	2.00E+01	2.10E+01
401	Particulates, < 2.5 um	Air	g	6.44E-01	2.85E+01	2.36E-02
402	Particulates, > 10 um	Air	g	6.30E+00	5.89E+01	7.74E-02
403	Particulates, > 10 um (process)	Air	g	5.96E+02	5.96E+02	6.27E+02
404	Particulates, > 2.5 um, and < 10um	Air	g	2.51E+00	3.79E+02	3.63E-02
405	Pentane	Air	g	1.95E+00	3.09E+00	2.04E+00
406	Phenol	Air	mg	1.37E-01	6.73E+00	1.38E-01
407	Phenol, pentachloro-	Air	µg	1.69E+00	2.83E+02	4.51E-01
408	Phosphine	Air	ng	7.97E-03	7.44E+01	2.52E-03
409	Phosphorus	Air	mg	1.73E-02	4.09E+00	4.78E-03
410	Phosphorus, total	Air	mg	1.89E+01	1.89E+01	1.99E+01
411	Platinum	Air	µg	1.81E+01	1.82E+01	1.91E+01
412	Plutonium-238	Air	µBq	1.11E+00	1.26E+00	1.17E+00
413	Plutonium-241	Air	mBq	8.18E+02	8.18E+02	8.61E+02
414	Plutonium-alpha	Air	mBq	2.97E+01	2.97E+01	3.13E+01
415	Polonium-210	Air	Bq	1.34E+01	2.37E+01	1.41E+01
416	Polychlorinated biphenyls	Air	µg	3.61E-01	5.62E+01	1.32E-01
417	Potassium	Air	mg	2.91E+02	5.62E+02	3.05E+02
418	Potassium-40	Air	Bq	1.57E+00	2.89E+00	1.65E+00
419	Promethium-147	Air	mBq	2.53E+02	2.53E+02	2.66E+02
420	Propanal	Air	µg	1.10E+00	8.06E+00	7.02E-03
421	Propane	Air	g	1.72E+00	6.14E+00	1.80E+00
422	Propene	Air	mg	8.85E+01	1.36E+02	9.26E+01
423	Propionic acid	Air	mg	1.95E+00	5.07E+00	2.04E+00
424	Propylene oxide	Air	mg	1.30E-03	1.85E+00	3.00E-04
425	Protactinium-234	Air	mBq	3.01E+02	4.43E+02	3.14E+02
426	Radioactive species, other beta emitters	Air	Bq	6.85E-02	1.02E+01	1.87E-02
427	Radium-226	Air	Bq	1.09E+01	1.69E+01	1.14E+01
428	Radium-228	Air	Bq	7.75E-01	1.68E+00	8.14E-01
429	Radon-220	Air	Bq	6.79E+01	1.24E+02	7.14E+01
430	Radon-222	Air	kBq	6.74E+04	8.62E+04	7.06E+04
431	Ruthenium-103	Air	µBq	5.17E+00	5.39E+00	5.40E+00
432	Ruthenium-106	Air	Bq	2.97E+00	2.97E+00	3.13E+00
433	Scandium	Air	µg	1.55E+02	1.69E+02	1.63E+02
434	Selenium	Air	mg	1.19E+01	1.94E+01	1.25E+01
435	Silicon	Air	g	3.51E+00	3.66E+00	3.69E+00
436	Silicon tetrafluoride	Air	µg	1.87E-02	8.03E+00	1.77E-03
437	Silver	Air	µg	4.92E-02	5.01E+00	1.16E-02
438	Silver-110	Air	µBq	5.03E+02	5.05E+02	5.29E+02
439	Sodium	Air	mg	2.35E+02	3.04E+02	2.47E+02
440	Sodium chlorate	Air	µg	4.89E-01	9.50E+01	7.87E-02

Table B.1 (Continued)

No	Substance	Compartment	Unit	LS-cement	TiO2-cement	Plain cement
441	Sodium dichromate	Air	µg	2.60E+00	1.12E+02	1.39E+00
442	Sodium formate	Air	µg	6.69E-02	1.31E+02	1.52E-03
443	Sodium hydroxide	Air	µg	9.34E-02	8.63E+02	2.95E-02
444	Strontium	Air	mg	1.71E+01	2.37E+01	1.80E+01
445	Strontium-89	Air	µBq	8.92E+02	8.92E+02	9.39E+02
446	Strontium-90	Air	mBq	4.91E+02	4.91E+02	5.17E+02
447	Styrene	Air	µg	1.12E+00	2.41E+02	5.54E-01
448	Sulfate	Air	g	9.64E-03	4.59E+02	7.25E-03
449	Sulfur dioxide	Air	oz	3.98E-02	6.52E+01	5.44E-03
450	Sulfur hexafluoride	Air	mg	4.75E-02	5.26E+00	1.13E-02
451	Sulfur oxides	Air	kg	1.36E+00	1.36E+00	1.43E+00
452	Sulfuric acid	Air	µg	2.03E-02	1.81E+02	6.34E-03
453	t-Butyl methyl ether	Air	µg	3.19E+02	4.60E+02	3.36E+02
454	Technetium-99	Air	µBq	2.08E+01	2.08E+01	2.19E+01
455	Tellurium-123m	Air	mBq	2.24E+00	2.24E+00	2.36E+00
456	Terpenes	Air	µg	5.83E-01	3.54E+01	6.60E-03
457	Thallium	Air	µg	1.17E+02	2.44E+02	1.23E+02
458	Thorium	Air	µg	2.98E+02	3.16E+02	3.14E+02
459	Thorium-228	Air	mBq	6.54E+02	9.42E+02	6.88E+02
460	Thorium-230	Air	Bq	3.32E+00	3.86E+00	3.48E+00
461	Thorium-232	Air	mBq	4.16E+02	8.33E+02	4.37E+02
462	Thorium-234	Air	mBq	3.01E+02	4.43E+02	3.14E+02
463	Tin	Air	mg	3.51E-01	4.83E+00	3.46E-01
464	Titanium	Air	mg	4.52E+01	4.89E+01	4.75E+01
465	Toluene	Air	mg	2.67E+02	5.08E+02	2.79E+02
466	Uranium	Air	µg	3.31E+02	3.51E+02	3.48E+02
467	Uranium-234	Air	Bq	3.60E+00	5.27E+00	3.76E+00
468	Uranium-235	Air	mBq	1.75E+02	2.55E+02	1.82E+02
469	Uranium-238	Air	Bq	4.74E+00	7.44E+00	4.96E+00
470	Uranium alpha	Air	Bq	1.08E+01	1.85E+01	1.12E+01
471	Vanadium	Air	mg	3.68E+02	4.51E+02	3.87E+02
472	water	Air	g	9.20E-01	4.83E+00	4.77E-03
473	Xenon-131m	Air	Bq	1.19E+02	1.58E+02	1.22E+02
474	Xenon-133	Air	kBq	3.32E+01	3.44E+01	3.48E+01
475	Xenon-133m	Air	Bq	1.68E+01	2.18E+01	1.75E+01
476	Xenon-135	Air	kBq	5.73E+00	6.24E+00	5.98E+00
477	Xenon-135m	Air	Bq	6.10E+02	9.10E+02	6.11E+02
478	Xenon-137	Air	Bq	1.53E+01	2.14E+01	1.51E+01
479	Xenon-138	Air	Bq	1.64E+02	2.16E+02	1.65E+02
480	Xylene	Air	mg	5.36E+02	9.38E+02	5.62E+02
481	Zinc	Air	mg	2.32E+02	4.13E+02	2.40E+02
482	Zinc-65	Air	mBq	2.20E+00	2.25E+00	2.31E+00
483	Zirconium	Air	µg	2.48E+01	8.57E+01	2.58E+01
484	Zirconium-95	Air	µBq	4.18E+01	8.22E+01	3.63E+01
485	1,4-Butanediol	Water	ng	8.59E-02	7.11E+02	2.64E-02
486	4-Methyl-2-pentanone	Water	ng	5.70E-02	2.91E+01	3.71E-02
487	Acenaphthene	Water	µg	5.82E-02	4.41E+00	1.59E-03

Table B.1 (Continued)

No	Substance	Compartment	Unit	LS-cement	TiO2-cement	Plain cement
488	Acenaphthylene	Water	mg	6.09E+00	6.09E+00	6.41E+00
489	Acetaldehyde	Water	mg	1.15E-04	1.02E+00	3.60E-05
490	Acetic acid	Water	mg	7.14E-03	3.21E+00	1.26E-03
491	Acetone	Water	ng	1.36E-01	6.94E+01	8.85E-02
492	Acidity, unspecified	Water	mg	1.45E-02	1.06E+00	2.29E-03
493	Acids, unspecified	Water	mg	7.69E+00	7.69E+00	8.09E+00
494	Acrylate, ion	Water	µg	2.18E-02	2.04E+02	6.91E-03
495	Actinides, radioactive, unspecified	Water	Bq	3.04E-02	1.73E+00	6.80E-03
496	Aluminum	Water	g	2.38E+02	5.17E+02	2.51E+02
497	Americium-241	Water	Bq	1.24E+00	1.24E+00	1.30E+00
498	Ammonia, as N	Water	g	1.37E+00	1.37E+00	1.44E+00
499	Ammonium, ion	Water	mg	3.14E+00	8.99E+02	4.18E-01
500	Antimony	Water	mg	4.68E-01	6.73E+01	4.62E-01
501	Antimony-122	Water	mBq	6.61E+00	7.23E+00	6.84E+00
502	Antimony-124	Water	Bq	8.96E-01	1.18E+00	9.35E-01
503	Antimony-125	Water	mBq	6.16E+01	3.17E+02	5.74E+01
504	AOX, Adsorbable Organic Halogen as Cl	Water	mg	3.34E+00	7.74E+00	3.50E+00
505	Arsenic, ion	Water	mg	4.74E+02	6.26E+02	4.99E+02
506	Barite	Water	g	1.73E+01	3.08E+01	1.82E+01
507	Barium	Water	g	2.11E+01	2.25E+01	2.22E+01
508	Barium-140	Water	mBq	7.08E+00	9.79E+00	6.94E+00
509	Benzene	Water	mg	1.20E+02	1.90E+02	1.25E+02
510	Benzene, 1,2-dichloro-	Water	µg	2.89E-02	2.39E+02	8.88E-03
511	Benzene, chloro-	Water	mg	6.13E-04	4.94E+00	2.01E-04
512	Benzene, ethyl-	Water	mg	2.18E+01	3.86E+01	2.28E+01
513	Beryllium	Water	mg	5.73E-02	6.01E+00	5.04E-02
514	BOD5, Biological Oxygen Demand	Water	g	1.96E+00	1.67E+02	2.65E-01
515	Boron	Water	g	6.89E-02	1.02E+00	7.01E-02
516	Bromate	Water	g	4.48E-05	1.88E+00	1.71E-05
517	Bromine	Water	mg	6.74E+00	6.01E+02	2.41E-01
518	Butanol	Water	µg	6.33E-02	5.60E+02	1.98E-02
519	Butene	Water	µg	2.18E-01	1.38E+02	1.79E-01
520	Butyl acetate	Water	µg	8.23E-02	7.28E+02	2.57E-02
521	Butyrolactone	Water	µg	1.49E-04	1.24E+00	4.59E-05
522	Cadmium-109	Water	µBq	3.74E+01	3.74E+01	3.94E+01
523	Cadmium, ion	Water	mg	1.71E+01	2.63E+01	1.80E+01
524	Calcium, ion	Water	g	2.10E+02	8.65E+02	2.19E+02
525	Carbon-14	Water	Bq	6.24E+01	6.24E+01	6.57E+01
526	Carbonate	Water	mg	1.28E+00	6.52E+01	3.26E-01
527	Carboxylic acids, unspecified	Water	g	3.95E-02	3.17E+00	1.08E-03
528	Cerium-141	Water	mBq	1.21E+00	2.30E+00	1.07E+00
529	Cerium-144	Water	Bq	2.82E+01	2.82E+01	2.97E+01
530	Cesium	Water	mg	9.14E-01	1.61E+00	9.52E-01
531	Cesium-134	Water	Bq	6.31E+01	6.34E+01	6.65E+01

Table B.1 (Continued)

No	Substance	Compartment	Unit	LS-cement	TiO2-cement	Plain cement
532	Cesium-136	Water	µBq	7.82E+01	2.70E+02	4.57E+01
533	Cesium-137	Water	Bq	5.85E+02	7.80E+02	6.13E+02
534	Chlorate	Water	g	4.37E-04	1.43E+01	2.04E-04
535	Chloride	Water	kg	1.77E+00	2.73E+00	1.84E+00
536	Chlorinated solvents, unspecified	Water	mg	1.06E-01	4.26E+00	1.08E-01
537	Chlorine	Water	mg	5.01E+01	5.55E+01	5.00E+01
538	Chloroform	Water	µg	3.86E+02	3.97E+02	4.06E+02
539	Chromium-51	Water	mBq	1.88E+02	5.10E+02	1.60E+02
540	Chromium VI	Water	mg	4.10E+00	7.84E+02	1.41E+00
541	Chromium, ion	Water	g	2.37E+00	2.38E+00	2.50E+00
542	Cobalt	Water	mg	4.72E+02	7.63E+02	4.96E+02
543	Cobalt-57	Water	mBq	8.02E+00	1.41E+01	7.28E+00
544	Cobalt-58	Water	Bq	5.66E+00	7.97E+00	5.78E+00
545	Cobalt-60	Water	Bq	2.74E+02	2.76E+02	2.88E+02
546	COD, Chemical Oxygen Demand	Water	g	4.05E+00	2.10E+02	2.37E+00
547	Copper, ion	Water	g	1.18E+00	1.53E+00	1.24E+00
548	Cumene	Water	mg	6.43E-02	2.15E+01	9.35E-03
549	Curium alpha	Water	Bq	1.63E+00	1.63E+00	1.72E+00
550	Cyanide	Water	mg	8.33E+00	6.34E+01	8.56E+00
551	Dichromate	Water	µg	5.76E+00	4.03E+02	1.26E+00
552	DOC, Dissolved Organic Carbon	Water	g	6.77E-01	7.25E+01	1.26E-01
553	Ethane, 1,1,1-trichloro-, HCFC-140	Water	µg	4.13E+00	4.13E+00	4.35E+00
554	Ethane, 1,2-dichloro-	Water	µg	1.34E+00	1.08E+02	2.86E-01
555	Ethane, dichloro-	Water	µg	6.31E+02	6.31E+02	6.64E+02
556	Ethane, hexachloro-	Water	ng	1.40E+01	1.40E+01	1.47E+01
557	Ethanol	Water	mg	1.46E-04	1.29E+00	4.55E-05
558	Ethene	Water	mg	2.47E-02	4.44E+00	3.82E-03
559	Ethene, chloro-	Water	µg	6.01E-01	1.96E+01	5.87E-01
560	Ethene, tetrachloro-	Water	µg	1.66E+00	1.66E+00	1.75E+00
561	Ethene, trichloro-	Water	µg	1.05E+02	1.05E+02	1.11E+02
562	Ethyl acetate	Water	ng	9.70E-03	8.79E+01	3.05E-03
563	Ethylene diamine	Water	ng	7.19E+00	1.11E+02	1.91E-01
564	Ethylene oxide	Water	µg	1.35E-02	9.67E+01	3.89E-03
565	Fatty acids as C	Water	g	4.57E+00	4.57E+00	4.82E+00
566	Fluoride	Water	g	5.67E-01	1.51E+01	5.93E-01
567	Fluosilicic acid	Water	mg	1.76E-02	4.13E+00	1.19E-03
568	Formaldehyde	Water	mg	1.42E-02	1.28E+00	1.14E-02
569	Glutaraldehyde	Water	mg	2.14E+00	3.81E+00	2.25E+00
570	Heat, waste	Water	MJ	2.38E+01	1.09E+02	2.48E+01
571	Hydrocarbons, aliphatic, alkanes, unspecified	Water	mg	1.19E+02	2.10E+02	1.24E+02
572	Hydrocarbons, aliphatic, alkenes, unspecified	Water	mg	1.09E+01	1.09E+01	1.15E+01

Table B.1 (Continued)

No	Substance	Compartment	Unit	LS-cement	TiO2-cement	Plain cement
573	Hydrocarbons, aliphatic, unsaturated	Water	mg	1.12E-01	8.51E+00	3.06E-03
574	Hydrocarbons, aromatic	Water	mg	5.51E+02	9.52E+02	5.75E+02
575	Hydrocarbons, unspecified	Water	mg	1.14E+01	2.83E+02	1.11E+01
576	Hydrogen-3, Tritium	Water	kBq	1.86E+03	2.31E+03	1.95E+03
577	Hydrogen peroxide	Water	mg	2.65E-01	2.21E+00	2.64E-01
578	Hydrogen sulfide	Water	mg	2.78E+01	7.90E+01	2.78E+01
579	Hydroxide	Water	mg	9.77E-04	6.42E+00	2.85E-04
580	Hypochlorite	Water	mg	1.97E+02	2.21E+02	2.08E+02
581	Hypochlorous acid	Water	mg	1.97E+02	1.97E+02	2.08E+02
582	Iodide	Water	mg	9.10E+01	1.63E+02	9.48E+01
583	Iodine-129	Water	Bq	1.79E+02	1.79E+02	1.88E+02
584	Iodine-131	Water	mBq	1.22E+02	1.73E+02	1.26E+02
585	Iodine-133	Water	mBq	3.00E+01	3.17E+01	3.13E+01
586	Iron	Water	g	9.98E+01	9.98E+01	1.05E+02
587	Iron-59	Water	µBq	2.21E+02	6.88E+02	1.43E+02
588	Iron, ion	Water	g	2.41E-01	1.55E+02	1.00E-01
589	Lanthanum-140	Water	mBq	1.99E+00	4.88E+00	1.55E+00
590	Lead	Water	g	1.22E+00	1.34E+00	1.28E+00
591	Lead-210	Water	Bq	3.58E+00	9.05E+00	3.75E+00
592	Lithium, ion	Water	mg	1.46E-02	7.46E+00	9.52E-03
593	m-Xylene	Water	ng	4.12E-01	2.10E+02	2.68E-01
594	Magnesium	Water	g	1.91E+02	3.02E+02	2.01E+02
595	Manganese	Water	g	4.97E+00	5.69E+00	5.23E+00
596	Manganese-54	Water	Bq	4.19E+01	4.20E+01	4.41E+01
597	Mercury	Water	mg	1.10E-01	3.04E+00	1.10E-01
598	Methane, dichloro-, HCC-30	Water	mg	8.09E+00	2.45E+01	8.41E+00
599	Methane, tetrachloro-, CFC-10	Water	µg	2.54E+00	2.54E+00	2.67E+00
600	Methanol	Water	mg	1.17E-02	5.48E+01	2.92E-03
601	Methyl acrylate	Water	mg	2.04E-04	1.91E+00	6.47E-05
602	Methyl amine	Water	ng	5.38E-02	4.45E+02	1.65E-02
603	Methyl formate	Water	ng	1.61E-02	1.51E+02	5.11E-03
604	Molybdenum	Water	mg	6.19E+02	6.62E+02	6.51E+02
605	Molybdenum-99	Water	mBq	6.77E-01	1.67E+00	5.24E-01
606	Neptunium-237	Water	mBq	7.88E+01	7.88E+01	8.29E+01
607	Nickel, ion	Water	g	1.20E+00	2.54E+00	1.25E+00
608	Niobium-95	Water	mBq	4.50E+00	2.61E+01	4.05E+00
609	Nitrate	Water	g	1.65E+00	6.52E+00	1.73E+00
610	Nitrite	Water	mg	4.80E+01	8.95E+01	5.05E+01
611	Nitrogen	Water	mg	1.70E+00	3.87E+02	3.57E-01
612	Nitrogen, organic bound	Water	mg	1.34E+02	5.91E+02	1.40E+02
613	Nitrogen, total	Water	g	1.16E+00	1.16E+00	1.22E+00
614	o-Xylene	Water	ng	3.00E-01	1.53E+02	1.95E-01
615	Oils, unspecified	Water	g	1.72E+01	6.29E+01	1.75E+01
616	PAH, polycyclic aromatic hydrocarbons	Water	mg	1.21E+01	1.66E+01	1.26E+01
617	Paraffins	Water	ng	2.57E-01	1.54E+02	4.95E-02

Table B.1 (Continued)

No	Substance	Compartment	Unit	LS-cement	TiO2-cement	Plain cement
618	Phenol	Water	mg	8.78E-01	7.47E+01	2.46E-02
619	Phenols, unspecified	Water	mg	1.25E+02	1.25E+02	1.32E+02
620	Phosphate	Water	g	1.42E+01	2.18E+01	1.49E+01
621	Phosphorus	Water	mg	9.14E-02	2.51E+01	2.29E-02
622	Phosphorus compounds, unspecified	Water	µg	5.35E+02	5.35E+02	5.63E+02
623	Phthalate, dimethyl tere-	Water	µg	3.89E+00	3.89E+00	4.09E+00
624	Phthalate, dioctyl-	Water	ng	8.72E+01	8.72E+01	9.18E+01
625	Phthalate, p-dibutyl-	Water	ng	6.17E+02	6.17E+02	6.49E+02
626	Plutonium-241	Water	Bq	1.22E+02	1.22E+02	1.28E+02
627	Plutonium-alpha	Water	Bq	4.90E+00	4.90E+00	5.16E+00
628	Polonium-210	Water	Bq	3.58E+00	1.06E+01	3.75E+00
629	Potassium	Water	g	7.52E+01	7.52E+01	7.92E+01
630	Potassium-40	Water	Bq	4.49E+00	7.91E+00	4.71E+00
631	Potassium, ion	Water	g	6.48E-02	1.17E+01	8.83E-03
632	Propene	Water	mg	2.67E-02	1.21E+01	4.28E-03
633	Propylene oxide	Water	mg	3.13E-03	4.46E+00	7.21E-04
634	Protactinium-234	Water	Bq	5.57E+00	8.19E+00	5.81E+00
635	Radioactive species, alpha emitters	Water	mBq	4.39E-01	9.63E+00	4.32E-01
636	Radioactive species, from fission and activation	Water	Bq	3.69E+00	3.69E+00	3.88E+00
637	Radioactive species, Nuclides, unspecified	Water	Bq	1.82E+01	1.04E+03	4.08E+00
638	Radium-224	Water	Bq	4.55E+01	8.05E+01	4.74E+01
639	Radium-226	Water	kBq	2.28E+01	2.45E+01	2.40E+01
640	Radium-228	Water	Bq	9.10E+01	1.61E+02	9.48E+01
641	Rubidium	Water	mg	9.58E-02	7.20E+00	3.05E-03
642	Ruthenium	Water	mg	9.03E+00	9.03E+00	9.51E+00
643	Ruthenium-103	Water	mBq	2.21E+00	2.42E+00	2.29E+00
644	Ruthenium-106	Water	Bq	2.97E+02	2.97E+02	3.13E+02
645	Salts, unspecified	Water	g	6.54E+01	6.54E+01	6.88E+01
646	Scandium	Water	mg	2.67E-02	1.29E+01	8.57E-03
647	Selenium	Water	g	1.18E+00	1.19E+00	1.24E+00
648	Silicon	Water	oz	7.27E-02	1.66E+02	1.75E-02
649	Silver	Water	µg	6.06E+02	6.06E+02	6.38E+02
650	Silver-110	Water	Bq	3.60E+00	5.31E+00	3.65E+00
651	Silver, ion	Water	mg	8.49E-03	1.67E+00	3.22E-04
652	Sodium-24	Water	mBq	2.01E+02	2.09E+02	2.10E+02
653	Sodium formate	Water	µg	1.61E-01	3.15E+02	3.65E-03
654	Sodium, ion	Water	g	5.28E+02	8.81E+02	5.52E+02
655	Solids, inorganic	Water	g	1.79E-01	6.72E+01	4.99E-02
656	Solved solids	Water	g	5.36E-02	1.10E+02	6.33E-03
657	Solved substances	Water	g	1.01E+02	1.01E+02	1.07E+02
658	Strontium	Water	g	8.29E+00	1.03E+01	8.71E+00
659	Strontium-89	Water	mBq	1.84E+01	4.95E+01	1.62E+01
660	Strontium-90	Water	Bq	6.97E+01	1.51E+03	6.51E+01

Table B.1 (Continued)

No	Substance	Compartment	Unit	LS-cement	TiO2-cement	Plain cement
661	Sulfate	Water	kg	1.16E+00	1.14E+01	1.22E+00
662	Sulfide	Water	mg	2.91E+01	3.33E+01	3.06E+01
663	Sulfite	Water	mg	2.04E-01	6.49E+01	5.85E-02
664	Sulfur	Water	mg	1.45E+00	1.43E+02	3.89E-02
665	Sulfur trioxide	Water	mg	3.08E+01	3.08E+01	3.24E+01
666	Suspended solids, unspecified	Water	g	1.45E-01	1.57E+02	1.31E-02
667	t-Butyl methyl ether	Water	mg	4.33E-02	4.58E+00	2.83E-02
668	Technetium-99	Water	Bq	3.13E+01	3.13E+01	3.29E+01
669	Technetium-99m	Water	mBq	8.23E+00	3.12E+01	4.31E+00
670	Tellurium-123m	Water	mBq	8.48E-01	3.10E+01	4.15E-01
671	Tellurium-132	Water	µBq	1.25E+02	1.83E+02	1.21E+02
672	Thallium	Water	mg	1.61E-02	2.70E+00	1.47E-02
673	Thorium-228	Water	Bq	1.82E+02	3.22E+02	1.89E+02
674	Thorium-230	Water	Bq	8.70E+02	1.23E+03	9.09E+02
675	Thorium-232	Water	Bq	8.37E-01	1.41E+00	8.79E-01
676	Thorium-234	Water	Bq	5.62E+00	8.24E+00	5.86E+00
677	Tin, ion	Water	mg	4.21E-01	2.53E+01	3.71E-01
678	Titanium, ion	Water	oz	5.00E-01	3.59E+01	5.26E-01
679	TOC, Total Organic Carbon	Water	g	3.14E+01	1.03E+02	3.24E+01
680	Toluene	Water	mg	1.00E+02	1.97E+02	1.04E+02
681	Tributyltin compounds	Water	mg	6.06E+00	2.26E+01	6.37E+00
682	Triethylene glycol	Water	mg	8.51E+01	1.27E+02	8.96E+01
683	Tungsten	Water	mg	1.22E+00	1.06E+01	1.26E+00
684	Undissolved substances	Water	g	5.91E+01	5.91E+01	6.22E+01
685	Uranium-234	Water	Bq	7.43E+00	1.06E+01	7.77E+00
686	Uranium-235	Water	Bq	1.11E+01	1.63E+01	1.16E+01
687	Uranium-238	Water	Bq	1.88E+01	2.95E+01	1.96E+01
688	Uranium alpha	Water	Bq	3.64E+02	5.15E+02	3.80E+02
689	Vanadium, ion	Water	g	1.19E+00	1.92E+00	1.25E+00
690	VOC, volatile organic compounds as C	Water	mg	3.15E+02	3.15E+02	3.32E+02
691	VOC, volatile organic compounds, unspecified origin	Water	mg	3.41E+00	2.55E+02	1.20E-01
692	Xylene	Water	mg	8.65E+01	1.60E+02	9.01E+01
693	Yttrium-90	Water	µBq	7.47E+02	7.47E+02	7.86E+02
694	Zinc-65	Water	mBq	4.44E+02	5.46E+02	4.48E+02
695	Zinc, ion	Water	g	2.42E+00	3.94E+00	2.55E+00
696	Zirconium-95	Water	Bq	2.53E+00	2.53E+00	2.66E+00
697	2,4-D	Soil	µg	2.35E-01	1.44E+01	2.66E-03
698	Aclonifen	Soil	µg	3.20E-02	1.78E+01	1.11E-02
699	Aldrin	Soil	µg	2.39E-04	2.21E+00	7.56E-05
700	Aluminum	Soil	g	1.15E+00	1.88E+00	1.21E+00
701	Antimony	Soil	ng	7.89E-01	2.43E+02	7.08E-01
702	Arsenic	Soil	µg	4.61E+02	7.50E+02	4.84E+02
703	Atrazine	Soil	ng	6.28E-02	5.81E+02	1.98E-02
704	Barium	Soil	mg	2.02E+00	3.26E+02	6.31E-02
705	Benomyl	Soil	ng	1.49E+00	9.08E+01	1.69E-02

Table B.1 (Continued)

No	Substance	Compartment	Unit	LS-cement	TiO2-cement	Plain cement
706	Bentazone	Soil	µg	1.63E-02	9.08E+00	5.67E-03
707	Boron	Soil	mg	7.95E-02	9.26E+00	9.83E-03
708	Cadmium	Soil	µg	2.54E+01	9.24E+01	2.66E+01
709	Calcium	Soil	g	4.62E+00	7.74E+00	4.84E+00
710	Carbetamide	Soil	µg	2.02E-02	3.47E+00	2.11E-03
711	Carbofuran	Soil	µg	8.20E-01	4.98E+01	9.28E-03
712	Carbon	Soil	g	3.57E+00	6.11E+00	3.74E+00
713	Chloride	Soil	g	2.80E-02	1.61E+01	4.68E-03
714	Chlorothalonil	Soil	µg	1.42E+01	2.47E+02	1.02E-01
715	Chromium	Soil	mg	5.77E+00	9.56E+00	6.05E+00
716	Chromium VI	Soil	mg	2.21E-01	1.55E+01	4.84E-02
717	Cobalt	Soil	µg	2.45E+01	7.43E+01	2.57E+01
718	Copper	Soil	mg	2.62E-01	1.22E+01	1.59E-01
719	Cypermethrin	Soil	µg	1.17E-01	7.11E+00	1.36E-03
720	Fenpiclonil	Soil	µg	5.60E-01	1.03E+01	4.40E-03
721	Fluoride	Soil	mg	3.51E-01	4.31E+01	3.91E-02
722	Glyphosate	Soil	mg	4.65E-03	4.19E+00	7.90E-04
723	Heat, waste	Soil	MJ	3.32E+00	5.04E+00	3.47E+00
724	Iron	Soil	g	2.31E+00	1.12E+01	2.42E+00
725	Lead	Soil	mg	5.58E-01	1.49E+00	5.86E-01
726	Linuron	Soil	µg	2.47E-01	1.38E+02	8.56E-02
727	Magnesium	Soil	mg	3.44E+00	5.82E+02	1.65E-01
728	Mancozeb	Soil	µg	1.85E+01	3.20E+02	1.33E-01
729	Manganese	Soil	mg	4.63E+01	9.85E+01	4.84E+01
730	Mercury	Soil	µg	3.44E+00	8.40E+00	3.61E+00
731	Metaldehyde	Soil	ng	7.44E+00	7.16E+02	4.23E-01
732	Metolachlor	Soil	µg	1.79E+00	9.92E+02	6.19E-01
733	Metribuzin	Soil	µg	6.50E-01	1.13E+01	4.67E-03
734	Molybdenum	Soil	µg	2.93E-02	2.07E+01	7.59E-03
735	Napropamide	Soil	µg	1.32E-02	1.27E+00	7.49E-04
736	Nickel	Soil	µg	1.84E+02	7.42E+02	1.93E+02
737	Nitrogen	Soil	mg	1.02E+00	1.02E+00	1.07E+00
738	Oils, biogenic	Soil	mg	1.76E+01	9.06E+01	1.85E+01
739	Oils, unspecified	Soil	g	1.36E+00	4.71E+01	8.59E-01
740	Orbencarb	Soil	µg	3.51E+00	6.09E+01	2.52E-02
741	Phosphorus	Soil	mg	5.93E+01	1.04E+02	6.21E+01
742	Pirimicarb	Soil	ng	1.55E+00	8.59E+02	5.36E-01
743	Potassium	Soil	mg	1.76E+00	2.98E+02	1.53E-01
744	Silicon	Soil	mg	9.70E-01	2.71E+02	1.79E-01
745	Sodium	Soil	g	8.11E-03	1.38E+00	2.67E-04
746	Strontium	Soil	mg	4.07E-02	6.54E+00	1.27E-03
747	Sulfur	Soil	g	6.93E-01	1.15E+00	7.27E-01
748	Sulfuric acid	Soil	ng	1.20E-02	1.12E+02	3.79E-03
749	Tebutam	Soil	µg	3.12E-02	3.00E+00	1.78E-03
750	Teflubenzuron	Soil	ng	4.33E+01	7.52E+02	3.11E-01
751	Thiram	Soil	ng	2.65E+00	1.61E+02	3.00E-02
752	Tin	Soil	µg	2.50E-02	6.72E+01	2.30E-03

Table B.1 (Continued)

No	Substance	Compartment	Unit	LS-cement	TiO2-cement	Plain cement
753	Titanium	Soil	mg	8.84E-03	1.76E+00	2.75E-03
754	Vanadium	Soil	µg	2.53E-01	5.04E+01	7.88E-02
755	Zinc	Soil	mg	1.85E+01	6.98E+01	1.94E+01

REFERENCES

1. Worrell, E., et al., *Carbon dioxide emissions from the global cement industry.* Annual Review of Energy and the Environment, 2001. **26**: p. 303-329.

2. Kapur, A., et al., *The contemporary cement cycle of the United States.* Journal of Material Cycles and Waste Management, 2009. **11**(2): p. 155-165.

3. U.S.EPA, *Inventory of U.S. greenhouse gas emissions and sinks 1990-2009*, EPA, Editor. 2011: Washington. DC. p. 1-459.

4. Vukotic, L., Fenner, R.A., and Symons, K., *Assessing embodied energy of building structural elements.* Proceedings of the Institution of Civil Engineers-Engineering Sustainability, 2010. **163**(3): p. 147-158.

5. Soubbotina, T.P. and Sheram, K.A., *Beyond economic growth - Meeting the challenges of global development*. 2000, Washington D. C.: The World Bank.

6. Kelly, T.D. and Matos, G.R. *Cement statistics*. Historical statistics for mineral and material commodities in the United States: U.S. Geological Survey Data Series 140 2013 [cited 2010 07-20-2010]; Available from: http://pubs.usgs.gov/ds/2005/140/.

7. Gartner, E.M. and Macphee, D.E., *A physico-chemical basis for novel cementitious binders.* Cement and Concrete Research, 2011. **41**(7): p. 736-749.

8. Dai, H.C., Cao, G.J., and Su, H.Z., *Management and construction of the Three Gorges Project.* Journal of Construction Engineering and Management-Asce, 2006. **132**(6): p. 615-619.

9. Mehta, P.K. and Monteiro, P.J.M., *Concrete - Microstructure, properties and materials*. 2006, New York: McGraw-Hill.

10. Habert, G., et al., *Cement production technology improvement compared to factor 4 objectives.* Cement and Concrete Research, 2010. **40**(5): p. 820-826.

11. Schokker, A.J., *The Sustainable Concrete Guide - Strategies and Examples*. 2010, Farmington Hills, MI: U.S. Green Concrete Council.

12. Sanchez, F. and Sobolev, K., *Nanotechnology in concrete - A review.* Construction and Building Materials, 2010. **24**(11): p. 2060-2071.

13. Bijen, J., *Benefits of slag and fly ash.* Construction and Building Materials, 1996. **10**(5): p. 309-314.

14. Lawrence, P., Cyr, M., and Ringot, E., *Mineral admixtures in mortars effect of type, amount and fineness of fine constituents on compressive strength.* Cement and Concrete Research, 2005. **35**(6): p. 1092-1105.

15. Gutteridge, W.A. and Dalziel, J.A., *Filler cement: The effect of the secondary component on the hydration of Portland cement: Part 2: Fine hydraulic binders.* Cement and Concrete Research, 1990. **20**(6): p. 853-861.

16. Gutteridge, W.A. and Dalziel, J.A., *Filler cement: The effect of the secondary component on the hydration of Portland cement: Part I. A fine non-hydraulic filler.* Cement and Concrete Research, 1990. **20**(5): p. 778-782.

17. Moosberg-Bustnes, H., Lagerblad, B., and Forssberg, E., *The function of fillers in concrete.* Materials and Structures, 2004. **37**(266): p. 74-81.

18. Carp, O., Huisman, C.L., and Reller, A., *Photoinduced reactivity of titanium dioxide.* Progress in Solid State Chemistry, 2004. **32**(1-2): p. 33-177.

19. Diamantonis, N., et al., *Investigations about the influence of fine additives on the viscosity of cement paste for self-compacting concrete.* Construction and Building Materials. **24**(8): p. 1518-1522.

20. Soroka, I. and Stern, N., *Calcareous fillers and the compressive strength of portland cement.* Cement and Concrete Research, 1976. **6**(3): p. 367-376.

21. Cyr, M., Lawrence, P., and Ringot, E., *Efficiency of mineral admixtures in mortars: Quantification of the physical and chemical effects of fine admixtures in relation with compressive strength.* Cement and Concrete Research, 2006. **36**(2): p. 264-277.

22. Lothenbach, B., et al., *Influence of limestone on the hydration of Portland cements.* Cement and Concrete Research, 2008. **38**(6): p. 848-860.

23. Bouasker, M., et al., *Chemical shrinkage of cement pastes and mortars at very early age: Effect of limestone filler and granular inclusions.* Cement & Concrete Composites, 2008. **30**(1): p. 13-22.

24. Bentz, D.P., et al., *Influence of silica fume on diffusivity in cement-based materials I. Experimental and computer modeling studies on cement pastes.* Cement and Concrete Research, 2000. **30**(6): p. 953-962.

25. Ye, Q., et al., *Influence of nano-SiO2 addition on properties of hardened cement paste as compared with silica fume.* Construction and Building Materials, 2007. **21**(3): p. 539-545.

26. Senff, L., et al., *Mortars with nano-SiO2 and micro-SiO2 investigated by experimental design.* Construction and Building Materials, 2010. **24**(8): p. 1432-1437.

27. Fujishima, A. and Honda, K., *Electrochemical Photolysis of Water at a Semiconductor Electrode.* Nature, 1972. **238**(5358): p. 37-38.

28. Cassar, L., et al. *White Cement for architectural concrete, possessing photocatalytic properties*. in *11th International Congress on the Chemistry of Cement*. 2003. Durban.

29. Banerjee, S., et al., *Physics and chemistry of photocatalytic titanium dioxide: Visualization of bactericidal activity using atomic force microscopy.* Current Science, 2006. **90**(10): p. 1378-1383.

30. Giannantonio, D.J., et al., *Effects of concrete properties and nutrients on fungal colonization and fouling.* International Biodeterioration & Biodegradation, 2009. **63**(3): p. 252-259.

31. Husken, G., Hunger, M., and Brouwers, H.J.H., *Experimental study of photocatalytic concrete products for air purification.* Building and Environment, 2009. **44**(12): p. 2463-2474.

32. Kawakami, M., Furumura, T., and Tokushige, H. *NOx removal effects and physical properties of cement mortar incorporating titanium dioxide powder*. in *International RILEM Symposium of Photocatalysis, Environment and Construction Materials*. 2007. Florence, Italy: RILEM Publications S. A. R. L.

33. Folli, A., et al., *Rhodamine B Discolouration on TiO2 in the Cement Environment: A Look at Fundamental Aspects of the Self-cleaning Effect in Concretes.* Journal of Advanced Oxidation Technologies, 2009. **12**(1): p. 126-133.

34. Diamanti, M.V., Ormellese, M., and Pedeferri, M., *Characterization of photocatalytic and superhydrophilic properties of mortars containing titanium dioxide.* Cement and Concrete Research, 2008. **38**(11): p. 1349-1353.

35. Bowering, N., Walker, G.S., and Harrison, P.G., *Photocatalytic decomposition and reduction reactions of nitric oxide over Degussa P25.* Applied Catalysis B-Environmental, 2006. **62**(3-4): p. 208-216.

36. Maggos, T., et al., *Application of photocatalytic technology for NOx removal.* Applied Physics a-Materials Science & Processing, 2007. **89**(1): p. 81-84.

37. Poon, C.S. and Cheung, E., *NO removal efficiency of photocatalytic paving blocks prepared with recycled materials.* Construction and Building Materials, 2007. **21**(8): p. 1746-1753.

38. Ruot, B., et al., *TiO2-containing cement pastes and mortars: Measurements of the photocatalytic efficiency using a rhodamine B-based colourimetric test.* Solar Energy, 2009. **83**(10): p. 1794-1801.

39. Maggos, T., et al., *Photocatalytic degradation of NOx in a pilot street canyon configuration using TiO2-mortar panels.* Environmental Monitoring and Assessment, 2008. **136**(1-3): p. 35-44.

40. Beeldens, A. *Air purification by road materials: Results of the test project in Antwerp*. in *International RILEM Symposium on Photocatalysis, Environment, and Construction Materials - TDP 2007*. 2007. Florence, Italy: Rilem Publications.

41. Tanaka, K., Capule, M.F.V., and Hisanaga, T., *Effect of crytallinity of TiO_2 on its photocatalytic action.* Chemical Physics Letters, 1991. **187**(1-2): p. 73-76.

42. Dylla, H., et al., *Evaluation of Environmental Effectiveness of Titanium Dioxide Photocatalyst Coating for Concrete Pavement.* Transportation Research Record: Journal of the Transportation Research Board, 2010. **2164**(1): p. 46-51.

43. Sahmaran, M., Christianto, H.A., and Yaman, I.O., *The effect of chemical admixtures and mineral additives on the properties of self-compacting mortars.* Cement & Concrete Composites, 2006. **28**(5): p. 432-440.

44. Damtoft, J.S., et al., *Sustainable development and climate change initiatives.* Cement and Concrete Research, 2008. **38**(2): p. 115-127.

45. *ASTM C595, 2013 "Standard Specification for Blended Hydraulic Cements"*, ASTM International: West Conshohocken, PA.

46. *Canadian Standards Association, CAN/CSA-A5-98, "Portland Cement" 1998*, Canadian Standards Association: Ontario, Canada.

47. Bentz, D.P., et al., *Limestone Fillers Conserve Cement. Part 1: An analysis based on Powers' model.* Concrete International, 2009(Nov): p. 41-46.

48. *Comité Européen de Normalisation, EN 197-1, "Cement-Part 1: Composition Specifications and Conformity Criteria for Common Cements"*. 2000, Comité Européen de Normalisation: Brussels, Belgium.

49. Hawkins, P., Tennis, P., and Detwiler, R., *The Use of Limestone in Portland Cement: A State-of-the-Art Review*. 2005, Portland Cement Association: Skokie, Illinois, USA.

50. *ASTM C150, 2012 "Standard Specification for Portland Cement"*, ASTM International: West Conshohocken, PA.

51. Bentz, D.P., *Replacement of "coarse" cement particles by inert fillers in low w/c ratio concretes II. Experimental validation.* Cement and Concrete Research, 2005. **35**(1): p. 185-188.

52. Flores, I., et al., *Performance of Cement Systems with Nano-SiO2 Particles Produced by Using the Sol-Gel Method.* Transportation Research Record, (2141): p. 10-14.

53. Jayapalan, A.R., et al., *Influence of Additions of Anatase TiO2 Nanoparticles on Early-Age Properties of Cement-Based Materials.* Transportation Research Record, 2010(2141): p. 41-46.

54. Matschei, T., Lothenbach, B., and Glasser, F.P., *The role of calcium carbonate in cement hydration.* Cement and Concrete Research, 2007. **37**(4): p. 551-558.

55. Powers, T.C. and Brownyard, T.L., *Studies of the physical properties of hardened portland cement paste*, in *Bulletin 22*. 1948, Research Laboratories of the Portland Cement Association: Chicago.

56. Powers, T.C., *Structure and physical properties of hardened portland cement paste.* Journal of the American Ceramic Society, 1958. **41**(1): p. 1-6.

57. Gleize, P.J.P., Cyr, M., and Escadeillas, G., *Effects of metakaolin on autogenous shrinkage of cement pastes.* Cement & Concrete Composites, 2007. **29**(2): p. 80-87.

58. Bentz, D.P. and Peltz, M.A., *Reducing thermal and autogenous shrinkage contributions to early-age cracking.* Aci Materials Journal, 2008. **105**(4): p. 414-420.

59. Bentz, D.P. and Jensen, O.M., *Mitigation strategies for autogenous shrinkage cracking.* Cement & Concrete Composites, 2004. **26**(6): p. 677-685.

60. Wild, S., Khatib, J.M., and Roose, L.J., *Chemical shrinkage and autogenous shrinkage of Portland cement metakaolin pastes.* Advances in Cement Research, 1998. **10**(3): p. 109-119.

61. Lawrence, P., Cyr, M., and Ringot, E., *Mineral admixtures in mortars - Effect of inert materials on short-term hydration.* Cement and Concrete Research, 2003. **33**(12): p. 1939-1947.

62. Cyr, M., Lawrence, P., and Ringot, E., *Mineral admixtures in mortars - Quantification of the physical effects of inert materials on short-term hydration.* Cement and Concrete Research, 2005. **35**(4): p. 719-730.

63. Lee, B.Y. and Kurtis, K.E., *Influence of TiO_2 Nanoparticles on Early C_3S Hydration.* Journal of the American Ceramic Society, 2010. **93**(10): p. 3399-3405.

64. Schindler, A.K., *Effect of temperature on hydration of cementitious materials.* Aci Materials Journal, 2004. **101**(1): p. 72-81.

65. Schindler, A.K. and Folliard, K.J., *Heat of hydration models for cementitious materials.* ACI Materials Journal, 2005. **102**(1): p. 24-33.

66. Poole, J.L., et al., *Methods for calculating activation energy for portland cement.* ACI Materials Journal, 2007. **104**(1): p. 86-94.

67. Kada-Benameur, H., Wirquin, E., and Duthoit, B., *Determination of apparent activation energy of concrete by isothermal calorimetry.* Cement and Concrete Research, 2000. **30**(2): p. 301-305.

68. Glasstone, S., Laidler, K.J., and Eyring, H., *The theory of rate processes: The kinetics of chemical reactions, viscosity, diffusion and electrochemical phenomena*. 1st ed. 1941, New York, London: McGraw-Hill.

69. *ASTM C 1074, 2011 "Standard Practice for Estimating Concrete Strength by the Maturity Method"*. 2011, ASTM International: West Conshohocken, PA.

70. FitzGerald, S.A., et al., *In situ quasi-elastic neutron scattering study of the hydration of tricalcium silicate.* Chemistry of Materials, 1998. **10**(1): p. 397-402.

71. Thomas, J.J. and Jennings, H.M., *Effects of D2O and mixing on the early hydration kinetics of tricalcium silicate.* Chemistry of Materials, 1999. **11**(7): p. 1907-1914.

72. Kjellsen, K.O. and Detwiler, R.J., *Reaction kinetics of portland cement mortars hydrated at different temperatures.* Cement and Concrete Research, 1992. **22**(1): p. 112-120.

73. Poole, J.L., et al., *Effect of Chemical Admixtures on Apparent Activation Energy of Cementitious Systems.* Journal of Materials in Civil Engineering, 2011. **23**(12): p. 1654-1661.

74. Fujii, K. and Kondo, W., *Kinetics of the Hydration of Tricalcium Silicate.* Journal of the American Ceramic Society, 1974. **57**(11): p. 492-497.

75. FitzGerald, S.A., et al., *A neutron scattering study of the role of diffusion in the hydration of tricalcium silicate.* Cement and Concrete Research, 2002. **32**(3): p. 409-413.

76. D'Aloia, L. and Chanvillard, G., *Determining the "apparent" activation energy of concrete Ea - Numerical simulations of the heat of hydration of cement.* Cement and Concrete Research, 2002. **32**(8): p. 1277-1289.

77. Riding, K.A., et al., *New Model for Estimating Apparent Activation Energy of Cementitious Systems.* ACI Materials Journal, 2011. **108**(5): p. 550-557.

78. Wirquin, E., Broda, M., and Duthoit, B., *Determination of the apparent activation energy of one concrete by calorimetric and mechanical means - Influence of a superplasticizer.* Cement and Concrete Research, 2002. **32**(8): p. 1207-1213.

79. Ma, W.P., et al., *Calorimetric study of cement blends containing fly-ash, silica fume and slag at elevated temperatures.* Cement Concrete and Aggregates, 1994. **16**(2): p. 93-99.

80. Scrivener, K.L. and Kirkpatrick, R.J., *Innovation in use and research on cementitious material.* Cement and Concrete Research, 2008. **38**(2): p. 128-136.

81. Zhang, J., et al., *Early hydration and setting of oil well cement.* Cement and Concrete Research, 2010. **40**(7): p. 1023-1033.

82. Pane, I. and Hansen, W., *Concrete hydration and mechanical properties under nonisothermal conditions.* ACI Materials Journal, 2002. **99**(6): p. 534-542.

83. Hansen, P.F. and Pedersen, E.J., *Maturity computer for controlled curing and hardening of concrete.* Nordisk Betong, 1977. **1**(19): p. 21-25.

84. Riding, K.A., et al., *Modeling Hydration of Cementitious Systems.* ACI Materials Journal, 2012. **109**(2): p. 225-234.

85. Swamy, R.N., *Holistic design: key to sustainability in concrete construction.* Proceedings of the Institution of Civil Engineers-Structures and Buildings, 2001. **146**(4): p. 371-379.

86. Bentz, D.P., et al., *Limestone fillers conserve cement. Part 2: Durability issues and the effects of limestone fineness on mixtures* Concrete International, 2009(Dec): p. 35-39.

87. Diamond, S., *Mercury porosimetry - An inappropriate method for the measurement of pore size distributions in cement-based materials.* Cement and Concrete Research, 2000. **30**(10): p. 1517-1525.

88. Gonen, T. and Yazicioglu, S., *The influence of compaction pores on sorptivity and carbonation of concrete.* Construction and Building Materials, 2007. **21**(5): p. 1040-1045.

89. Aligizaki, K.K., *Pore Structure of Cement-Based Materials: Tesing, Interpreation and Requirements*. Modern Concrete Technology, ed. A. Bentur and S. Mindess. Vol. 12. 2006, New York: Taylor & Francis.

90. Garboczi, E.J. and Bentz, D.P., *Computer Simulation of the Diffusivity of Cement-Based Materials.* Journal of Materials Science, 1992. **27**(8): p. 2083-2092.

91. Bentz, D.P. and Garboczi, E.J., *Percolation of Phases in a 3-Dimensional Cement Paste Microstructural Model.* Cement and Concrete Research, 1991. **21**(2-3): p. 325-344.

92. Linsebigler, A.L., Lu, G.Q., and Yates, J.T., *Photocatalysis on TiO_2 surfaces - Principles, mechanisms, and selected results.* Chemical Reviews, 1995. **95**(3): p. 735-758.

93. Bianchi, C.L., et al. *The Role of the Synthetic Procedure of Nano-Crystalline TiO_2 on the Photodegradation of Toluene*. in *International RILEM Symposium on Photocatalysis, Environment, and Construction Materials - TDP 2007*. 2007. Florence, Italy: Rilem Publications.

94. Blake, D.M., et al., *Application of the photocatalytic chemistry of titanium dioxide to disinfection and the killing of cancer cells.* Separation and Purification Methods, 1999. **28**(1): p. 1-50.

95. Allen, N.S., et al., *Photocatalytic titania based surfaces: Environmental benefits.* Polymer Degradation and Stability, 2008. **93**(9): p. 1632-1646.

96. Alberici, R.M. and Jardim, W.F., *Photocatalytic destruction of VOCs in the gas-phase using titanium dioxide.* Applied Catalysis B: Environmental, 1997. **14**(1-2): p. 55-68.

97. Seinfeld, J.H. and Pandis, S.N., *Atmospheric Chemistry and Physics - From Air Pollution to Climate Change*. 2nd ed. 2006, Hoboken, New Jersey: John Wiley & Sons , Inc.

98. Zivica, V. and Bajza, A., *Acidic attack of cement based materials - a review. Part 1. Principle of acidic attack.* Construction and Building Materials, 2001. **15**(8): p. 331-340.

99. Bell, F.G., *Durability of carbonate rock as building stone with comments on its preservation.* Environmental Geology, 1993. **21**(4): p. 187-200.

100. Schlatter, C., *Environmental-Pollution and Human Health.* Science of the Total Environment, 1994. **143**(1): p. 93-101.

101. Devahasdin, S., et al., *TiO2 photocatalytic oxidation of nitric oxide: transient behavior and reaction kinetics.* Journal of Photochemistry and Photobiology A: Chemistry, 2003. **156**(1-3): p. 161-170.

102. Chen, J. and Poon, C.-s., *Photocatalytic Cementitious Materials: Influence of the Microstructure of Cement Paste on Photocatalytic Pollution Degradation.* Environmental Science & Technology, 2009. **43**(23): p. 8948-8952.

103. ISO, *ISO 22197-1 - Fine ceramics (advanced ceramics, advanced technical ceramics) — Test method for air-purification performance of semiconducting photocatalytic materials — Part 1: Removal of nitric oxide*. 2007.

104. JIS, *JIS R 1701-1: Fine ceramics (advanced ceramics, advanced technical ceramics) - Test method for air purification performance of photocatalytic materials - Part 1: Removal of nitric oxide*. 2004, Japanese Standards Association: Tokyo, Japan.

105. UNI, *UNI 11247-1 - Determination of the catalytic degradation of nitrous dioxides by photocatalytic inorganic materials*. 2008.

106. Hassan, M.M., et al., *Evaluation of the durability of titanium dioxide photocatalyst coating for concrete pavement.* Construction and Building Materials, 2010. **24**(8): p. 1456-1461.

107. Chen, J. and Poon, C.-S., *Photocatalytic activity of titanium dioxide modified concrete materials - Influence of utilizing recycled glass cullets as aggregates.* Journal of Environmental Management, 2009. **90**(11): p. 3436-3442.

108. Folli, A. and Macphee, D.E. *Thermodynamic and kinetic considerations of the oxidation of nitrogen oxides on photocatalytic cementitious materials*. in *Nanotechnology in Construction - 4th International Symposium (NICOM4)*. 2012. Crete, Greece.

109. Lackhoff, M., et al., *Photocatalytic activity of semiconductor-modified cement-influence of semiconductor type and cement ageing.* Applied Catalysis B-Environmental, 2003. **43**(3): p. 205-216.

110. WCED, *Our Common Future*. 1987, United Nations World Commission on Environment and Development: Oxford: Oxford University Press.

111. Seghezzo, L., *The five dimensions of sustainability.* Environmental Politics, 2009. **18**(4): p. 539-556.

112. Somerville, G., *Sustainability - its implications for concrete research.* Magazine of Concrete Research, 2001. **53**(1): p. 1-2.

113. Pulselli, R.M., et al., *Specific emergy of cement and concrete: An energy-based appraisal of building materials and their transport.* Ecological Indicators, 2008. **8**(5): p. 647-656.

114. Schonsleben, P., et al., *The changing concept of sustainability and economic opportunities for energy-intensive industries.* Cirp Annals-Manufacturing Technology. **59**(1): p. 477-480.

115. Horvath, A., *Construction materials and the environment.* Annual Review of Environment and Resources, 2004. **29**: p. 181-204.

116. Buchanan, A.H. and Honey, B.G., *Energy and carbon-dioxide implications of building construction.* Energy and Buildings, 1994. **20**(3): p. 205-217.

117. VanGeem, M., *Achieving sustainability with precast concrete.* Pci Journal, 2006. **51**(1): p. 42-+.

118. Van den Heede, P. and De Belie, N., *Environmental impact and life cycle assessment (LCA) of traditional and ˜green" concretes: Literature review and theoretical calculations.* Cement and Concrete Composites. **34**(4): p. 431-442.

119. Huntzinger, D.N. and Eatmon, T.D., *A life-cycle assessment of Portland cement manufacturing: comparing the traditional process with alternative technologies.* Journal of Cleaner Production, 2009. **17**(7): p. 668-675.

120. Chidiac, S.E., *Sustainability of Civil Engineering Structures - Durability of concrete.* Cement & Concrete Composites, 2009. **31**(8): p. 513-514.

121. ISO, *ISO 14040:2006 - Environmental management - Life cycle assessment - Principles and framework* 2006.

122. Habert, G. and Roussel, N., *Study of two concrete mix-design strategies to reach carbon mitigation objectives.* Cement and Concrete Composites, 2009. **31**(6): p. 397-402.

123. Hassan, M.M., *Quantification of the Environmental Benefits of Ultrafine/Nanotitanium Dioxide Photocatalyst Coatings for Concrete Pavement Using Hybrid Life-Cycle Assessment.* Journal of Infrastructure Systems, 2010. **16**(2): p. 160-166.

124. Grubb, G.F. and Bakshi, B.R., *Life Cycle of Titanium Dioxide Nanoparticle Production Impact of Emissions and Use of Resources.* Journal of Industrial Ecology, 2011. **15**(1): p. 81-95.

125. Colvin, V.L., *The potential environmental impact of engineered nanomaterials.* Nature Biotechnology, 2003. **21**(10): p. 1166-1170.

126. Osborne, G.J., *Durability of Portland blast-furnace slag cement concrete.* Cement & Concrete Composites, 1999. **21**(1): p. 11-21.

127. Schwarz, N., Cam, H., and Neithalath, N., *Influence of a fine glass powder on the durability characteristics of concrete and its comparison to fly ash.* Cement & Concrete Composites, 2008. **30**(6): p. 486-496.

128. Szalay, A.Z.Z., *What is missing from the concept of the new European Building Directive?* Building and Environment, 2007. **42**(4): p. 1761-1769.

129. *ASTM C 305, 2006 "Standard practice for mechanical mixing of hydraulic cement pastes and mortars of plastic consistency"*. 2006, ASTM International: West Conshohocken, PA.

130. *ASTM C 191, 2008 "Standard Test Method for Time of Setting of Hydraulic Cement by Vicat Needle"*. 2008, ASTM International: West Conshohocken, PA.

131. *ASTM C 1437, 2007 "Standard Test Method for Flow of Hydraulic Cement Mortar"*. 2007, ASTM International: West Conshohocken, PA.

132. *ASTM C 1679, 2008 "Standard practice for measuring hydration kinetics of hydraulic cementitious mixtures using isothermal calorimetry"*. 2008, ASTM International: West Conshohocken, PA.

133. *ASTM C 1702, 2009 "Standard test method for measurement of heat of hydration of hydraulic cementitious materials using isothermal conduction calorimetry"*. 2009, ASTM International: West Conshohocken, PA.

134. *ASTM C 1608, 2007 "Standard test method for chemical shrinkage of hydraulic cement paste"*. 2007, ASTM International: West Conshohocken, PA.

135. *ASTM C 1698, 2009 "Standard Test Method for Autogenous Strain of Cement Paste and Mortar"*. 2009, ASTM International: West Conshohocken, PA.

136. Jensen, O.M. and Hansen, P.F., *Water-entrained cement-based materials I. Principles and theoretical background.* Cement and Concrete Research, 2001. **31**(4): p. 647-654.

137. Taylor, H.F.W., *Cement Chemistry*. Second ed. 1997: Thomas Telford Limited.

138. *ASTM C 1581, 2009 "Standard Test Method for Determining Age of Cracking and Induced Tensile Stress Characteristics of Mortar and Concrete under Restrained Shrinkage"*. 2009, ASTM International: West Conshohocken, PA.

139. Mohr, B.J. and Hood, K.L., *Influence of bleed water reabsorption on cement paste autogenous deformation.* Cement and Concrete Research, 2010. **40**(2): p. 220-225.

140. Thomas, J.J., Jennings, H.M., and Chen, J.J., *Influence of Nucleation Seeding on the Hydration Mechanisms of Tricalcium Silicate and Cement.* Journal of Physical Chemistry C, 2009. **113**(11): p. 4327-4334.

141. Thomas, J.J., *A new approach to modeling the nucleation and growth kinetics of tricalcium silicate hydration.* Journal of the American Ceramic Society, 2007. **90**(10): p. 3282-3288.

142. *ASTM C192/C192M 2012 "Standard Practice for Making Concrete Test Specimen in the Laboratory"*, ASTM International: West Conshohocken, PA.

143. *ASTM C305, 2006 "Standard practice for mechanical mixing of hydraulic cement pastes and mortars of plastic consistency"*, ASTM International: West Conshohocken, PA.

144. Brunauer, S., Emmett, P.H., and Teller, E., *Adsorption of Gases in Multimolecular Layers.* Journal of the American Chemical Society, 1938. **60**(2): p. 309-319.

145. Barrett, E.P., Joyner, L.G., and Halenda, P.P., *The Determination of Pore Volume and Area Distributions in Porous Substances I. Compuations from nitrogen isotherms.* Journal of the American Chemical Society, 1951. **73**(1): p. 373-380.

146. Odler, I., *The BET-specific surface area of hydrated Portland cement and related materials.* Cement and Concrete Research, 2003. **33**(12): p. 2049-2056.

147. Juenger, M.C.G. and Jennings, H.M., *The use of nitrogen adsorption to assess the microstructure of cement paste.* Cement and Concrete Research, 2001. **31**(6): p. 883-892.

148. *ASTM C1202, 2010 "Standard Test Method for Electrical Indication of Concrete's Ability to Resist Chloride Ion Penetration"*, ASTM International: West Conshohocken, PA.

149. Stanish, K.D., Hooton, R.D., and Thomas, M.D.A., *Testing the chloride penetration resistance of concrete: A literature review (FHWA contract DTFH61-97-R-00022: Prediction of chloride penetration in concrete)*. 1997, University of Toronto Department of Civil Engineering: Toronto, ON, Canada.

150. Obla, K.H., et al., *Properties of concrete containing ultra-fine fly ash.* Aci Materials Journal, 2003. **100**(5): p. 426-433.

151. *ASTM C 1202, 2010 "Standard Test Method for Electrical Indication of Concrete's Ability to Resist Chloride Ion Penetration"*. 2010, ASTM International: West Conshohocken, PA.

152. Chini, A.R., Muszynski, L.C., and Hicks, J.K., *Determination of acceptance permeability characteristics for performance-related specifications for portland cement concrete (Grant BC 354-41)*. 2003, M. E. Rinker, Sr. School of Building Construction, University of Florida: Tallahassee, FL.

153. Wee, T.H., Suryavanshi, A.K., and Tin, S.S., *Evaluation of rapid chloride permeability test (RCPT) results for concrete containing mineral admixtures.* Aci Materials Journal, 2000. **97**(2): p. 221-232.

154. Polder, R.B., *Test methods for on site measurement of resistivity of concrete - a RILEM TC-154 technical recommendation.* Construction and Building Materials, 2001. **15**(2-3): p. 125-131.

155. Garrault, S., Behr, T., and Nonat, A., *Formation of the C-S-H layer during early hydration of tricalcium silicate grains with different sizes.* Journal of Physical Chemistry B, 2006. **110**(1): p. 270-275.

156. Vuk, T., et al., *The effects of limestone addition, clinker type and fineness on properties of Portland cement.* Cement and Concrete Research, 2001. **31**(1): p. 135-139.

157. Tsivilis, S., et al., *An analysis of the properties of Portland limestone cements and concrete.* Cement & Concrete Composites, 2002. **24**(3-4): p. 371-378.

158. Thomas, J.J., Jennings, H.M., and Allen, A.J., *Relationships between Composition and Density of Tobermorite, Jennite, and Nanoscale CaO-SiO2-H2O.* Journal of Physical Chemistry C, 2010. **114**(17): p. 7594-7601.

159. Odler, I. and KÃ¶ster, H., *Investigation on the structure of fully hydrated portland cement and tricalcium silicate pastes. III. Specific surface area and permeability.* Cement and Concrete Research, 1991. **21**(6): p. 975-982.

160. Dalton, J.S., et al., *Photocatalytic oxidation of NOx gases using TiO2: a surface spectroscopic approach.* Environmental Pollution, 2002. **120**(2): p. 415-422.

161. EPA, *Primary National Ambient Air Quality Standards for Nitrogen Dioxide; Final Rule*, in *Federal Register*. 2010. p. 6473-6537.

162. *Council Directive 1999/30/EC, Relating to limit values for sulphur dioxide, nitrogen dioxide and oxides of nitrogen, particulate matter and lead in ambient air*. Official Journal of the European Communities, 1999.

163. *Ministry of the Environment Government of Japan, Law 70 of 1992: The Law Concerning Special Measures for Total Emission Reduction of Nitrogen Oxides from Automobiles in Specified Areas*.

164. Linkous, C.A., et al., *Photocatalytic inhibition of algae growth using TiO2, WO3, and cocatalyst modifications.* Environmental Science & Technology, 2000. **34**(22): p. 4754-4758.

165. Erickson, J. *Route 141 testing baffles researchers*. 2013 [cited 2013 May 06]; Available from: http://www.newsmagazinenetwork.com/2013040132964/route-141-testing-baffles-researchers/.

166. Lee, B.Y., et al., *Photocatalytic Cement Exposed to Nitrogen Oxides: Effect of Oxidation and Binding.* Cement and Concrete Research, submitted.

167. Bacsa, R.R. and Kiwi, J., *Effect of rutile phase on the photocatalytic properties of nanocrystalline titania during the degradation of p-coumaric acid.* Applied Catalysis B: Environmental, 1998. **16**(1): p. 19-29.

168. Kurtis, K.E., et al., *Examining cement-based materials by laser scanning confocal microscopy.* Cement & Concrete Composites, 2003. **25**(7): p. 695-701.

169. Lee, B.Y., *Effect of titanium dioxide nanoparticles on early age and long term properties of cementitious materials*, in *Civil and Environmental Engineering*. 2012, Georgia Institute of Technology: Atlanta.

170. Jayapalan, A.R., *Properties of cement-based materials in the presence of nano and micro particle additives*, in *Civil and Environmental Engineering*. 2013, Georgia Institute of Technology: Atlanta - in preparation.

171. Hurum, D.C., et al., *Explaining the enhanced photocatalytic activity of Degussa P25 mixed-phase TiO2 using EPR.* Journal of Physical Chemistry B, 2003. **107**(19): p. 4545-4549.

172. Campillo, I., et al., *Improvement of initial mechanical strength by nanoalumina in belite cements.* Materials Letters, 2007. **61**(8-9): p. 1889-1892.

173. Jo, B.W., et al., *Characteristics of cement mortar with nano-SiO2 particles.* Construction and Building Materials, 2007. **21**(6): p. 1351-1355.

174. Sanchez, F. and Ince, C., *Microstructure and macroscopic properties of hybrid carbon nanofiber/silica fume cement composites.* Composites Science and Technology, 2009. **69**(7-8): p. 1310-1318.

175. Cardenas, H.E. and Struble, L.J., *Electrokinetic nanoparticle treatment of hardened cement paste for reduction of permeability.* Journal of Materials in Civil Engineering, 2006. **18**(4): p. 554-560.

176. Konsta-Gdoutos, M.S., Metaxa, Z.S., and Shah, S.P., *Highly dispersed carbon nanotube reinforced cement based materials.* Cement and Concrete Research, 2010. **40**(7): p. 1052-1059.

177. Hui, L., Xiao, H.G., and Ou, J.P., *A study on mechanical and pressure-sensitive properties of cement mortar with nanophase materials.* Cement and Concrete Research, 2004. **34**(3): p. 435-438.

178. Lee, J., Mahendra, S., and Alvarez, P.J.J., *Nanomaterials in the Construction Industry: A Review of Their Applications and Environmental Health and Safety Considerations.* Acs Nano, 2010. **4**(7): p. 3580-3590.

179. Pacheco-Torgal, F. and Jalali, S., *Nanotechnology: Advantages and drawbacks in the field of construction and building materials.* Construction and Building Materials, 2011. **25**(2): p. 582-590.

180. Lippiatt, B., Greig, A.L., and Lavappa, P., *BEES (Building for Environmental and Economic Sustainability)*. 2010, NIST (National Institute of Standards and Technology) Engineering Laboratory.

181. Hutchison, J.E., *Greener nanoscience: A proactive approach to advancing applications and reducing implications of nanotechnology.* Acs Nano, 2008. **2**(3): p. 395-402.

182. Rittmann, B.E., *Opportunities for renewable bioenergy using microorganisms.* Biotechnology and Bioengineering, 2008. **100**(2): p. 203-212.

183. Brennan, L. and Owende, P., *Biofuels from microalgae-A review of technologies for production, processing, and extractions of biofuels and co-products.* Renewable & Sustainable Energy Reviews, 2010. **14**(2): p. 557-577.

184. *Ambient Air Surveillance Report*. 2004, Environmental Protection Division - Air Protection Branch, Georgia Department of Natural Resources: Atlanta.

185. Stir, M., Nicula, R., and Burkel, E., *Pressure-temperature phase diagrams of pure and Ag-doped nanocrystalline TiO2 photocatalysts.* Journal of the European Ceramic Society, 2006. **26**(9): p. 1547-1553.

186. Menendez-Flores, V.M., et al., *Controlled structure of anatase TiO2 nanoparticles by using organic additives in a microwave process.* Applied Catalysis a-General, 2011. **406**(1-2): p. 119-123.

187. Jayapalan, A.R., Lee, B.Y., and Kurtis, K.E., *Can 'Nano' be 'Green'? Comparing Efficacy of Nano and Microparticles in Cementitious Materials - submitted to.* Cement & Concrete Composites, 2012.

188. Hashimoto, K., Irie, H., and Fujishima, A., *TiO2 photocatalysis: A historical overview and future prospects.* Japanese Journal of Applied Physics Part 1-Regular Papers Brief Communications & Review Papers, 2005. **44**(12): p. 8269-8285.

189. Xie, X.L., Mai, Y.W., and Zhou, X.P., *Dispersion and alignment of carbon nanotubes in polymer matrix: A review.* Materials Science & Engineering R-Reports, 2005. **49**(4): p. 89-112.